ESA Climate Change Initiative aerosol_cci

Option 3 Absorbing Aerosol Round Robin

Version 1.2

Document reference: Aerosol Absorption

DOCUMENT STATUS SHEET

	FUNCTION	NAME	DATE	SIGNATURE
LEAD AUTHOR	Research scientist	Martin de Graaf	15.12.2017 23.02.2018 15.03.2018	Martin de Graaf Digitally signed by Martin de Graaf Date: 2018.03.15 15:09:36 +01'00'
CONTRIBUTING AUTHORS		Jan Griesfeller Michael Schulz Thomas Popp		
REVIEWED BY		Pepijn Veefkind Thomas Popp	15.12.2017 01.02.2018 23.02.2018	
ISSUED BY	Project manager			
APPROVED BY	Technical Officer (ESA)			

EXECUTIVE SUMMARY

The Aerosol CCI aerosol absorption round robin exercise was designed to compare aerosol products using various available satellite products and verification tools. Four events were selected covering different types of absorbing aerosols: Saharan dust over northern Africa in summer of 2006, biomass burning aerosols over the Sahel in winter 2005/2006, transported mineral dust over Barbados in summer 2007 and industrial pollution over Europe in May 2008. These events were used to compare the following satellite retrievals; SYNAER developed at DLR, AATSR_SU developed at Swansea University, FAME-A developed at the Free University of Berlin, ORAC AATSR developed for Aerosol CCI, OMAERUV developed at NASA Goddard, GRASP developed at the University of Lille, and the Multi-sensor AAI developed at KNMI. Furthermore, AAOT and SSA were compared on a global scale. The correct retrieval of these quantities world-wide would mean a major step for climate research, which is what satellites can provide, given accurate retrievals.

The round robin exercise summarized in this report will show the challenges in retrieving aerosol absorption properties from space-based instruments. A growing dataset of AOT from various instruments covering several decades is being generated, but the retrieval of AAOT and SSA from space suffers from large inconsistencies. These quantities are important for climate studies on a global scale, and therefore deserve attention from the satellite community. The proper retrieval of these quantities should be a focus for the coming years.

CHANGE LOG

Issue	Date	Modified Items / Reason for Change
0.1	2017-01-01	Document creation
0.2	2017-03-30	Updated for internal review
0.3	2017-10-10	Updated for internal review
0.4	2017-10-01	Penultimate version for approval
1.0	2017-12-15	Final version
1.1	2018-02-01	Science leader review, layout changes (RID_O3_v1.1_001)
1.2	2018-03-15	Clarifications and improvements responding to changes requested by ESA (RID_O3_v1.1_002 – RID_O3_v1.1_031) + science leader review

TABLE OF CONTENTS

Change Log **3**
List of Tables **4**
List of Figures **5**
1 INTRODUCTION **8**
1.1 Scope 8
1.2 References 8
2 Description of the algorithms **11**
2.1 SU_AATSR 11
2.2 FAME-A 11
2.3 SYNAER 11
2.4 OMAERUV 12
2.5 Multi-sensor AAI 12
2.6 GRASP 12
2.7 ORAC AATSR 13
3 Mineral dust over the Sahara **14**
3.1 Aerosol Optical Thickness over the Sahara 14
3.2 Absorbing aerosol optical thickness and single scattering albedo 19
3.3 AERONET AAOT and SSA 21
4 Biomass burning aerosols over the Sahel region **24**
4.1 Aerosol Optical Thickness over the Sahel 24
4.2 Absorbing aerosol optical thickness and single scattering albedo 29
5 Biomass burning aerosols over Central South Africa **34**
5.1 Absorbing aerosol optical thickness and single scattering albedo 35
5.2 SYNAER data 37
5.3 GRASP data 37
6 Tropical Atlantic Ocean **42**
6.1 FAME-A data 42
6.2 ORAC AATSR data 44
6.3 Absorption Aerosol Optical Thickness 45
6.4 Saharan dust 46
7 Global Absorption Aerosol Optical Thickness **48**
8 Global Single Scattering Albedo **50**
9 Absorbing AOT validation against AERONET **52**
9.1 Maps 52
9.2 Comparison to observations 53
9.3 Zonal mean at observation sites 55
9.4 Bias at observation sites 56
9.5 Summary tables 57
10 Conclusions **59**
11 Recommendations **60**

List of Tables

1 Statistics table AAOT daily values for the whole year 2008 WORLD 58
2 Statistics table AOT daily values for the whole year 2008 WORLD 58
3 statistics table AAOT daily values for the whole year 2008 SAF 58
4 statistics table AOT daily values for the whole year 2008 SAF 58

List of Figures

1 SU_AATSR and OMAERUV AOT averaged from 1 July - 31 August 2006. 14
2 SU_AATSR and OMAERUV AOT from 1 July - 31 August 2006 averaged over the area shown in Figure 1. 15
3 AOT at AERONET station Tammanrasset, OMAERUV AOT and SU_AATSR AOT around that station, from 1 July - 31 August 2006. 16
4 AOT at AERONET station Ras el Ain, OMAERUV AOT and SU_AATSR AOT around that station, from 1 July - 31 August 2006. 17
5 AOT at AERONET station Izana, OMAERUV AOT and SU_AATSR AOT around that station, from 1 July - 31 August 2006. 18
6 AAOT (top panels) from SU_AATSR (left) and OMAERUV (right) and SSA (lower panels) averaged from 1 July – 31 August 2006. 19
7 SU_AATSR AAOT at 550 nm, OMAERUV AAOT at 354 nm, 388 nm, and 500 nm, SU_AATSR SSA (550 nm) and OMAERUV SSA (354, 388, and 500 nm) from 1 July – 31 August 2006 averaged over the area shown in Figure 6. 20
8 SU_AATSR versus OMAERUV AAOT and SSA for all regridded data over the Sahara region shown in Figure 1 and the period shown in Figure 7. 21
9 Absorbing Aerosol Optical Thickness from 1 July – 31 August 2006 from AERONET, SU_AATSR and OMAERUV around station (a) Tamanrasset, (b) Ras El Ain, and (c) Izana. The satellite data were averaged over the same areas as in Figures 3-5 22
10 Single scattering albedo from 1 July – 31 August 2006 from AERONET, SU_AATSR and OMAERUV around station (a) Tamanrasset, (b) Ras El Ain, and (c) Izana. The satellite data were averaged over the same areas as in Figures 3-5 23
11 AOT derived from SU_AATSR (left) and OMAERUV (right) data, averaged from 1 November 2005 – 28 February 2006. 24
12 SU_AATSR and OMAERUV AOT from 1 November 2005 – 28 February 2006 averaged over the area shown in Figure 11. 25
13 AOT at AERONET station Ilorin, OMAERUV AOT and SU_AATSR AOT around that station, from 1 November 2005 – 28 February 2006. 26
14 AOT at AERONET station Djougou, OMAERUV AOT and SU_AATSR AOT around that station, from 1 November 2005 – 28 February 2006. 27
15 AOT at AERONET station Dakar, OMAERUV AOT and SU_AATSR AOT around that station, from 1 November 2005 – 28 February 2006. 28
16 AAOT (top panel) and SSA (bottom) derived from SU_AATSR (left) and OMAERUV (right) data, averaged from 1 November 2005 – 28 February 2006. 29
17 SU_AATSR and OMAERUV AAOT and SSA from 1 November 2005 – 28 February 2006 averaged over the area shown in Figure 11. The top panel shows the SU_AATSR AAOT at 550 nm, the next panel the OMAERUV AAOT at 354 nm, 388 nm, and 500 nm. The lower panels show the SSA, first from SU_AATSR at 550 nm, the lowest panel showing the OMAERUV SSA at 354 nm, 388 nm, and 500 nm. 30
18 SU_AATSR and OMAERUV AAOT (left panel) and SSA (right panel) from 1 November 2005 – 28 February 2006 averaged over the area shown in Figure 11. 31
19 Absorbing Aerosol Optical Thickness from 1 November 2005 – 28 February 2006 from AERONET, SU_AATSR and OMAERUV around station (a) Ilorin, (b) Djougou, and (c) Dakar. The satellite data were averaged over the same areas as in Figures 13-15. 32

20 Single scattering albedo from 1 November 2005 – 28 February 2006 from AERONET, SU_AATSR and OMAERUV around station (a) Ilorin, (b) Djougou, and (c) Dakar. The satellite data were averaged over the same areas as in Figures 13-15 33
21 Multi sensor AAI at $1^\circ \times 1^\circ$ grid (left) and the OMAER UVAI at a $0.25^\circ \times 0.25^\circ$ grid, averaged from 1 August – 31 September 2006 over the area shown. The left plot shows the location of the Mongu AERONET station, and the averaging boxes that were used to average OMAERUV data around the station. 34
22 (Left panel) Comparison of multi-sensor AAI data and OMAR UVAI data regridded to a $1^\circ \times 1^\circ$ grid, from 1 August – 31 September 2006, for all data between $0 - 35^\circ$S and $0 - 40^\circ$E (see Figure 21. (Right panel) OMAERUV AAOT versus UVAI data for the same period and area as the left panel, except at the original $0.25^\circ \times 0.25^\circ$ grid. 35
23 SU_AATSR versus OMAERUV AAOT and SSA for all regridded data in central-south Africa (around Mongu station). 35
24 SU_AATSR versus OMAERUV AAOT and SSA for all regridded data Mongu station. 36
25 SYNAER AOT (left), AAOT (middle), and SSA (right), averaged from 1 July – 31 September 2006 over the area shown. 37
26 OMAERUV, SU_AATSR, SYNAER, and GRASP AAOT averaged per day versus daily AERONET station Mongu data. The area over which is averaged is indicated in Fig 21, the smaller rectangle for OMAERUV, and the wider rectangle for the three other datasets. The OMAERUV AAOT is at 500 nm, from SU_AATSR at 550 nm, from SYNAER at 550 nm and from GRASP at 440 and 670 nm. The orange data are Mongu station AAOT data at 674 nm, while the black dots were computed by simple averaging of Mongu AAOTs at 674 nm and 441 nm (to compare with 500 nm), or 441 nm for comparison with GRASP at 440 nm. 38
27 OMAERUV, SU_AATSR, SYNAER, and GRASP SSA averaged per day versus daily AERONET station Mongu SSA. The area over which is averaged is indicated in Fig 21, the smaller rectangle for OMAERUV, and the wider rectangle for the three other datasets. The OMAERUV SSA is at 500 nm, from SU_AATSR at 550 nm, from SYNAER at 550 nm and from GRASP at 440 and 670 nm. The orange data are Mongu station SSA data at 674 nm, while the black dots were computed by simple averaging of Mongu SSAs at 674 nm and 441 nm (to compare with 500 nm), or 441 nm for comparison with GRASP at 440 nm. 39
28 Comparison of SU_AATSR AAOT (left panel) and SSA (right panel) to that from SYNAER. The data were regridded to $0.5^\circ \times 0.5^\circ$ grid and averaged from 1 July to 30 September 2006. 40
29 FAME-A AOT and SSA in sunglint areas (upper panels) and SU_AATSR AOT and SSA (lower panels) averaged from 1 June to 31 August 2007 over the tropical Atlantic Ocean. 42
30 Upper panel: AOT (500 to 555 nm, see caption) from 1 June to 31 August 2007 averaged over the tropical Atlantic Ocean from the different algorithms compared to AOT from La Parguera AERONET station; Lower panel: SSA from three algorithms from 1 June to 31 August 2007 averaged over the tropical Atlantic Ocean compared to SSA from La Parguera AERONET station. Blue and yellow data are AERONET L1.5 data at 441 nm and 674 nm, respectively, the green line is a simple average of these data. 43
31 ORAC AATSR v3.02 AOT and AAOT over the tropical northeast Atlantic, averaged from 1 June to 31 August 2007. 44
32 ORAC AATSR v3.02 AAOT over the Atlantic, averaged from 1 to 30 June August 2007. 45
33 Satellite AOT and AAOT averaged over tropical northeast Atlantic around La Parguera AERONET station compared to AOT and AAOT from this AERONET station. Data were daily averaged from 1 June –31 August 2007. 45
34 FAME-A AOT and SSA in sunglint areas averaged from 1 June to 31 August 2007 over the tropical Atlantic Ocean. 46
35 Satellite SSA over the tropical Atlantic Ocean, averaged from 1 June to 31 August 2007, compared to AERONET SSA from Dakar and Capo Verde stations. 47
36 Absorption Aerosol Optical Thickness from various retrievals, averaged from July to September 2007. All data were regridded to a $1^\circ \times 1^\circ$ global grid. All available data from this period was used. 48
37 Single scattering albedo from various retrievals, averaged from July to September 2007. All data were regridded to a $1^\circ \times 1^\circ$ global grid. All available data from this period was used. (Figure continued on next page.) 50

37 (Cont.) Single scattering albedo from various retrievals, averaged from July to September 2007. All data were regridded to a $1^\circ \times 1^\circ$ global grid. All available data from this period was used. 51
38 World maps of absorbing AOT 52
39 Maps of absorbing AOT in the southern Africa region 53
40 Scatterplots of absorbing AOT for the WORLD region 54
41 Scatterplots for the South Africa region 55
42 Zonal means of absorbing and total AOT 56
43 Bias at observational stations 57

1 INTRODUCTION

1.1 Scope

This report described the results from the Aerosol-CCI Absorbing Aerosol Round Robin Excercise, defined in the Aerosol-CCI2 GMECV proposal [*DLR*, 2012]. The absorbing aerosol properties, retrieved from several participating algorithms, are compared under different circumstances, showing their capability for the retrieval of microphysical absorption properties of aerosols using satellite measurements. The original participating teams and algorithms were defined in the proposal document. A few changes were made regarding the proposed algiorithms. From KNMI, the Absorbing Aerosol Index (AAI) from OMI and GOME-2, was proposed, and AAOT from OMI. The former data set was replaced by the Multi-sensor AAI developed at KNMI, which combines not only GOME-2 and OMI AAI, but also includes AAI from the TOMS series, SCIAMACHY and GOME-2 series. The AAOT from OMI was not available, because the aerosol height retrieval algorithm was not yet functional. The SU_AATSR v4.21 data set was tested for both SSA and AAOT as proposed. From DLR a data set called SYNAER, and from the Free University of Berlin a data set called FAME-A were specifically processed for this option. However, both data sets were delivered late in the project, and are only covered in the later sections of the report.

Next to the proposed algorithms, a number of additional data sets were included, to increase the comparison capabilities. From NASA Goddard, the OMAERUV data set was included, covering the AAOT and SSA. This data set is included throughout the report. At a later stage, the ORAC AATSR developed for Aerosol CCI, and GRASP data set, developed at the University of Lille, were also added to the project. These data sets were delivered very late in the project and were added in the later sections of the report.

Several cases are used to compare different sensitivities of the algorithm for different absorbing aerosols. The case are: dust over the Sahara, biomass burning aerosols over the Sahel, biomass burning aerosols over central south Africa, Dust over the tropical Atlantic Ocean, and global comparison of the data. In section 9, a comparison is presented of Aerosol-CCI data sets only.

1.2 References

Bond, T. C., et al., Bounding the role of black carbon in the climate system: A scientific assessment, *J. Geophys. Res.*, *118*(11), 5380–5552, 10.1002/jgrd.50171, 2013.

de Graaf, M., P. Stammes, O. Torres, and R. B. A. Koelemeijer, Absorbing Aerosol Index: Sensitivity Analysis, application to GOME and comparison with TOMS, *J. Geophys. Res.*, *110*, D01201, 10.1029/2004JD005178, 2005.

de Graaf, M., P. Stammes, and I. Aben, Temporal and spectral variation of desert dust and biomass burning aerosol scenes from 1995 – 2000 using GOME, *Atmos. Chem. Phys. Disc.*, *6*, 1321–1353, 2006.

de Leeuw, G., and T. Holzer-Popp, Algorithm theoretical basis document (atbd) synaer envisat, *Tech. rep.*, FMI/DLR, 2012.

DLR, Proposal for phase 2 of the climate change initiative (gmecv) option proposal, *Tech. rep.*, DLR, 2012.

Filipitsch, F., AATSR Aerosol Absorption Retrieval over Ocean, *Aerosol CCI*, *Aerosol_cci_AATSR_Aerosol_Absortion_VR_v1.0.pdf*(1.0), 19, 2006.

Hasekamp, O. P., and J. Landgraf, Retrieval of aerosol properties over the ocean from multispectral single-viewing-angle measurements of intensity and polarization: Retrieval approach, information content, and sensitivity study, *J. Geophys. Res.*, *110*, D20207, 10.1029/2005JD006212, 2005.

Herman, J. R., P. K. Bhartia, O. Torres, C. Hsu, C. Seftor, and E. A. Celarier, Global distributions of UV-absorbing aerosols from NIMBUS 7/TOMS data, *J. Geophys. Res.*, *102*, D14, 10.1029/96JD03680, 1997.

Kahn, R. A., and B. J. Gaitley, An analysis of global aerosol type as retrieved by misr, *Journal of Geophysical Research: Atmospheres*, *120*(9), 4248–4281, 10.1002/2015JD023322, 2015.

Kaufman, Y. J., D. Tanré, and O. Boucher, A satellite view of aerosols in the climate system, *Nature*, *419*, 215–223, 10.1038/nature01091, 2002.

Kokhanovsky, A., et al., Space-based remote sensing of atmospheric aerosols: The multi-angle spectro-polarimetric frontier, *Earth-Science Reviews*, *145*(Supplement C), 85 – 116, https://doi.org/10.1016/j.earscirev.2015.01.012, 2015.

Kokhanovsky, A. A., et al., The inter-comparison of major satellite aerosol retrieval algorithms using simulated intensity and polarization characteristics of reflected light, *Atmospheric Measurement Techniques*, *3*(4), 909–932, 10.5194/amt-3-909-2010, 2010.

North, P., A. Heckel, W. Davies, S. Bevan, and W. Grey, Algorithm theoretical basis document (atbd) instruments: Atsr-2 and aatsr algorithm: Su-atsr, *Tech. rep.*, Swansea U., Swansea, UK, 2012.

Swap, R. J., H. J. Annegarn, J. T. Suttles, M. D. King, S. Platnick, J. L. Privette, and R. J. Scholes, Africa burning: A thematic analysis of the southern african regional science initiative (safari 2000), *J. Geophys. Res.*, *108*(D13), 10.1029/2003JD003747, 2003.

Thomas, G., C. Poulsen, R. Siddans, E. Carboni, R. Grainger, and A. Povey, Algorithm theoretical basis document (atbd) aatsr optimal retrieval of aerosol and cloud (orac), *Tech. rep.*, Swansea U., Swansea, UK, 2015.

Tilstra, L. G., M. de Graaf, I. Aben, and P. Stammes, In-flight degradation correction of SCIAMACHY UV reflectances and Absorbing Aerosol Index, *J. Geophys. Res.*, *117*, D06209, 10.1029/2011JD016957, 2012.

Torres, O., P. K. Bhartia, J. R. Herman, Z. Ahmad, and J. Gleason, Derivation of aerosol properties from satellite measurements of backscattered ultraviolet radiation: Theoretical basis, *J. Geophys. Res.*, *103*, D14, 10.1029/98JD00900, 1998.

Torres, O., P. K. Bhartia, J. R. Herman, A. Sinyuk, P. Ginoux, and B. Holben, A long-term record of aerosol optical depth from TOMS observations and comparison to AERONET measurements, *J. Atmos. Sci.*, *59*(3), 398–413, 10.1175/1520-0469, 2002.

Wu, L., O. Hasekamp, B. van Diedenhoven, and B. Cairns, Aerosol retrieval from multiangle, multispectral photopolarimetric measurements: importance of spectral range and angular resolution, *Atmospheric Measurement Techniques*, *8*(6), 2625–2638, 10.5194/amt-8-2625-2015, 2015.

Wu, Y., M. de Graaf, and M. Menenti, The sensitivity of aod retrieval to aerosol type and vertical distribution over land with modis data, *Remote Sensing*, *8*(9), 10.3390/rs8090765, 2016.

Definitions of terms

AATSR	Advanced Along Track Scanning Radiometer
AERONET	AEROsol robotic NETwork
AAI	Absorbing Aerosol Index
AAOT	Aerosol Absorbing Optical Thickness
AE	Ångström exponent
AOD	Aerosol Optical Depth
AOT	Aerosol Optical Thickness
ATSR	Along Track Scanning Radiometer
CCI	Climate Change Initiative
ENVISAT	ENVIronmetal SATellite
ESA	European Space Agency
FAME-A	Freie Universität Berlin AATSR-MERIS Retrieval Algorithm-Aerosol
FU	Freie Universität
GOME	Global Ozone Monitoring Exoperiment
MERIS	Medium Resolution Imaging Spectrometer
MODIS	Moderate Resolution Imaging SpectroRadiometer
MSAAI	Multi-sensor AAI
NASA	National Aeronautics and Space Administration
OMAERUV	Aura OMI Near-UV Aerosol Data Product
OMI	Ozone Monitoring Instrument
RAZ	Relative azimuth angle
SSA	Single scattering albedo
SCIAMACHY	SCanning Imaging Absorption spectroMeter for Atmospheric CHartographY
SU_AATSR	Swansea University AATSR Retrieval Algorithm
SZA	Solar zenith angle
SYNAER	Synergetic Aerosol Retrieval Algorithm
TOA	Top Of Atmosphere
TOMS	Total Ozone Mapping Spectrometer
UV	Ultra Violet
UVAI	UV Aerosol Index
VZA	Viewing zenith angle

2 Description of the algorithms

First a brief description is given of the participating algorithms and their characteristics. Note that all products and algorithms are described a great detail in their respective ATBDs.

2.1 SU_AATSR

The SU_AATSR v4.21 dataset contains the level-2 aerosol properties products from AATSR satellite observations, which is available from 2002–2012. The data were processed by an algorithm developed at Swansea University, and are available on a global $10 \times 10\,\mathrm{km}^2$ scale. The main relevant products that are available are AOT at 550, 670, 870 and 1600 nm plus uncertainties, single scattering albedo (SSA) at 550 nm, a fine mode AOT at 550 nm, a dust AOT at 550 nm, and absorbing AOT (AAOT) at 550 nm, derived from retrieved total AOT and fine mode AOT, and one (Ångström exponent AE) valid for 550–870 nm.

The algorithm is described in [*North et al.*, 2012]. It is based on Lookup Tables generated by forward calculations of atmospheric properties by a radiative transfer model for a range of surface and atmospheric conditions. These lookup tables are the basis for aerosol retrievals and surface reflectance over land. The lookup table consists of the geometric, atmospheric and surface parameters. They provide modeled TOA reflectances depending on 6 dimensions: solar zenith angle (SZA), relative azimuth angle, view zenith angle (VZA), Lambertian surface albedo, AOD and surface pressure.

The table is calculated at 13 MERIS and 4 AATSR spectral channels. Aerosol optical properties (AOD, Angstrom, single scattering albedo and phase functions) are defined by up to 40 predefined aerosol models. Channels with strong absorption bands (i.e. MERIS channel 11 and 15) are excluded to avoid interference from oxygen and water vapor absorption. The remaining weaker water vapor absorption in other bands and the absorption by ozone can be decoupled and are not included in the lookup table. A total of 680 tables are computed in this way.

The data are available online, from 2002–2012 with daily global coverage.

2.2 FAME-A

At FU Berlin a new innovative algorithm called FAME-A quantifies aerosol absorption over the ocean in sunglint contaminated regions from Advanced Along Track Scanning Radiometer (AATSR) Top Of Atmosphere (TOA) radiation measurements. The method is described in detail by *Filipitsch* [2006]: The FAME-A algorithm retrieve the SSA and AOD on a pixel by pixel passes. A criteria of the retrieval is that one of the two AATSR view is brightened by sunglint contamination. Aerosol scattering increase the reflection in the off glint view and lowers the reflection in the glint region. An absorbing aerosol leads also to a decrease on the observed reflection within the glint in the off glint region is the increase due to the aerosol layer much lower. The sunglint is manly a function of wind speed and viewing geometry. The altering sun position leads to a continuously change in the viewing geometry on a yearly cycle [*Filipitsch*, 2006]. In these areas the single scattering albedo (SSA) and Aerosol Optical Thickness (AOT) can be retrieved, as described by [*Kaufman et al.*, 2002].

For the current project FAME-A data were available from 1 June to 31 August 2007.

2.3 SYNAER

At DLR an algorithm is available called Synergetic Aerosol Retrieval Algorithm (SYNAER) applied to AATSR and SCIAMACHY onboard ENVISAT [*de Leeuw and Holzer-Popp*, 2012].

SYNAER exploits a combination of two instruments with complementary information content due to their respective spatial and spectral resolution and coverage. Through the combined information of both sensors SYNAER retrieves multi-spectral aerosol optical thickness (AOT) and an estimation of the aerosol type provided as choice of an aerosol type from a pre-defined representative set of typical atmospheric aerosol mixtures of four basic atmospheric

aerosol components agreed upon in Aerosol_cci: fine mode weakly absorbing and strongly absorbing, mineral dust and sea salt. SYNAER uses the four Aerosol_cci components to compare 36 pre-defined mixtures with the nadir measurements and tries to fit (with discrete steps) the 3 mixing fractions (coarse/fine, within fine: weak/strong absorbing, within coarse: dust/salt). From the selected mixture absorption can be calculated (AAOT and SSA).

For the current project SYNAER data were available from November 2005 until September 2006, and June to September 2007. Obviously, since two instruments have to be combined, the global coverage is less than for one instruments. Therefore, data have to averaged over a larger period than e.g. the AATSR data.

2.4 OMAERUV

The OMAERUV algorithm derives the aerosol index (AI), aerosol absorption optical thickness (AAOT) and the aerosol single scattering albedo (ASSA) from the OMI instrument on Aqua, based on the TOMS UV algorithm [*Torres et al.*, 2002]. This algorithm uses two wavelength bands in the near UV (at 360 and 380 nm), and has been shown to be a robust product.

The spectral aerosol absorption optical thickness (AAOT) is derived from the wavelength dependence of the radiances measured by OMI (at the 360 and 380 nm bands) and contains information on the aerosol concentration and on the size of the aerosol particles. Quantitative estimates of AAOT can be made only in relatively cloud-free scenes.

The aerosol single scattering albedo is derived at a wavelength of 380 nm and is related to the absorbing properties; different values indicate that the aerosols originate from different sources. The aerosol single scattering albedo is available as a research product.

The data are available at the native OMI resolution of 13 km $\times$ 24 km at nadir, to about 126 km $\times$ 42 km at the far off-nadir (56°). The OMI instrument has daily global coverage and data are available online from 2004 to the present day.

2.5 Multi-sensor AAI

The Multi-Sensor AAI (MS-AAI) data record consists of AAI data from the TOMS, GOME-1, SCIAMACHY, OMI, GOME-2A and GOME-2B instruments. The dataset covers the period 1978–2017. The AAI is a very robust parameter, which has been retrieved from UV-spectrometers for several decades [*Herman et al.*, 1997; *Torres et al.*, 2002; *de Graaf et al.*, 2006]. It is a measure of radiation changes in the UV, e.g. due to ozone and absorbing aerosols, and can be used qualitatively to detect elevated absorbing aerosols in the atmosphere. It is very sensitive to radiometric offsets, and can as such be used to monitor and correct instrumental drifts and degradation [*Tilstra et al.*, 2012]. The multi-sensor AAI combines data from many spectro(radio)meters, that have flown successively in the last 30 years, cleverly compensating for degradation errors and inter-instrumental offsets.

The MS-AAI is a radiation measurement, but has been shown to be almost exclusively sensitive to absorbing aerosols, when ozone absorption, surface elevation, and polarization are properly taken into account. It has to be screened for sunglint and solar eclipses, but is equally valid over both land and sea surfaces and almost insensitive to underlying clouds.

The data are available online from 1978–2017 as daily gridded level 3 data at a $1^\circ \times 1^\circ$ resolution.

2.6 GRASP

General Retrieval of Aerosol and Surface Properties (GRASP) is an open source, highly accurate aerosol retrieval algorithm that processes properties of aerosol- and land-surface-reflectance. It infers nearly 50 aerosol and surface parameters including particle size distribution, the spectral index of refraction, the degree of sphericity and absorption. The algorithm is designed for the enhanced characterization of aerosol properties from spectral, multi-angular polarimetric remote sensing observations. GRASP works under different conditions, including bright

surfaces such as deserts, where the reflectance overwhelms the signal of aerosols. GRASP is highly versatile and allows input from a wide variety of satellite and surface measurements. Documentation for the open source code is available on-line: *https://www.grasp-open.com/doc/*

For CCI, PARASOL data were processed for 2005-2013 for 4 selected zones (1200x1200 km zones, centered at Banizoumbou, Mongu, Kanpur, and Beijing AERONET stations).

2.7 ORAC AATSR

Optimal Retrieval of Aerosol and Cloud (ORAC) is a dual-view aerosol retrieval scheme for use over both land and ocean surfaces. Applied to Advanced Along Track Scanning Radiometer (AATSR) measurements in the aerosol_cci project, ORAC retrieves both aerosol optical depth and effective radius, as well as the surface reflectance at each of the four AATSR short-wave channels, using a mixture of pre-defined aerosol components. The algorithm has also been shown to have limited skill at selecting aerosol type from a range of possibilities (represented by differing mixtures of aerosol components). ORAC is built around the optimal-estimation retrieval formalism, and thus provides full uncertainty propagation (from estimates of measurement noise, forward model uncertainty and *a priori* constraint), the ability to apply *a priori* constraints in a mathematically rigorous and consistent way, and extensive retrieval statistics and diagnostics [*Thomas et al.*, 2015].

Global ORAC v3.02 data are available on the Aerosol-CCI website, data from 1 June to 31 August 2007 were used in this project.

3 Mineral dust over the Sahara

The northern part of Africa is prone to dust events, especially in boreal summer, when the sun is overhead. During strong wind gusts, the atmosphere is typically loaded with mineral dust aerosols, especially from strong local sources like the Bodélé depression in Chad and generally in the entire Sahara desert. Desert dust is an absorbing aerosol, absorbing radiation in both the shortwave and longwave spectral ranges. The CCI absorbing aerosol products will be compared using the strong signals over the Sahara desert region.

3.1 Aerosol Optical Thickness over the Sahara

Before showing the absorbing quantities of the aerosol products, first an overview is given of the aerosol loading in general and the AOT of the various products. The AOT is a base product for aerosol retrievals, which can be used to quantitatively compare retrievals from different instruments, before introducing complexities from different retrieval methods, which are needed to derive the absorbing properties of aerosols. An overview of the average AOT over the Sahara region from July to August 2006 is introduced first, to show the mineral dust loading derived by various instruments and methods.

The AOT derived over the Sahara from SU_AATSR and OMAERUV data, averaged from 1 July – 31 August 2006, is shown in Figure 1. Note that the AOT from AATRS is derived at 550 nm, while the AOT form OMAERUV is derived at 500 nm. In order to compare the data sets and average the data over a longer period, all the data points were regridded to a regular grid of $0.25° \times 0.25°$. Generally, the SU_AATSR and OMAERUV AOT are in the same range (bearing in mind the wavelength difference). The spatial patterns look different for both instruments, indicating little agreement between the two. SU_AATSR AOT shows a strong land-sea contrast. OMAERUV AOT shows more continuity over coastlines, but suffers from much lower coverage over the ocean, resulting in s striped pattern due to low sampling during the selected period. The surface albedo may have a strong influence on the retrieved parameters. The highest AOT values coincide with strong local dust source regions, but if the surface albedo is dominant in the retrieval, the attribution of dust sources from satellite measurements must be treated with caution.

The AOT averaged over the Sahara region from 1 July – 31 August 2006 is shown in Figure 2, for all available wavelengths. In general, the OMAERUV shows much higher values, with local extreme values to more than 2.0, and no low values, while SU_AATSR shows moderate values between 0.0 and 1.0 or slightly above. This is in contrast to the spatial patterns in Figure 1, which showed higher values for SU_AATSR compared to OMAERUV. It is obvious that the correlation between the two products is low, and there is low confidence in the comparison between derived products.

To determine a further confidence in the AOT products, they are compared to AOT measurements from AERONET,

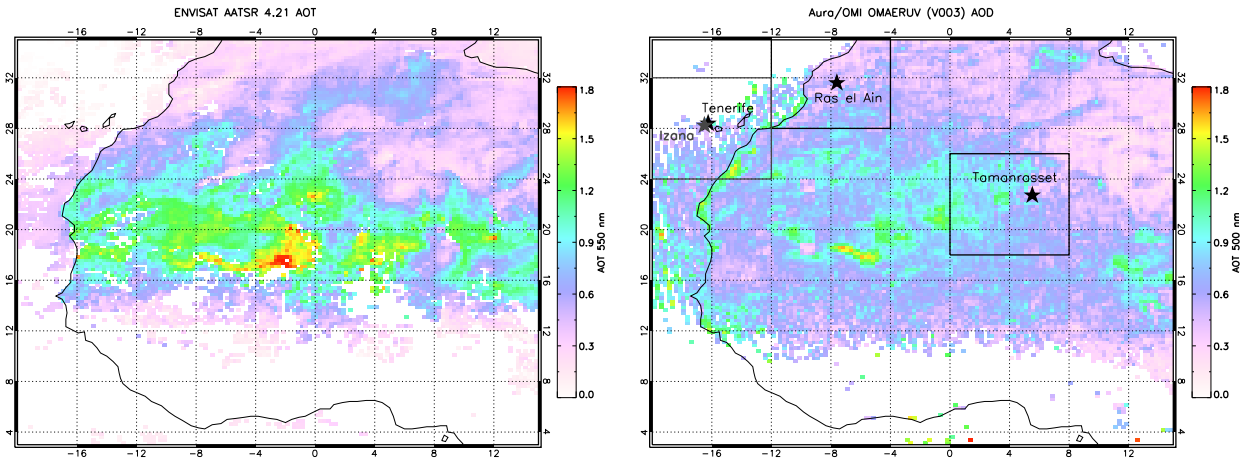

Figure 1: SU_AATSR and OMAERUV AOT averaged from 1 July - 31 August 2006.

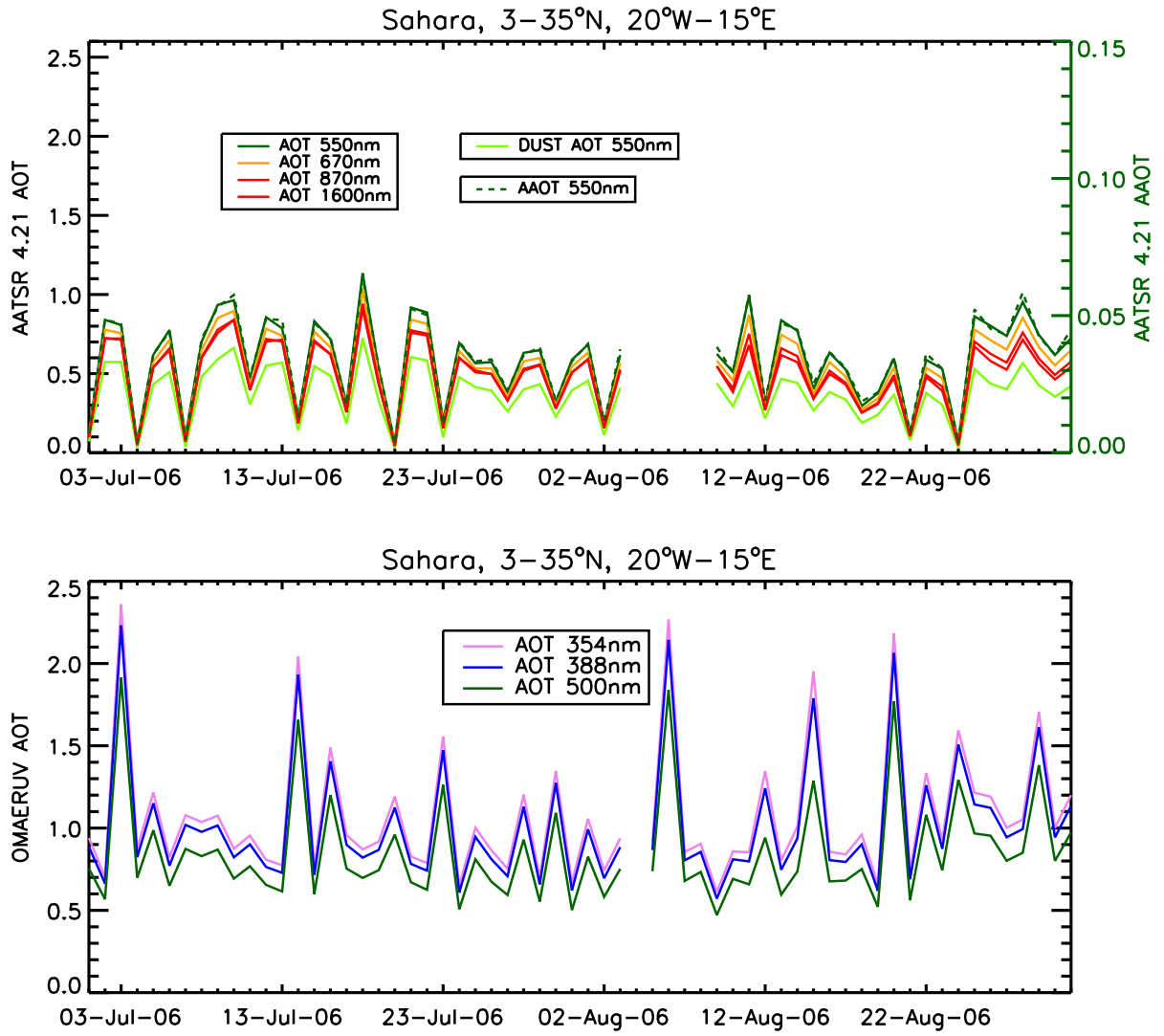

Figure 2: SU_AATSR and OMAERUV AOT from 1 July - 31 August 2006 averaged over the area shown in Figure 1.

which are spatial point measurements, but well calibrated and highly accurate since they are measured from the ground up and therefore are not sensitive to surface albedo uncertainties. Four AERONET stations were selected in the Sahara desert and its outflow region, indicated by stars in the right panel of Figure 1. The AOT averaged over the Sahara desert as a whole has little correlation to the AOT measurements of the AERONET stations around the desert, therefore a further refinement was made. Satellite data were averaged over smaller areas around the stations, as indicated by the rectangular boxes in the right panel of Figure 1. The averaging areas were a trade-off between the satellite data availability and the correlation between the averaged satellite data and the point source data from AERONET. For OMAERUV AOT the boxes were used as shown in Figure 1, while for SU_AATSR the boxes were increased by three degrees in all directions. Smaller boxes did not yield enough data points. The time series of the AOT measured by three of the AERONET stations (Tenerife is not shown, as it is comparable to Izana) for all available data from 1 July – 31 August 2006 is shown in the top panels of Figures 3 to 5. The middle panels show the times series of the OMAERUV AOT averaged over the boxes around the various stations, while the bottom panel show the same for the SU_AATSR AOT satellite derived data.

The area-averaged OMAERUV AOT shows some agreement with the AOT from various stations. Especially for station Ras el Ain the locations (occurrences) of the peak AOT correspond to peaks in the OMAERUV AOT. For

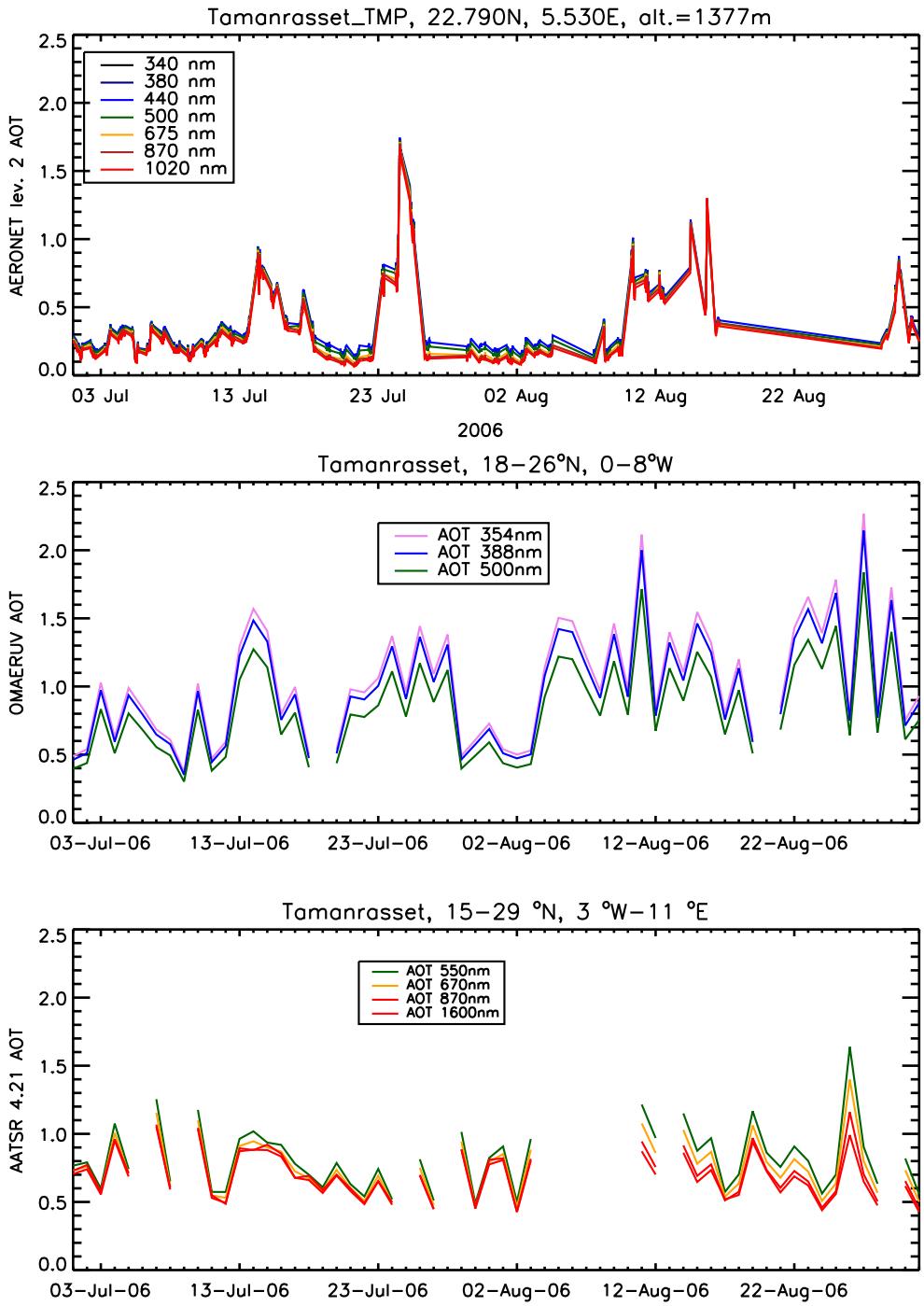

Figure 3: AOT at AERONET station Tammanrasset, OMAERUV AOT and SU_AATSR AOT around that station, from 1 July - 31 August 2006.

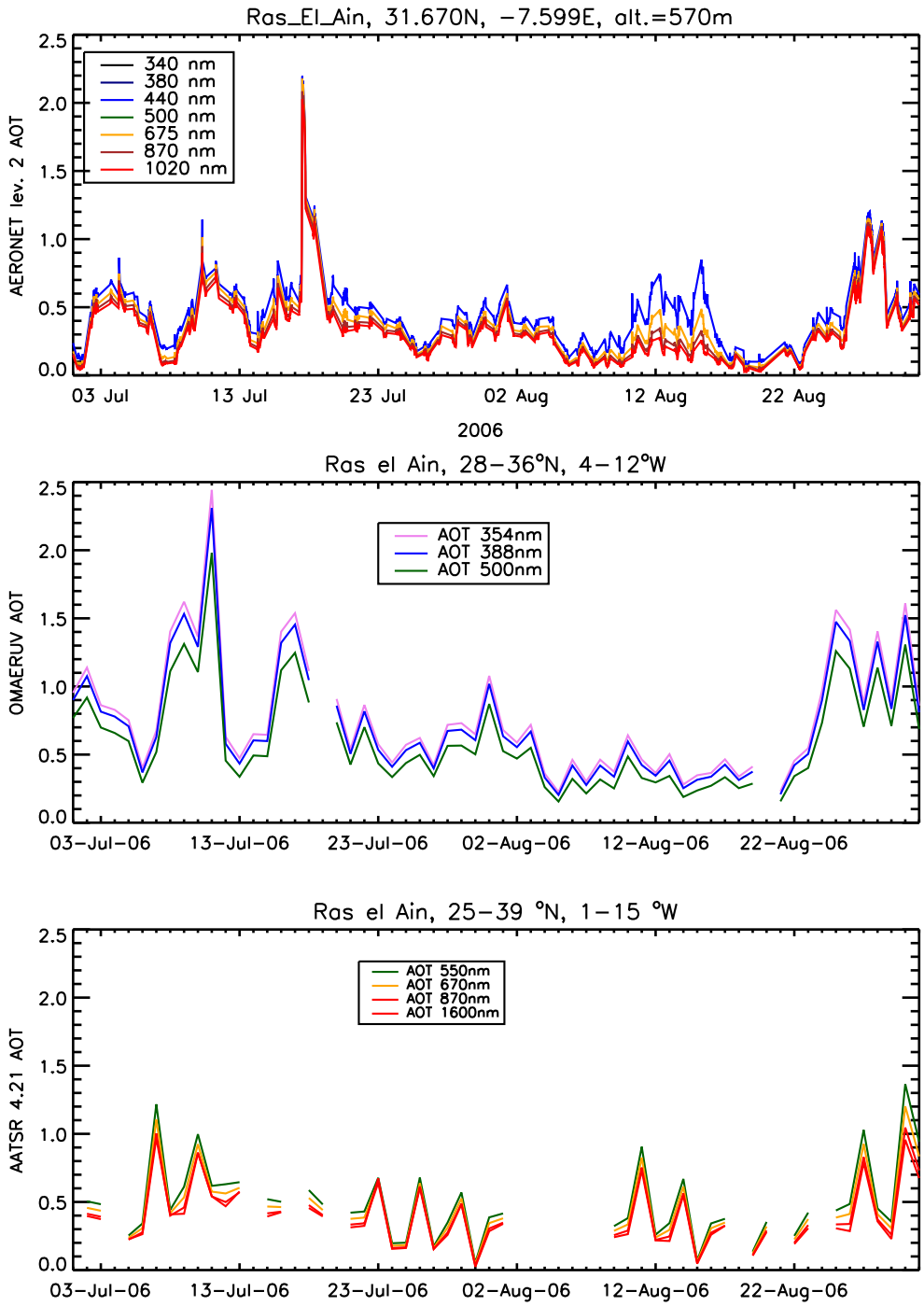

Figure 4: AOT at AERONET station Ras el Ain, OMAERUV AOT and SU_AATSR AOT around that station, from 1 July - 31 August 2006.

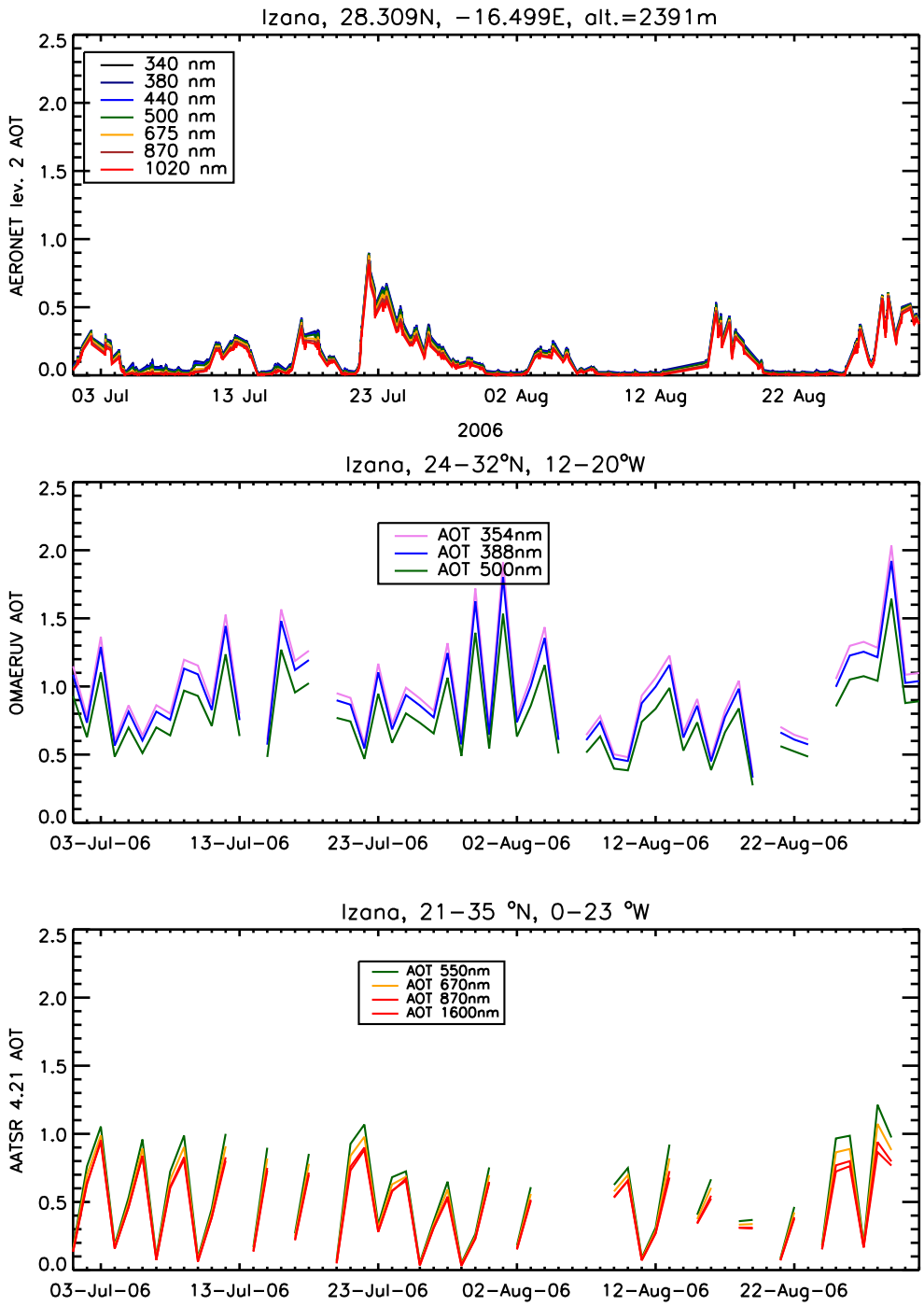

Figure 5: AOT at AERONET station Izana, OMAERUV AOT and SU_AATSR AOT around that station, from 1 July - 31 August 2006.

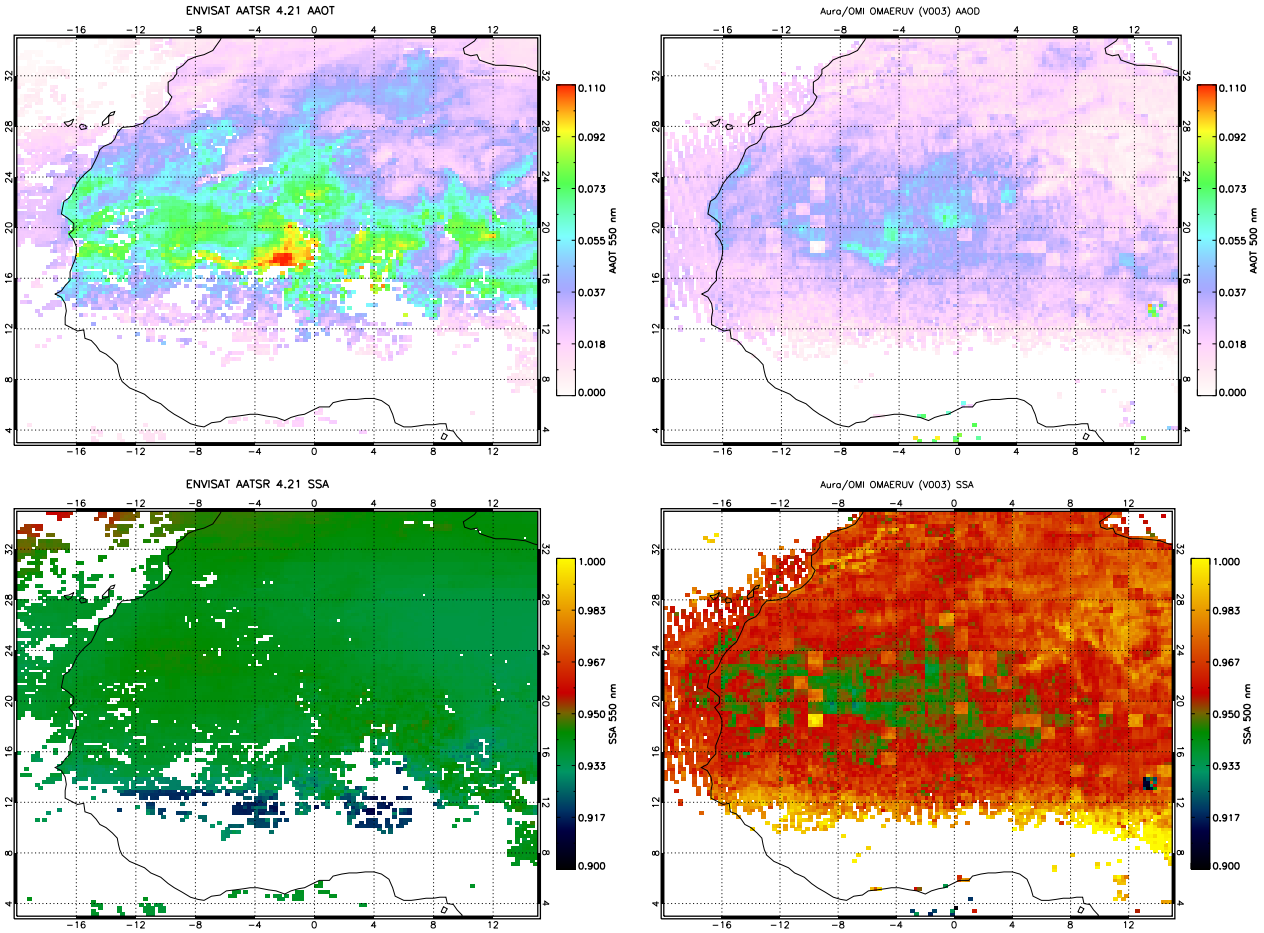

Figure 6: AAOT (top panels) from SU_AATSR (left) and OMAERUV (right) and SSA (lower panels) averaged from 1 July – 31 August 2006.

SU_AATSR the correlation is much lower, partly because of the larger averaging areas that had to be used. In general, the correlation between the AOT from SU_AATSR and AERONET is very low. The absolute AOT values derived from satellite and AERONET are quite different, but what is most striking is that the wavelength dependence of the satellite AOT product is much larger than that from AERONET. The difference in OMAERUV AOT between 354 nm and 500 nm is generally between 0.2 – 0.3, and the difference in SU_AATSR AOT between 550 nm and 1600 nm is around 0.2 – 0.4. In contrast, the difference of AERONET AOT between 440 nm and 1020 nm is never more than about 0.15. The wavelength dependence of the AOT is an important parameter for the absorbing properties of the aerosols. The large wavelength dependence in the satellite products indicate strong (assumed) absorption properties.

3.2 Absorbing aerosol optical thickness and single scattering albedo

The absorbing properties of mineral dust can be expressed in various ways, here we show the absorbing aerosol optical thickness (AAOT), which is the absorbing part of the AOT (in general a few procent) and the SSA, which is 1 minus the absorbing fraction of the total attenuation.

Figure 6 shows the spatial distribution of the AAOT and SSA over the Sahara averaged from 1 July – 31 August 2006 from SU_AATSR and OMAERUV. As expected the AAOT shows mostly the same distribution as the AOT in Figure 1, since it is largely determined by the AOT distribution as the absorption is a small part of the AOT. The differences are mostly caused by the treatment of the aerosol type (and hence SSA), which is shown in the bottom

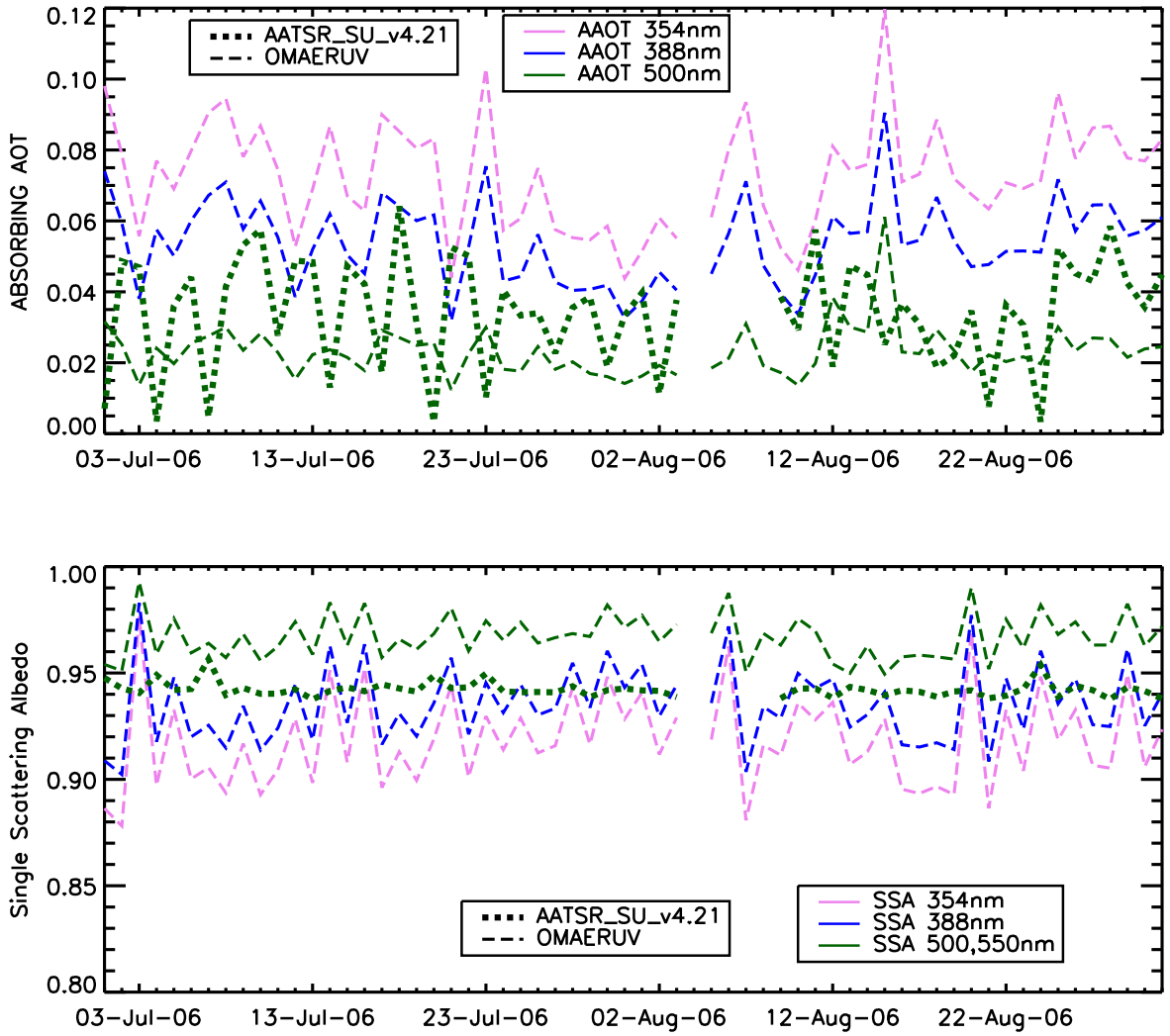

Figure 7: SU_AATSR AAOT at 550 nm, OMAERUV AAOT at 354 nm, 388 nm, and 500 nm, SU_AATSR SSA (550 nm) and OMAERUV SSA (354, 388, and 500 nm) from 1 July – 31 August 2006 averaged over the area shown in Figure 6.

panels of Figure 6. As these images show, the SSA from both algorithms is very different. The SU_AATSR SSA shows gradients in the east-west and north-south direction that are opposite to the OMAERUV gradients. Furthermore, the variation in SU_AATSR SSA is low, especially over the Sahara only, while the OMAERUV SSA shows much larger variations, from 0.9 to 1.00 over the Sahara region.

Figure 7 shows the AAOT and SSA from SU_AATSR and OMAERUV from 1 July – 31 August 2006 averaged over the area shown in Figure 6. As expected from the discussion above, the temporal behavior of all products is very different and the products are not correlated. The SU_AATSR AAOT shows a large range from about 0.0 to 0.08, while the OMAERUV AAOT (500 nm) shows a much smaller range from about 0.01 to 0.04 in general and one high value of 0.06 in August. In contrast, the SU_AATSR SSA shows a very small variation between 0.94 – 0.95, while the OMAERUV SSA (550 nm) ranges between 0.95 and 0.99. Next to a large difference in derived AOT, this indicates different assumptions on the aerosol mineral properties in the derivations.

To confirm the lack of correlation, scatterplots are shown in Figure 8 of the SU_AATSR versus OMAERUV AAOT and SSA. The data points are all the regridded data in the area shown in Figure 6 between 1 July and 31 August

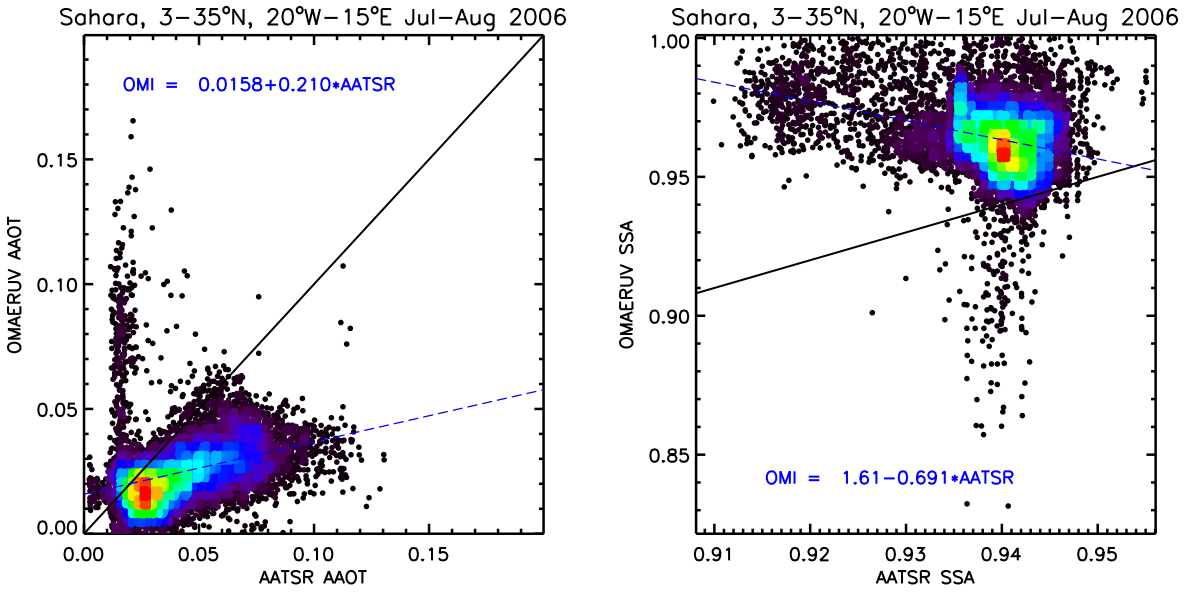

Figure 8: SU_AATSR versus OMAERUV AAOT and SSA for all regridded data over the Sahara region shown in Figure 1 and the period shown in Figure 7.

2006, filtered for AOT$>$ 0.2. The solid lines show the one-to-one line and the dashed line the linear least squares fit the data. As shown before, the correlation between the data sets is minimal. Also, the SU_AATSR data show a preference for SSA around 0.94 and AAOT around 0.02.

3.3 AERONET AAOT and SSA

In order to validate the satellite retrievals of Absorbing Aerosol Optical Thickness and Single Scattering Albedo, the satellite data were compared with AERONET data of AAOT and SSA. The results are shown in Figure 9 and 10. The top panels show the results from the AERONET station Tamanrasset, the middle panels show the results from station Ras El Ain and the bottom panels show Izana. The same averaging areas were used for the satellite products as for figures 3-5.

The results from the AERONET stations are sparse, but the available data shows that the AAOT from OMAERUV matches the AAOT from AERONET reasonably well. The amplitude of the AAOT variation is generally larger for OMAERUV than AERONET, but coincides well considering the different sampling of the satellite and ground-based data. Also the AAOT from SU_AATSR seems to be in the correct range.

An interesting event happened around Ras El Ain during the middle of August 2006, which is captured in the AERONET and OMAERUV data. It is clearer in the SSA data, shown in Figure 10. Generally, the SSA from OMAERUV is high compared to AERONET. The SU_AATSR SSA is in the same range as AERONET, but lacks temporal variation. During August around Ras El Ain (middle panel) the AERONET SSA drops sharply and the wavelength dependence is reversed compared to the other days. This means that all three stations are dust dominated during the period shown (SSA increases with wavelength), but station Ras El Ain may have experienced a non-dust dominated episode, like strong biomass burning, during August 2006. The drop in SSA is not replicated in the SU_AATSR data, while the OMAERUV data shows an increase in SSA and no reverse of wavelength dependence. This points to an attribution to scattering aerosols in the OMAERUV data, like e.g. marine aerosols, rather than absorbing aerosols.

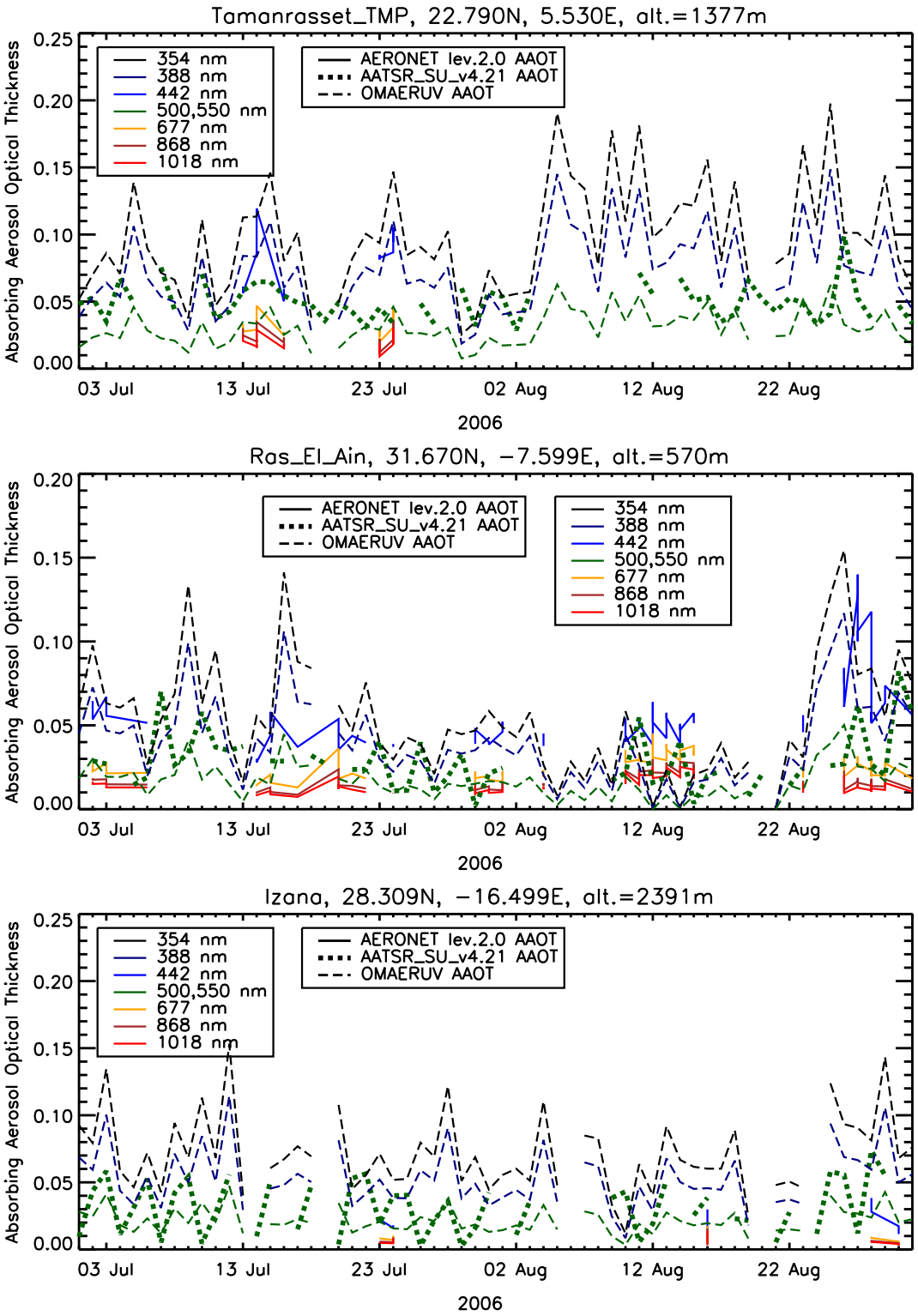

Figure 9: Absorbing Aerosol Optical Thickness from 1 July – 31 August 2006 from AERONET, SU_AATSR and OMAERUV around station (a) Tamanrasset, (b) Ras El Ain, and (c) Izana. The satellite data were averaged over the same areas as in Figures 3-5

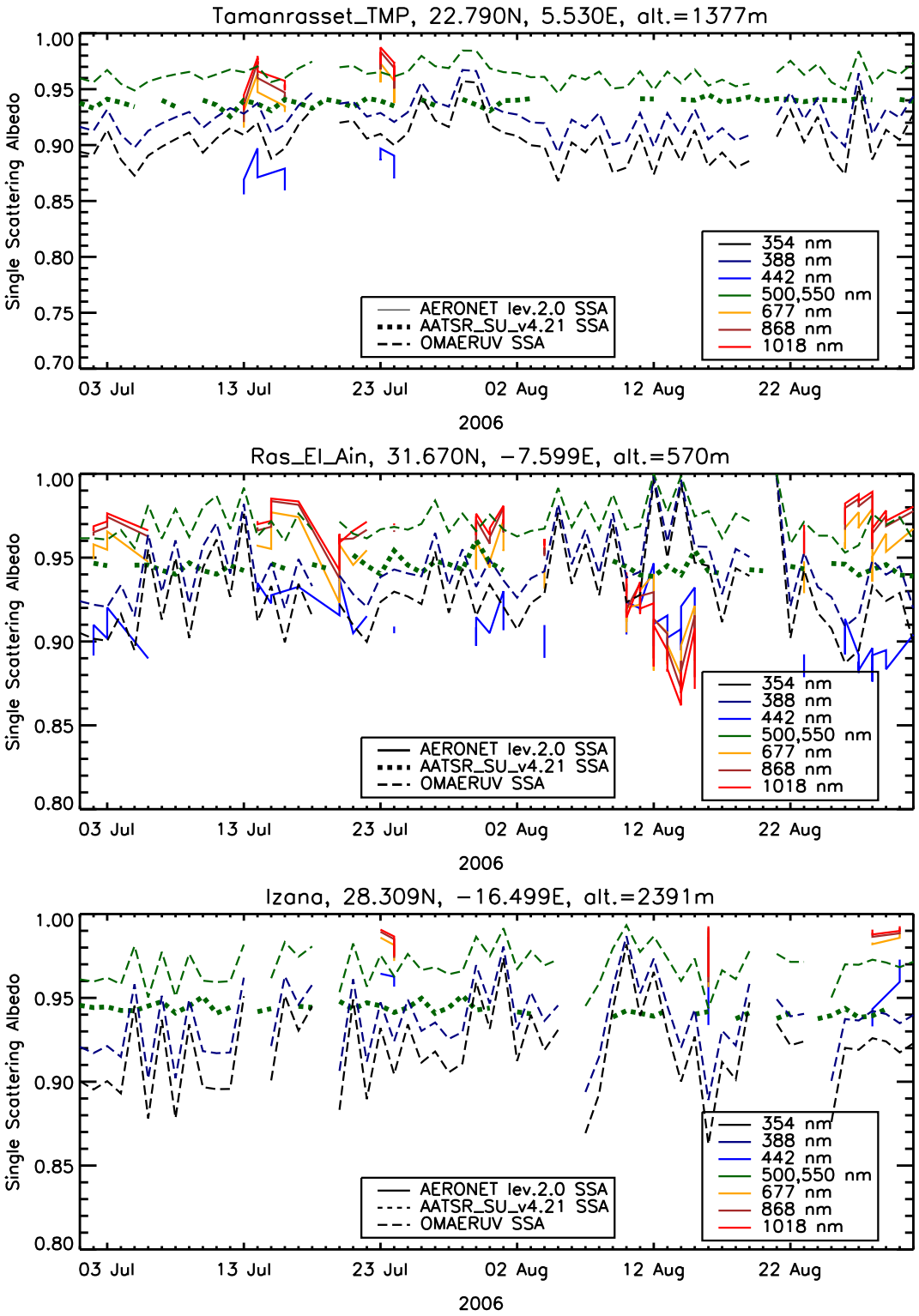

Figure 10: Single scattering albedo from 1 July – 31 August 2006 from AERONET, SU_AATSR and OMAERUV around station (a) Tamanrasset, (b) Ras El Ain, and (c) Izana. The satellite data were averaged over the same areas as in Figures 3-5

4 Biomass burning aerosols over the Sahel region

The tropical region of Africa experiences two dry and two wet seasons per year, as the sun moves overhead during the spring and autumn. Consequently, the Sahel region, in northern tropical Africa, is densely vegetated due to the abundance of water during the wet seasons, while the vegetation will burn during the dry period. The abundance of fuel produces huge amounts of biomass burning aerosols, or smoke, during vegetation fires. Smoke is an absorbing aerosol, due to the presence of black carbon and organic carbon. The amount of absorption and the wavelength dependence of the absorption (Ångström exponent AE) is determined by many factors, including the type of combustion (flaming versus smoldering, determining the black versus organic carbon fraction), chemical and physical aging of the smoke, water uptake, etc. In Africa smoke contains large fractions of organic carbon, due to many smoldering fires, contrary to industrial pollution, which often contains larger fractions of black carbon due to the highly optimized combustion processes in engines. Although black carbon is generally much more light absorbing than organic carbon, organic carbon has a very strong wavelength dependence in its light absorption properties. absorbing mainly in the UV. Furthermore, smoke generally consists of small particles, making it an efficient UV-absorbing aerosol.

The Sahel region is also prone to dust incursions. Both to the north and to the south, desert areas produce mineral dust aerosols, that are transported over large distances. Much of the aerosols found over the Sahel region is a mixture of local (and transported) smoke, transported mineral dust aerosols and marine aerosols from the nearby Atlantic Ocean.

4.1 Aerosol Optical Thickness over the Sahel

The aerosol loading over the Sahel region as derived by SU_AATSR and OMAERUV is given in Figure 11 averaged from 1 November 2005 to 28 February 2006, covering one dry season. In the figure SU_AATSR data is shown on the left, while OMAERUV data is shown on the right. The relationship between the two is low, but both show an increased AOT in the coastal regions.

In order to understand the correlation that can be expected between the two data sets, again temporal changes are compared of the AOT averaged over the Sahel region depicted in Figure 11, from 1 November 2005 – 28 February 2006. In Figure 12 the SU_AATSR and OMAERUV AOT are compared. Similarly Figure 11, it shows that SU_AATSR AOT is smaller than OMAERUV, between 0.0 – 0.8 for SU_AATSR, versus around 1.0, which peaks up to larger than 2.0 for OMAERUV AOT (500 nm). This signals again a low correlation between the data sets.

A more detailed analysis of the AOT is presented in Figures 13 – 15. The satellite AOT is compared to AERONET

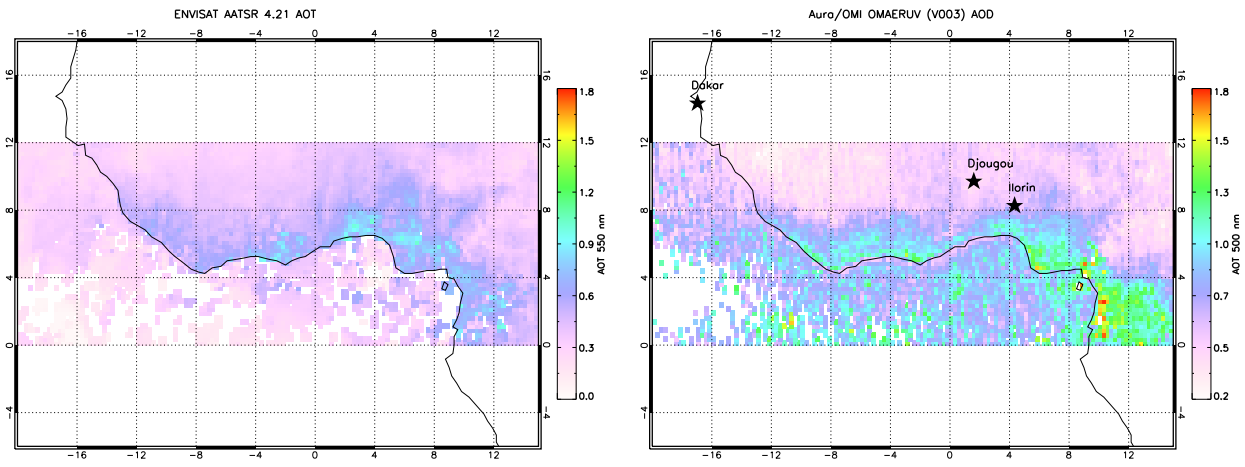

Figure 11: AOT derived from SU_AATSR (left) and OMAERUV (right) data, averaged from 1 November 2005 – 28 February 2006.

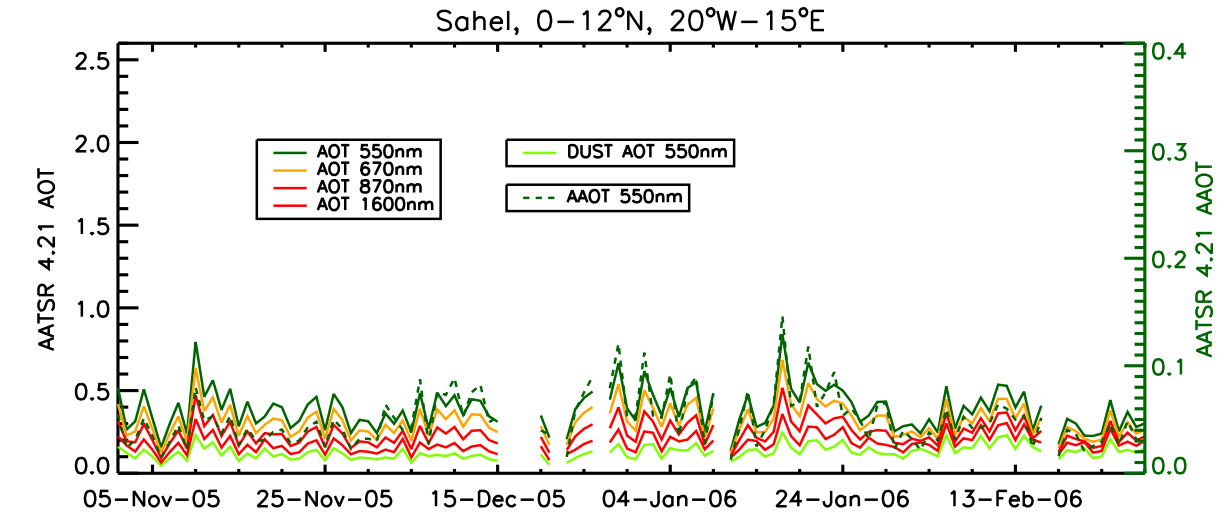

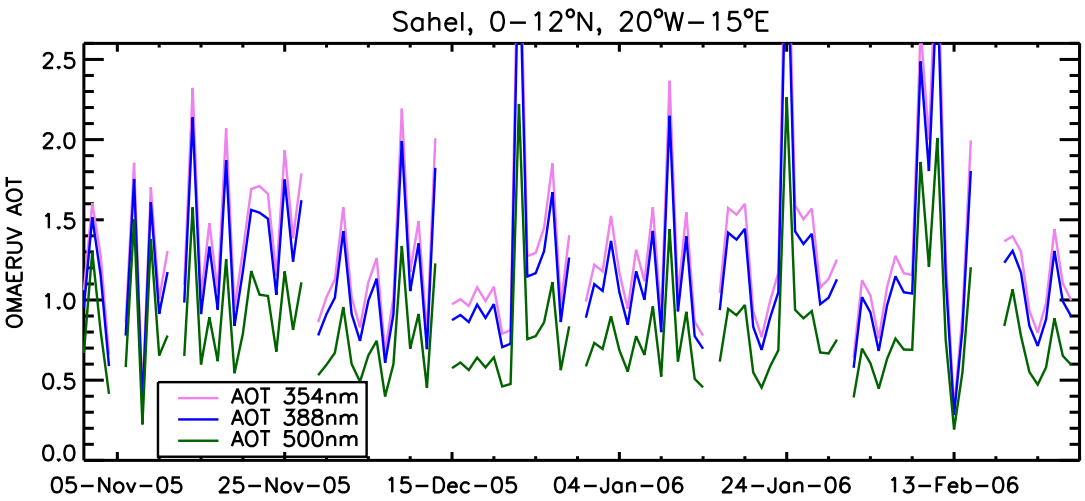

.

Figure 12: SU_AATSR and OMAERUV AOT from 1 November 2005 – 28 February 2006 averaged over the area shown in Figure 11.

AOT, using a selected area around the AERONET station to average the satellite data. Again, the selected area was larger for SU_AATSR, in order to have enough data points. The used areas are given in the plot titles. The correlation between OMAERUV AOT and the AOT from Ilorin (Figure 13) and Djougou (Figure 14) shows peaks in the AOT occurring at the same instances and absolute values of the AOT in the same range for both (compare 500 nm). The wavelength dependence of the AOT is also similar, the range between $380 - 500$ nm AERONET AOT being about $0.3 - 0.7$ at Ilorin, while the $388 - 500$ nm OMAERUV AOT is about $0.4 - 0.8$. The wavelength dependence of the SU_AATSR AOT is somewhat smaller than that from AERONET from $500 - 870$ nm, but reasonable. However, the temporal behavior of the SU_AATSR AOT is different from that for the AERONET station, probably because the larger averaging areas needed diminish the correlation.

For Dakar (Figure 15) no correlation can be found.

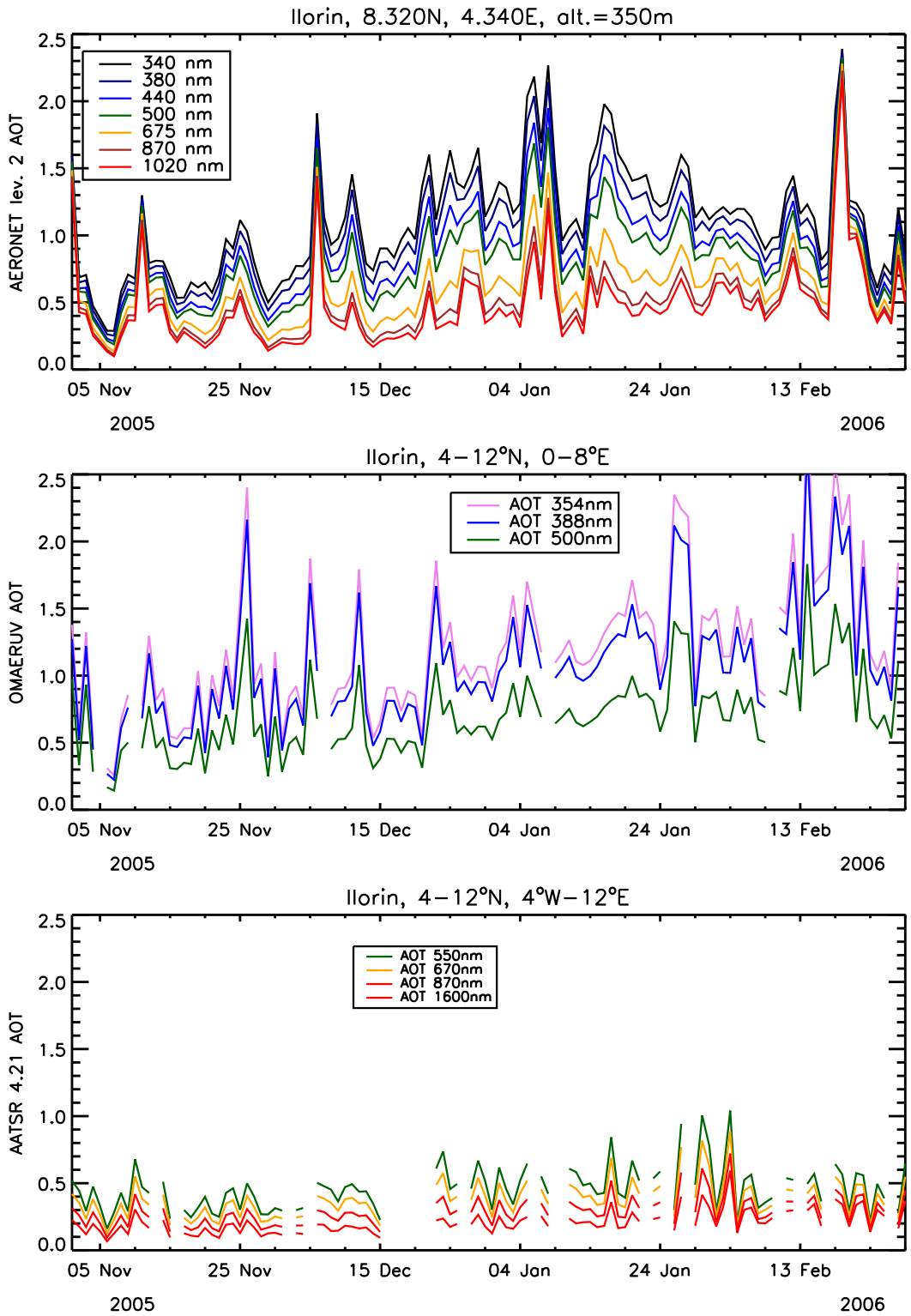

Figure 13: AOT at AERONET station Ilorin, OMAERUV AOT and SU_AATSR AOT around that station, from 1 November 2005 – 28 February 2006.

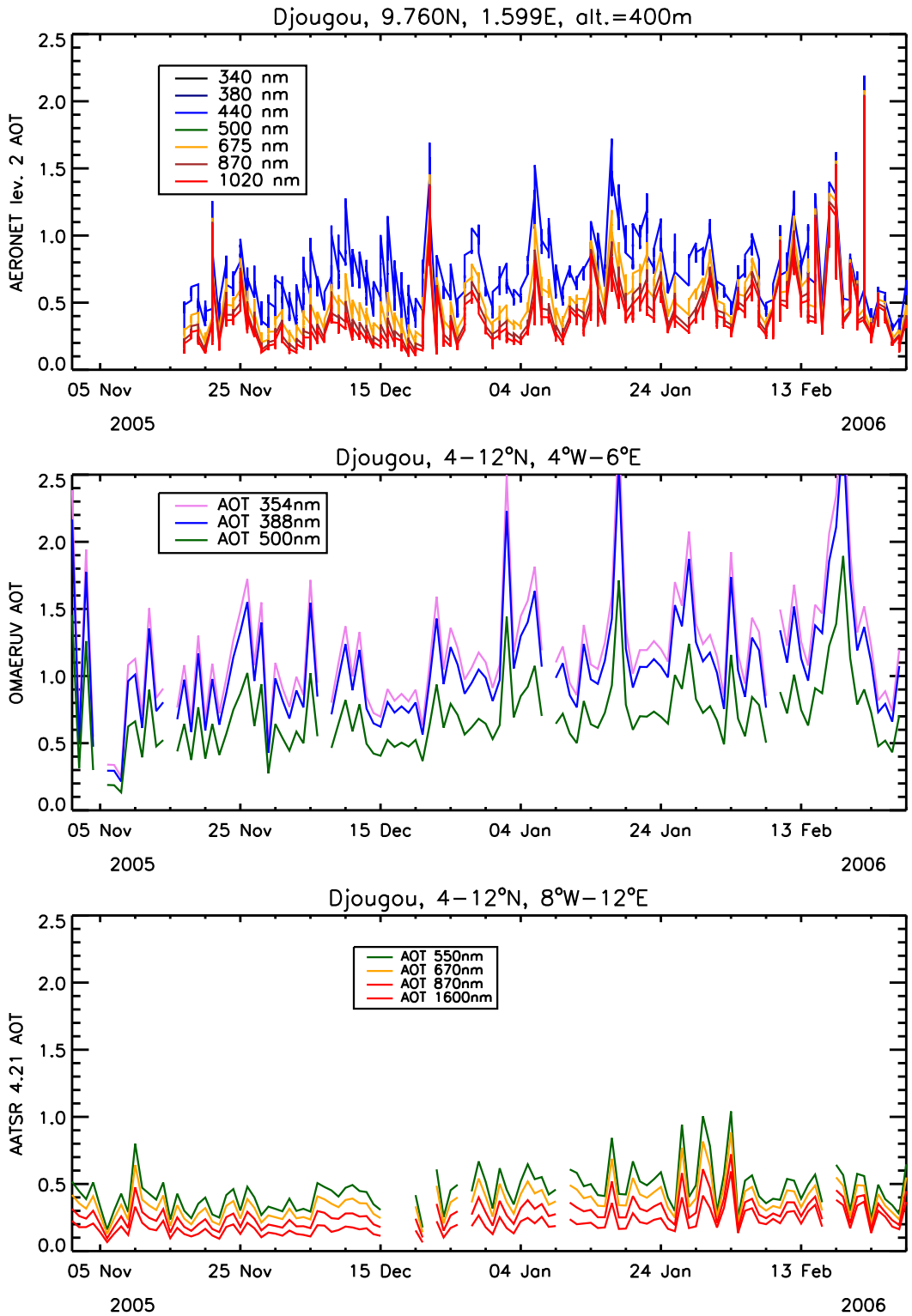

Figure 14: AOT at AERONET station Djougou, OMAERUV AOT and SU_AATSR AOT around that station, from 1 November 2005 – 28 February 2006.

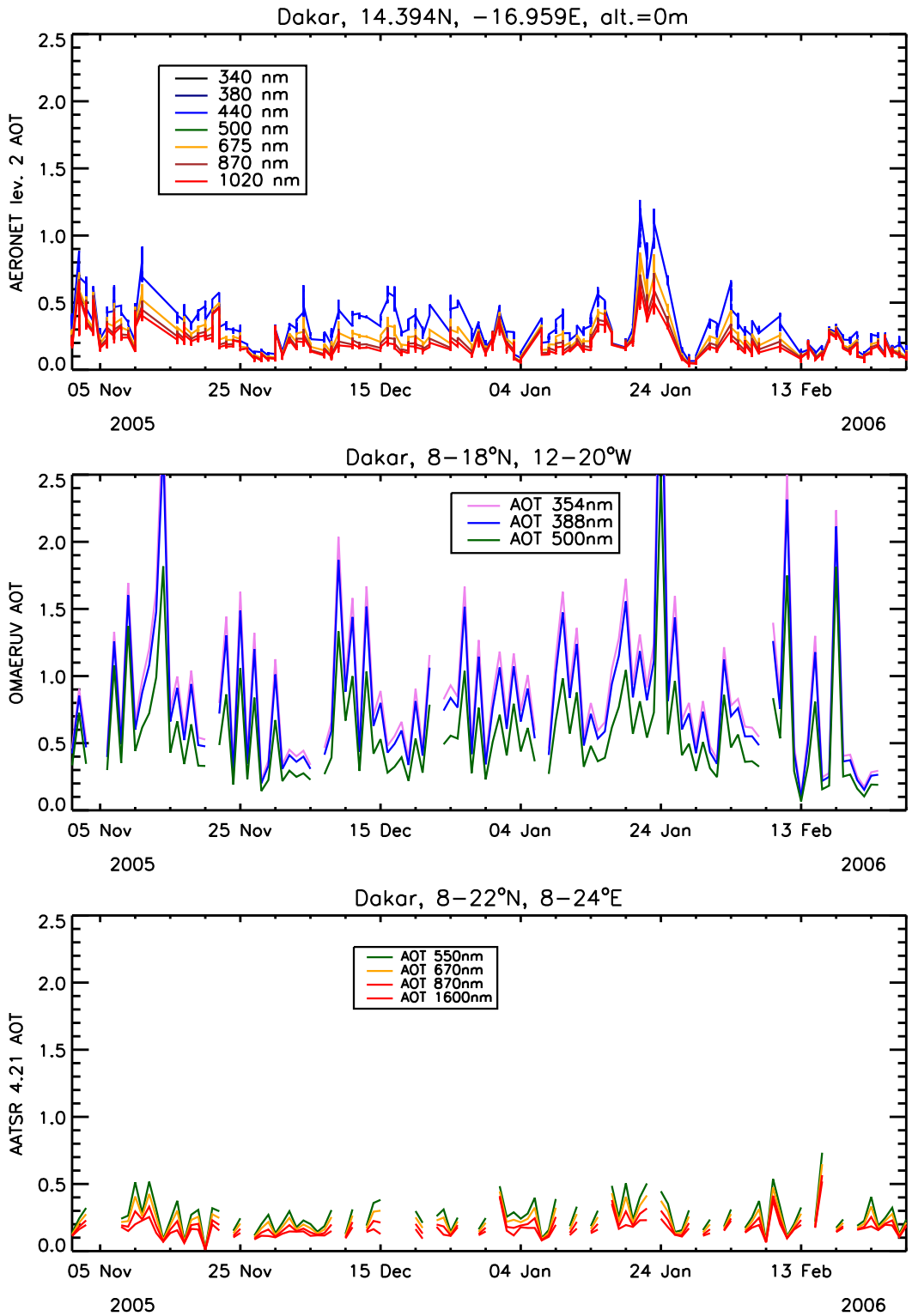

Figure 15: AOT at AERONET station Dakar, OMAERUV AOT and SU_AATSR AOT around that station, from 1 November 2005 – 28 February 2006.

4.2 Absorbing aerosol optical thickness and single scattering albedo

The Aborbing Aerosol Optical Thickness from both satellite instruments is shown in the top panels of Figure 16. The patterns look similar to the AOT patters of the respective instruments, especially for SU_AATSR, which can be explained by the small variation in absorbing properties of the aerosols over the region. The strong land-sea contrast for SU_AATSR, apparent in the AOT, becomes even more prominent in the AAOT. The SSA from both instruments (lower panels) seems to relate fairly well over land, but over the ocean the behavior of both is very different. This may again be due to sampling issues, as the ocean is often covered by clouds in this area. OMAERUV SSA over the ocean is clearly affected by under-sampling, while the SU_AATSR SSA is still very smooth over the ocean. For the Sahel region, the range in SSA values in is much closer agreement than it was for the Sahara.

The temporal variation of the absorbing aerosol optical thickness and single scattering albedo averaged over the Sahel region 1 November 2005 – 28 February 2006 is given in Figure 17. As expected, the time series look very different, and the ranges differ. The SU_AATSR (500 nm) and OMAERUV AAOT (550 nm) are in the same order of magnitude, but no correlation is found between the two. The SU_AATSR SSA shows an interesting temporal behavior, being very constant in November 2005, and showing a very large variation in December 2005 and January 2006, returning to a small variation in February 2006. An appealing explanation would be the incursion of transported mineral aerosols during part of the period with different single scattering albedos than that of local biomass burning aerosols. However, the Sahara case has shown that desert dust has a constant SSA, indicating a dominance of desert dust during the beginning and end of the shown period. Unfortunately, this is not in

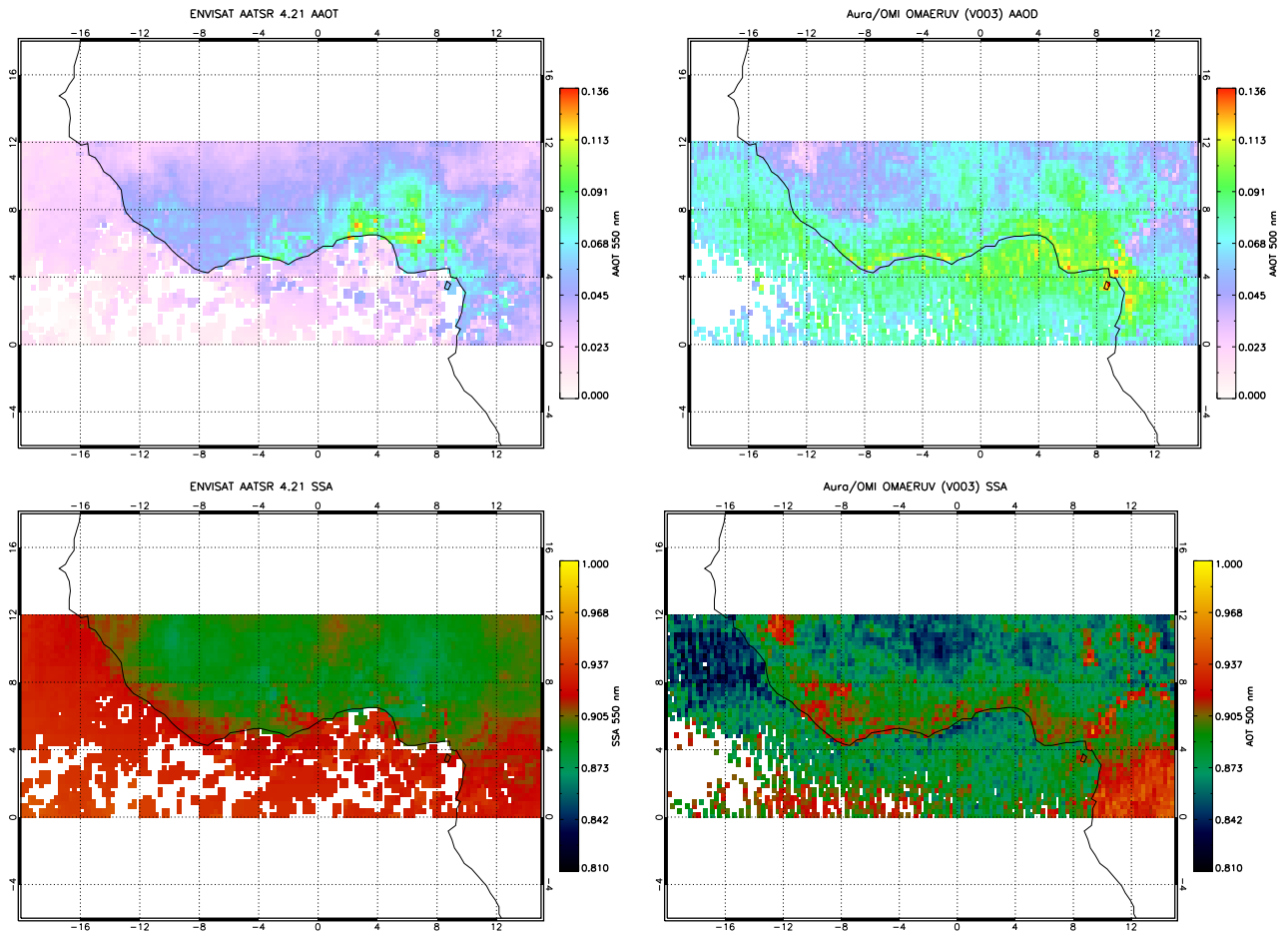

Figure 16: AAOT (top panel) and SSA (bottom) derived from SU_AATSR (left) and OMAERUV (right) data, averaged from 1 November 2005 – 28 February 2006.

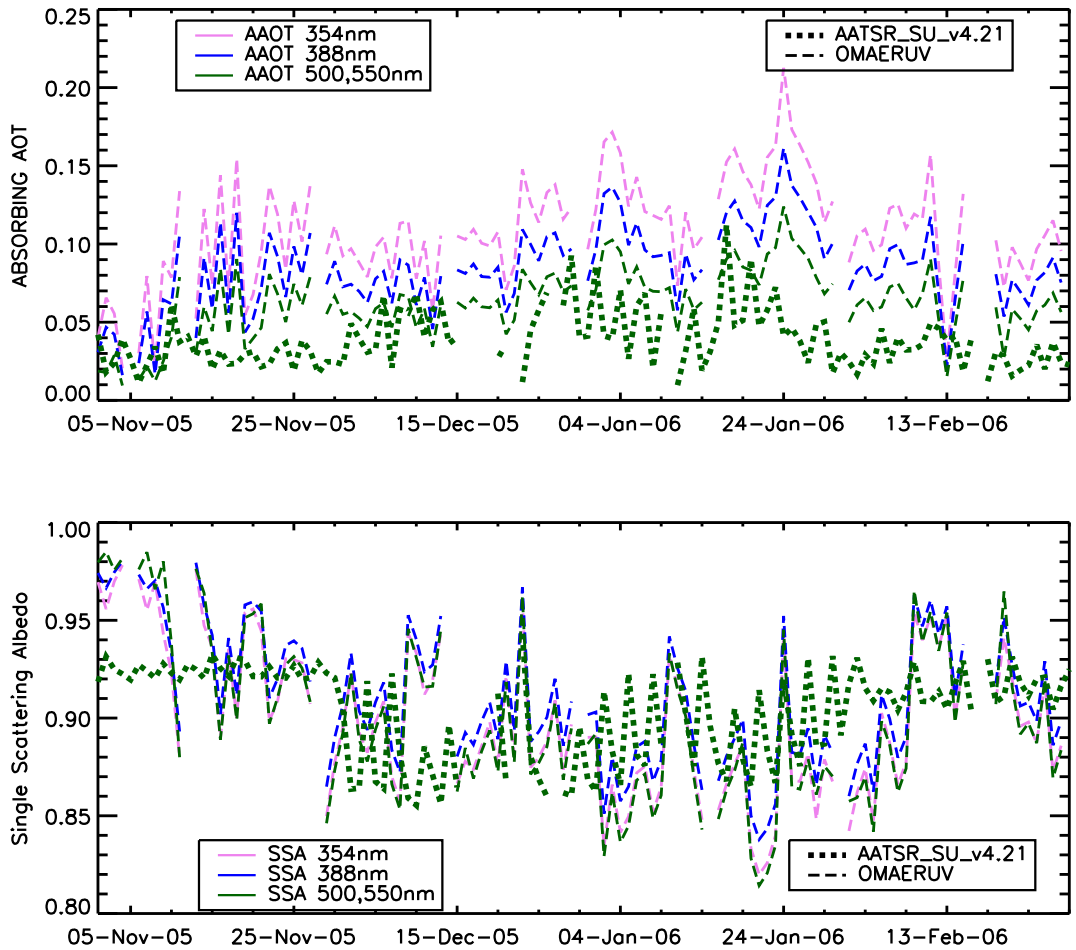

Figure 17: SU_AATSR and OMAERUV AAOT and SSA from 1 November 2005 – 28 February 2006 averaged over the area shown in Figure 11. The top panel shows the SU_AATSR AAOT at 550 nm, the next panel the OMAERUV AAOT at 354 nm, 388 nm, and 500 nm. The lower panels show the SSA, first from SU_AATSR at 550 nm, the lowest panel showing the OMAERUV SSA at 354 nm, 388 nm, and 500 nm.

correspondence with the SU_AATSR derived dust AOT, which is also shown in Figure 12. According to this plot, desert dust is present from January 2006 onward and also sporadically in November 2005, which should have reduced the SSA variation also during those times. The OMAERUV SSA shows no relation with the SU_AATSR SSA.

In Figure 18 scatter plots are shown of the SU_AATSR AAOT versus OMAERUV AAOT and the SU_AATSR SSA versus OMAERUV AAOT for all regridded data points between 1 November 2005 and 28 February 2006 over the Sahel region. The data were filtered for AOT$>$ 0.2. They again show that these products are not related for both instruments. The main feature in both plots is the separation of the SU_AATSR products into two strong hot spots. This is due to a different treatment of land and ocean data, also shown by the strong land-sea contrast. The high SSA values (centered around 0.93) are ocean data, while the data centered around 0.89 are the data over land. When only land data are considered, the correlation for AAOT improves considerably, whcih is shown by the blue line in Figure 18 (left).

The temporal variation of the SU_AATSR and OMAERUV AAOT and SSA data from 1 November 2005 – 28 February 2006 is given around three AERONET stations in Figures 19 and 20. In general, the AAOT from both satellites follow the same trend as the AERONET AAOT during the dry season, but satellite is somewhat lower than

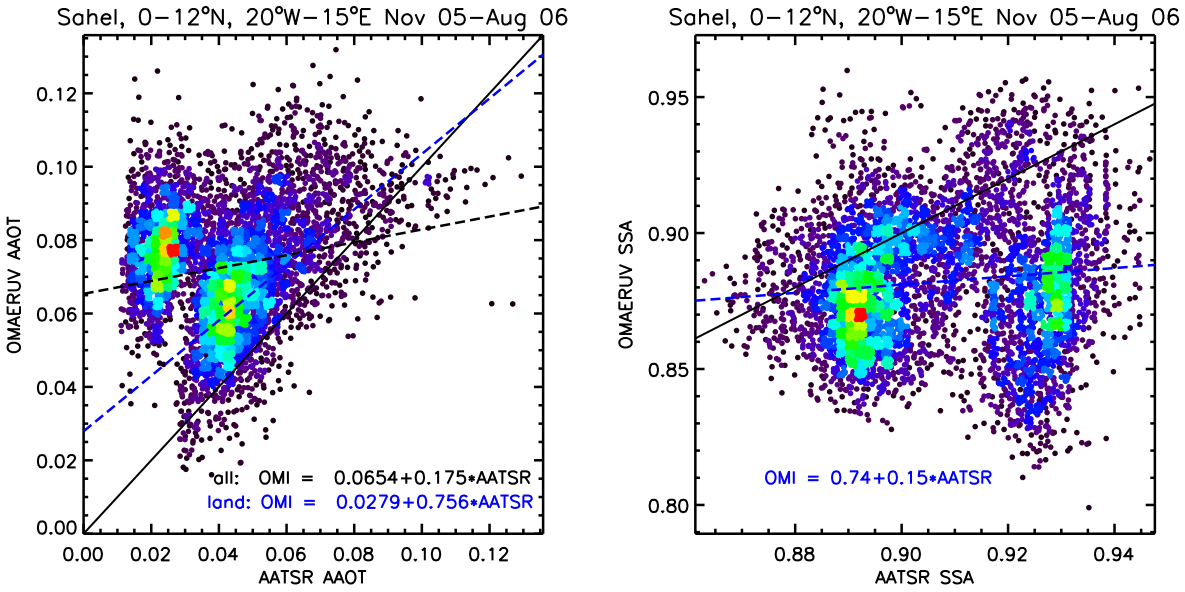

Figure 18: SU_AATSR and OMAERUV AAOT (left panel) and SSA (right panel) from 1 November 2005 – 28 February 2006 averaged over the area shown in Figure 11.

the ground-based. No clear correlation can be seen in details, but this is due mostly to the differences between the spatial averaging of satellite data and temporal averaging of the ground-based data. The same conclusion can be drawn from the SSA comparison in Figure 20. In general, the trend is the same for satellite and ground-based SSA, especially the comparison for Ilorin is good, although not in details. For AERONET station Ilorin and Dakar level 1.5 data has been used, because the level 2.0 was too sparse. From station Djougou can be concluded that the satellite SSA data is generally higher than the ground-based SSA, compensating for the lower AAOT. Again, it is clear that the OMAERUV data shows much more temporal variation in both AAOT and SSA, like AERONET, but the temporal variation of SU_AATSR seems too low, probably due to a strict constraint on the SSA.

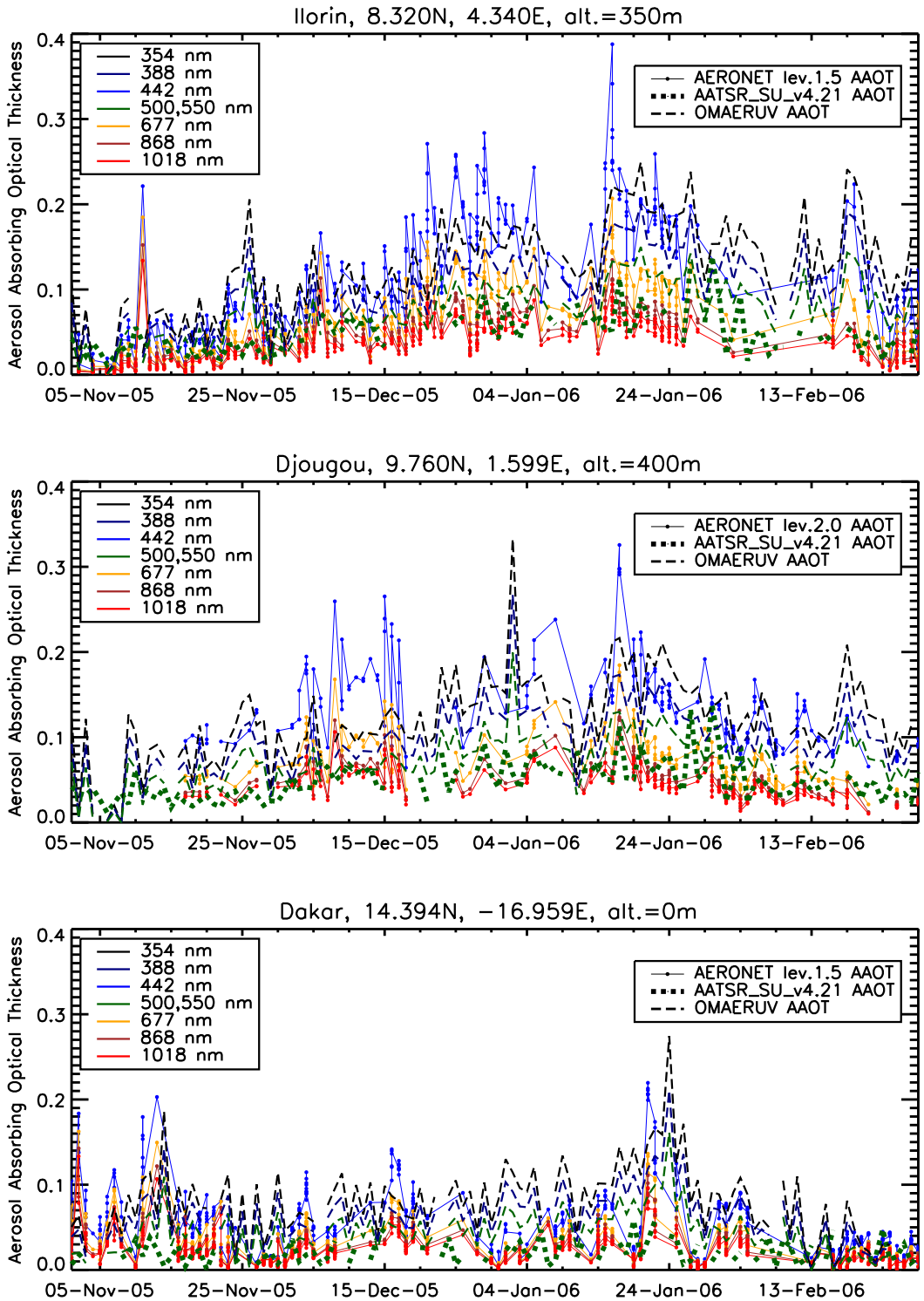

Figure 19: Absorbing Aerosol Optical Thickness from 1 November 2005 – 28 February 2006 from AERONET, SU_-AATSR and OMAERUV around station (a) Ilorin, (b) Djougou, and (c) Dakar. The satellite data were averaged over the same areas as in Figures 13-15

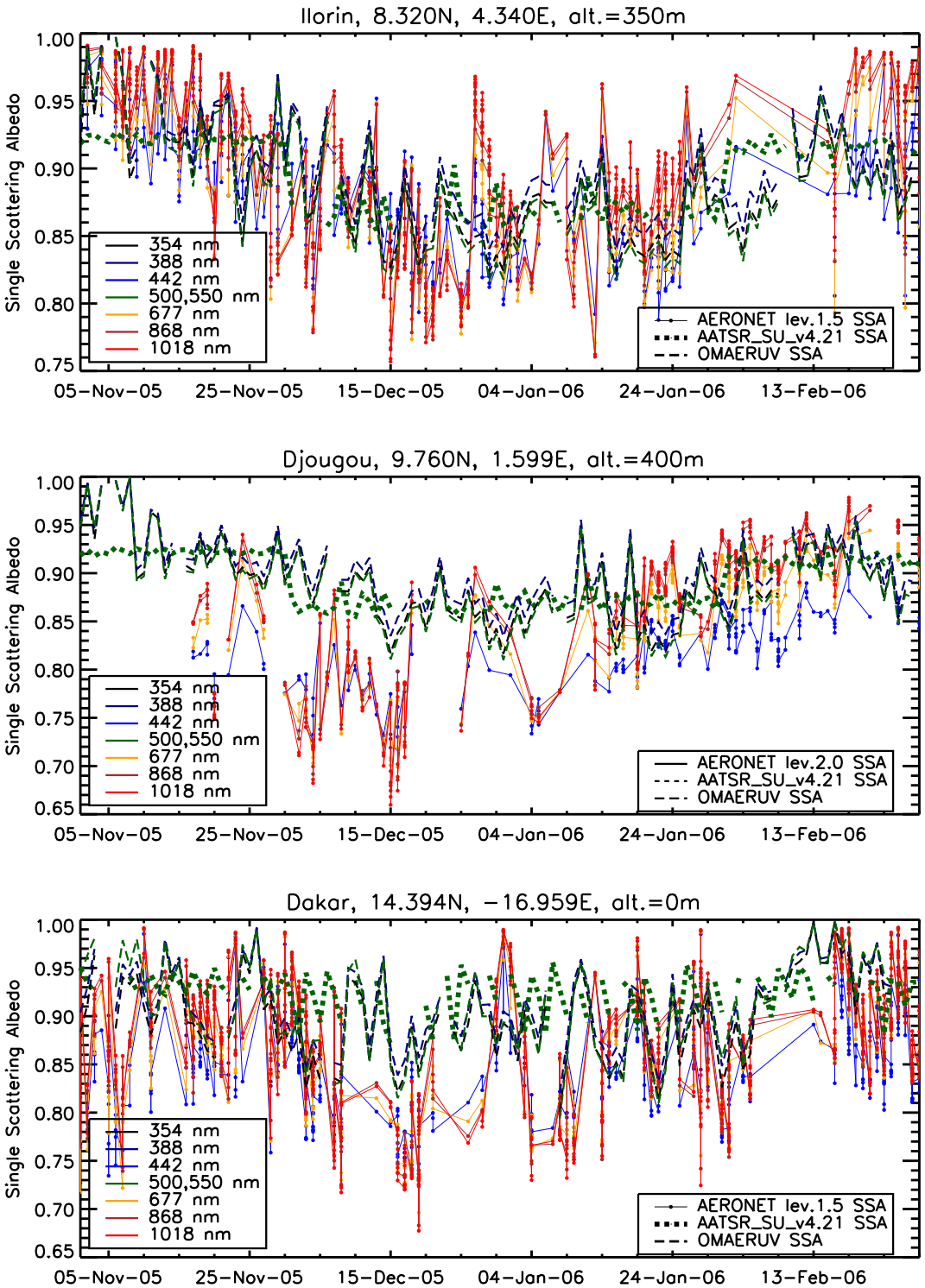

Figure 20: Single scattering albedo from 1 November 2005 – 28 February 2006 from AERONET, SU_AATSR and OMAERUV around station (a) Ilorin, (b) Djougou, and (c) Dakar. The satellite data were averaged over the same areas as in Figures 13-15

5 Biomass burning aerosols over Central South Africa

Central southern Africa is well-known as a monsoon area and experiences extreme droughts every year, during which dust and especially biomass burning smoke are abundant. The interior of the continent has an abundance of vegetation which burns during the dry season, especially regions like Zambia, Angola and the republic of Congo. The smoke from this biomass burning is often lofted into the free atmosphere, forming thick plumes of smoke between 2–5 kilometers in altitude. Depending on the prevailing large-scale circulation, this smoke can either be transported to the east over the south-east Atlantic Ocean, where it interacts with the semi-permanent stratocumulus deck over the ocean, or as 'rivers of smoke' south-west to the Indian Ocean [*Swap et al.*, 2003]. Either way, the elevated absorbing aerosols in the smoke plumes can be detected by satellite instruments, due to their high altitude and large absorption component. The southern African smoke has been extensively studied scientifically.

Absorbing Aerosol Index One of the main satellite products that has been used extensively is the Absorbing Aerosol Index (AAI) or UV Aerosol Index (UVAI), which is a color ratio in the UV, the positive part of which is indicating the presence of absorbing aerosols [e.g. *Torres et al.*, 1998; *de Graaf et al.*, 2005]. The AAI is available from many satellite instruments that cover the UV, like the TOMS series, the GOME series, SCIAMACHY, and OMI. Two examples are shown in Figure 21: The multi-sensor AAI, a multi-year composite AAI from all available instruments, developed for and available from Aerosol-CCI, and the NASA OMAERUV UVAI product from OMI. The multi-sensor AAI is currently available daily on a $1^\circ \times 1^\circ$ grid from 1978 to 2015, and the OMAERUV UVAI is available on a $0.25^\circ \times 0.25^\circ$ grid for the entire OMI mission. Note that the definition for the AAI and UVAI changes from instrument to instrument, because different combinations of wavelengths are used. For the multi-sensor AAI these differences have been reduced by combining the AAI during overlap periods of different instruments. Also, for the OMAERUV UVAI the reference wavelength is reversed compared to the definition of the multi-sensor AAI.

Figure 21 shows that in general the multi-sensor AAI and the OMAER UVAI compare well qualitatively. In these figures only the positive values were plotted, indicative of absorbing aerosols. To quantify the differences between the two quantities, the OMAER UVAI data were regridded to a $1^\circ \times 1^\circ$ grid and compared to the multi-sensor AAI data, see Figure 22. All the data in the area from 0–35°S and 0–40°E between 1 August and 31 September regridded to a $1^\circ \times 1^\circ$ grid were plotted. Note that now also negative values were used, which is essential when applying statistics. Figure 22 shows that the correlation is rather poor and that the multi-sensor AAI shows a much larger amplitude than the OMAER UVAI. Part of this can be explained by the different definition, but generally the correlation is not large.

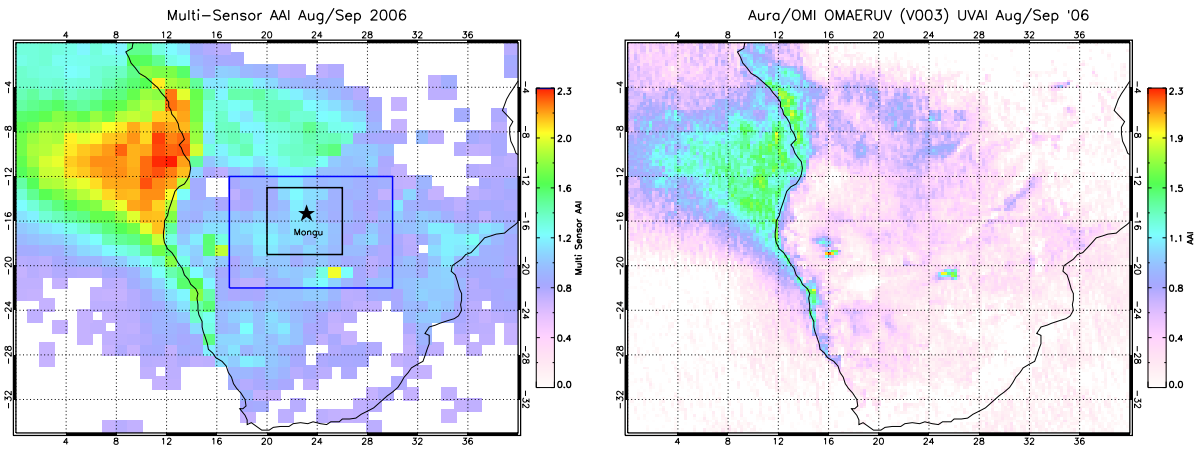

Figure 21: Multi sensor AAI at $1^\circ \times 1^\circ$ grid (left) and the OMAER UVAI at a $0.25^\circ \times 0.25^\circ$ grid, averaged from 1 August – 31 September 2006 over the area shown. The left plot shows the location of the Mongu AERONET station, and the averaging boxes that were used to average OMAERUV data around the station.

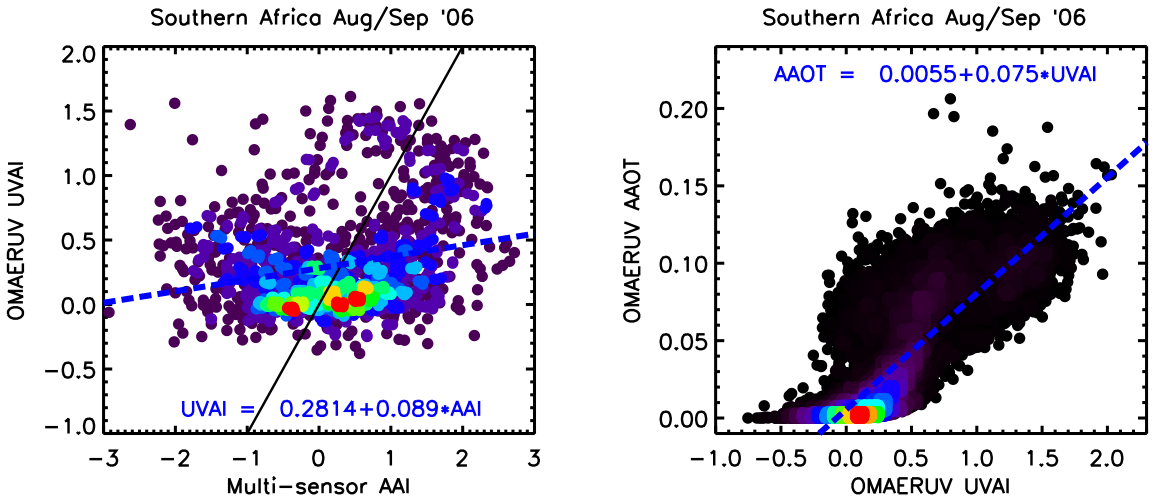

Figure 22: (Left panel) Comparison of multi-sensor AAI data and OMAR UVAI data regridded to a $1^\circ \times 1^\circ$ grid, from 1 August – 31 September 2006, for all data between $0-35^\circ$S and $0-40^\circ$E (see Figure 21. (Right panel) OMAERUV AAOT versus UVAI data for the same period and area as the left panel, except at the original $0.25^\circ \times 0.25^\circ$ grid.

5.1 Absorbing aerosol optical thickness and single scattering albedo

The right panel of Figure 22 shows the correlation of the OMAERUV AAOT with the OMAERUV UVAI, both at the original $0.25^\circ \times 0.25^\circ$ grid, for all data from 0–35°S and 0–40°E between 1 August and 31 September 2006. It shows a good correlation between the two products, which confirms the idea that the UVAI is sensitive to the absorbing part of aerosols. It must be mentioned here that both products are derived from the same instrument, which reduces the dependence of instrumental effects and calibration errors.

In Figure 23, the AAOT and SSA from SU_AATSR and OMAERUV are compared as before. The data were regridded to a $0.25^\circ \times 0.25^\circ$ grid, and filtered for AOT$>$ 0.2. All regridded data between 10–20°S and 15–30°E from

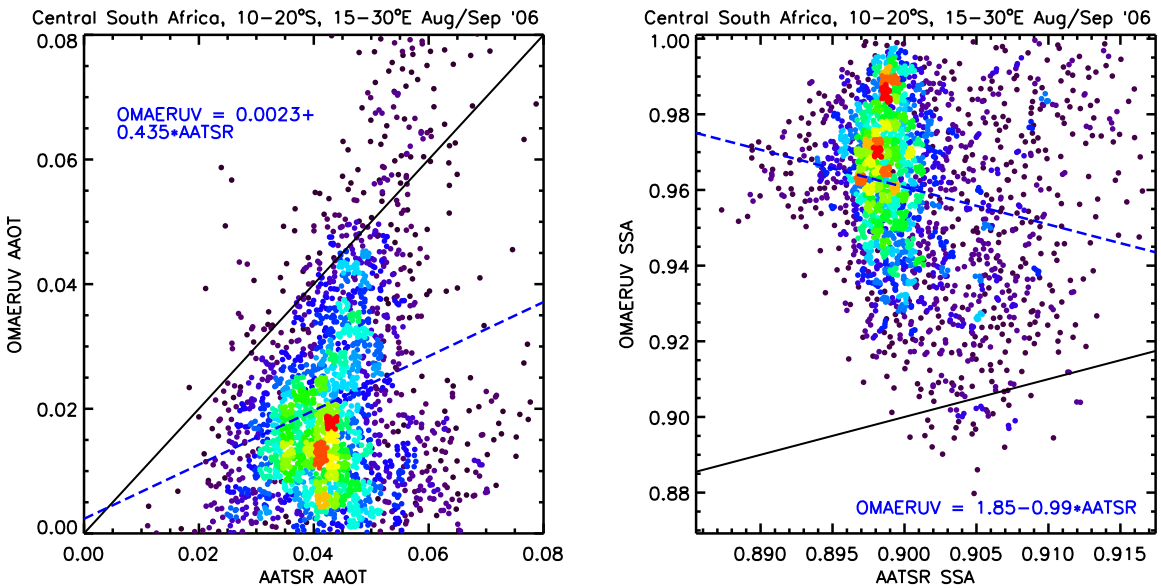

Figure 23: SU_AATSR versus OMAERUV AAOT and SSA for all regridded data in central-south Africa (around Mongu station).

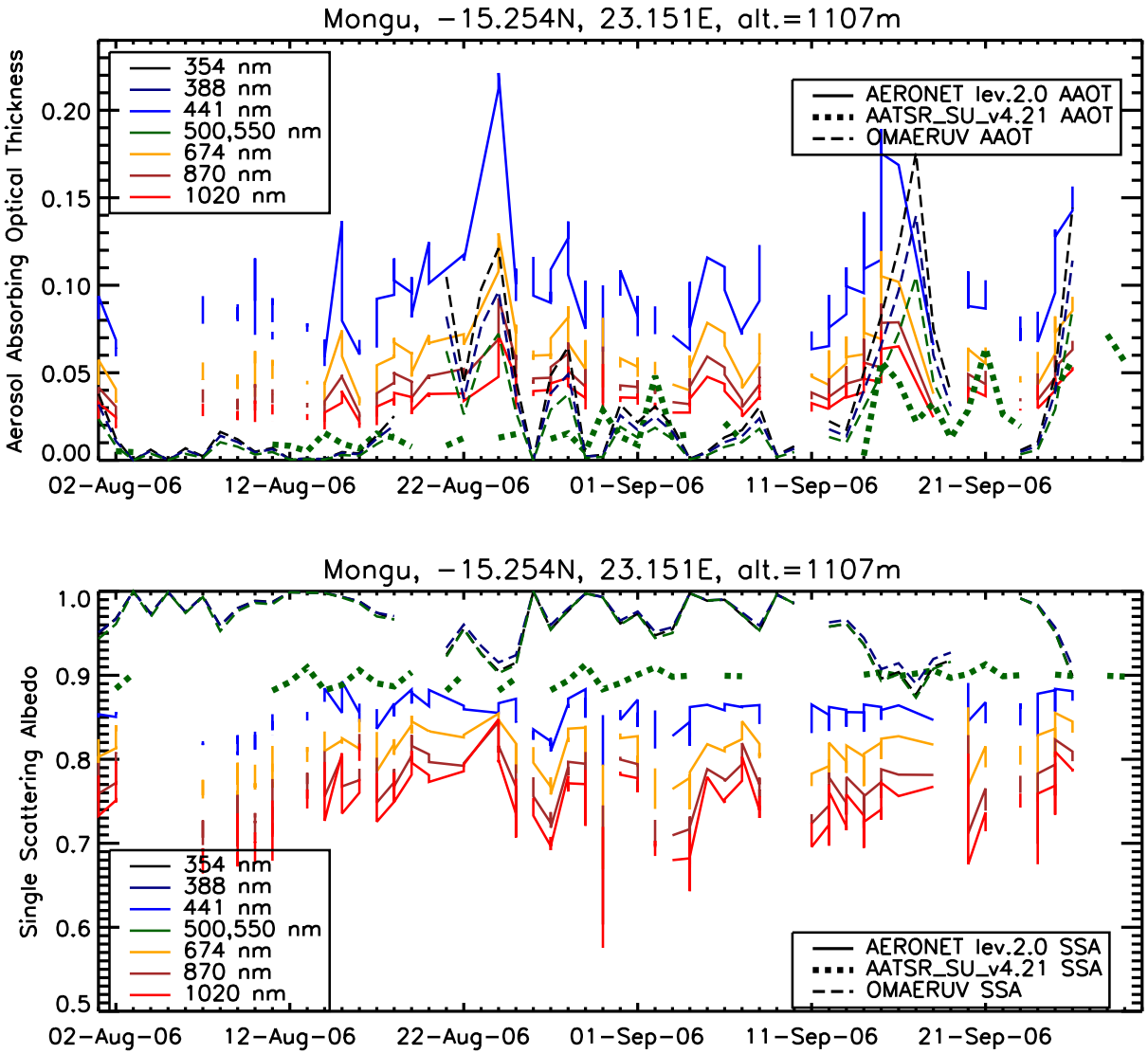

Figure 24: SU_AATSR versus OMAERUV AAOT and SSA for all regridded data Mongu station.

1 August to 31 September 2006 were plotted. The plot confirms the low correlation of the absorbing properties retrieved from both instruments, also for Central south Africa. In this case, since only data retrieved over land were used, no division in the data as seen in Figure 18 is found.

In order to compare the satellite data to a ground-based station, the AAOT and SSA derived from OMAERUV and SU_AATSR from 1 August – 31 September 2006 were averaged and compared to data from the AERONET station Mongu, indicated in Figure 21. The OMAERUV data were averaged over an area from 13–19°S and 20–26°E, which is the black box around Mongu station indicated in Figure 21. The SU_AATSR data were averaged over an area from 12–22°S and 17–30°E, which is the blue box around Mongu station indicated in Figure 21. The boxes were kept as small as possible to increase the correlation with the AERONET station, but the larger box was needed to increase the number of SU_AATSR data points, which are relatively sparse.

In Figure 24 the temporal variation of the OMAERUV and SU_AATSR AAOT and SSA are compared to the AAOT and SSA from Mongu AERONET station. The data show again and more clearly than before that the satellite AAOT is underestimated compared to the ground-based data, while the satellite SSA is overestimated compared to the ground-based data to compensate. In the current case especially the SSA from OMAERUV is much larger than

expected from the AERONET station. The OMAERUV SSA is around 0.95, indicating moderately absorbing aerosols at best, while the Mongu data indicate strong absorption with SSA at 500 nm to be lower than 0.85. The SU_AATSR SSA is closer with an SSA of around 0.9, but as always the SU_AATSR SSA seems to be heavily constrained, with little temporal variation. The wavelength dependence of the OMAERUV SSA is negligible, while the wavelength dependence of the AERONET SSA is very large, which points to a likely incorrect choice of aerosol model for this area at this time.

5.2 SYNAER data

The central south Africa case is also suitable to compare SYNAER data with other satellite data and AERONET. The SYNAER data have good coverage of this area, even though the data are sparse in general. To increase the coverage, the data were averaged over three months, instead of the two months before. Also, the data were gridded to a $0.5^\circ \times 0.5^\circ$ grid and averaged, to increase the number of points in a grid cell. Figure 25 shows the AOT, AAOT, and SSA over central south Africa, averaged from 1 July – 31 September 2006 from SYNAER data. Notice the extra month of July in the data, compared to Figure 21. The AOT and AAOT plot show a reasonable comparison to the AAI and UVAI in Figure 21 over the continent, showing that the SYNAER data are sensitive to absorbing aerosols. However, over the ocean the smoke plume that is very distinct in the AAI and UVAI is absent in the SYNAER data. This is probably due to the persistent cloud cover over the south-east Atlantic Ocean. The area is known for its extensive elevated smoke plumes which overly boundary layer clouds. The AAI and UVAI are not sensitive for cloud cover and will detect smoke that is overlying clouds, but the SYNAER data are cloud screened, leaving little data over the ocean.

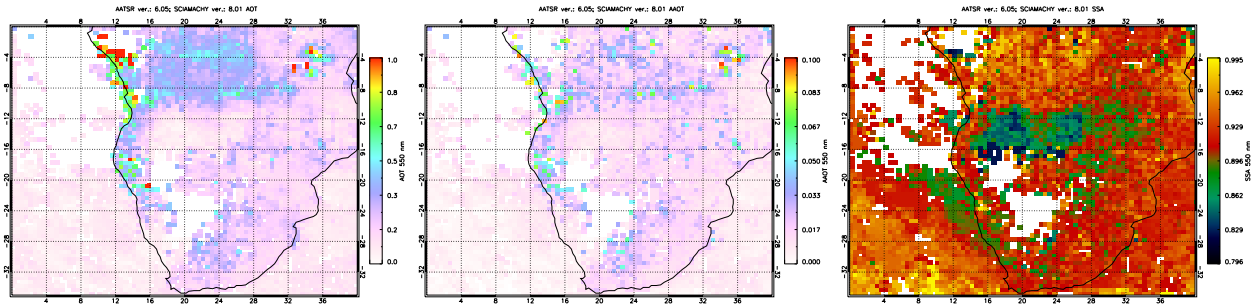

Figure 25: SYNAER AOT (left), AAOT (middle), and SSA (right), averaged from 1 July – 31 September 2006 over the area shown.

5.3 GRASP data

Central south Africa also provides a good opportunity to compare with GRASP/PARASOL data, since this data set was processed for a number of areas around important AERONET stations, one of them being Mongu. GRASP/PARASOL data are available from 2005–2013 for a 1200 $\times$ 1200 km^2 area around the AERONET station, which corresponds almost exactly with the wider rectangle in Figure 22: 9–21 °S, 16–30 °E. So the data can be compared to AERONET and the satellite retrievals described above. All level 2 data from 1 August to 30 September were regridded to a $0.25^\circ \times 0.25^\circ$ grid and averaged.

Comparing AAOT and SSA The AAOT data from all four satellite retrievals can now be compared to AERONET data from Mongu station, see Figure 26. This figure shows the averaged, regridded data satellite AAOT averaged over the area around Mongu station against daily averaged AAOT from Mongu. The four panels represent the data from OMAERUV (upper left), SU_AATSR (upper right), SYNAER (lower left), and GRASP/PARASOL (lower right), all regridded to a regular grid described above, and averaged over the area around the AERONET station Mongu as before. For all data sets, the period August and September 2006 was used, also SYNAER. Only AAOT and SSA

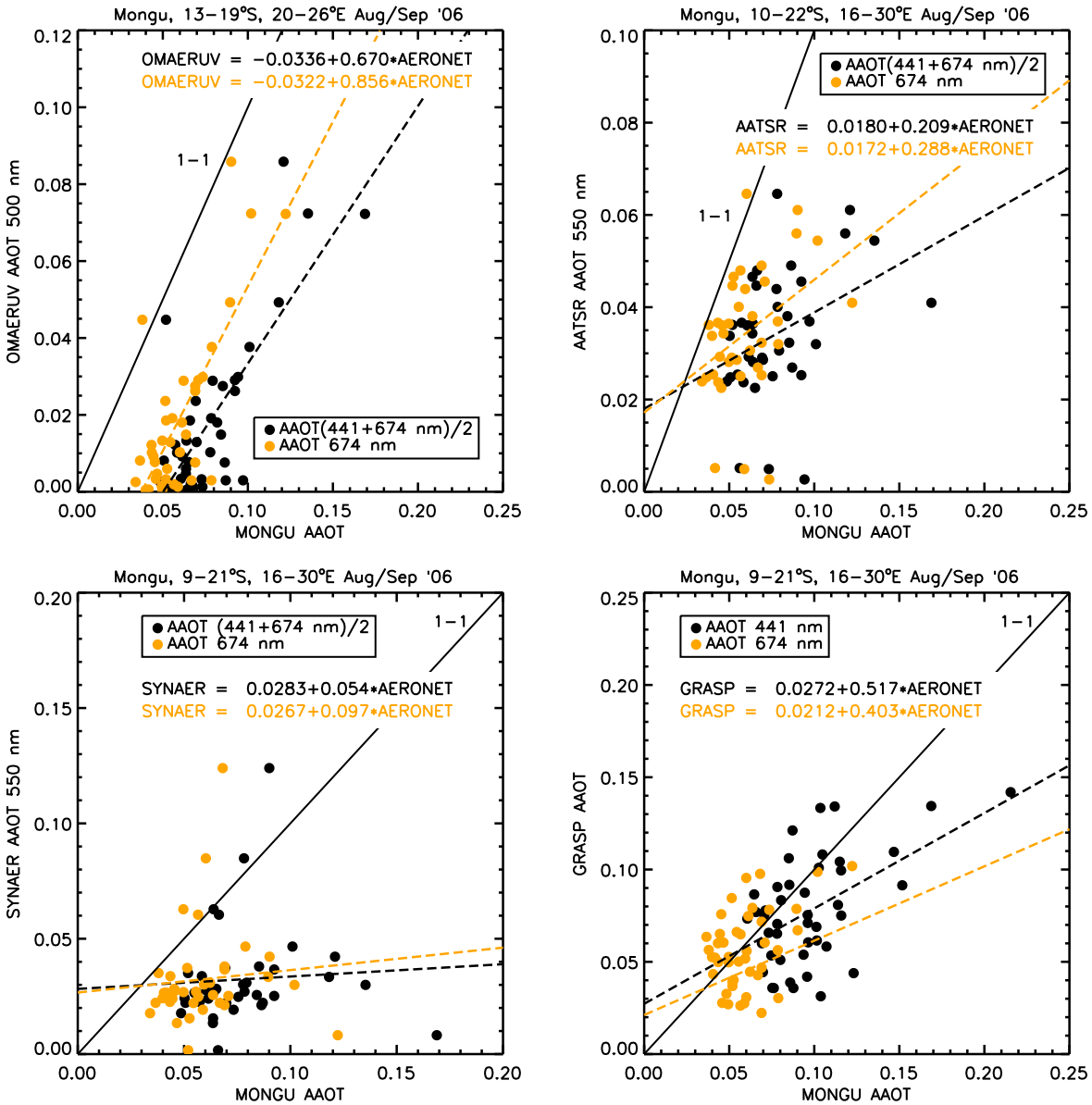

Figure 26: OMAERUV, SU_AATSR, SYNAER, and GRASP AAOT averaged per day versus daily AERONET station Mongu data. The area over which is averaged is indicated in Fig 21, the smaller rectangle for OMAERUV, and the wider rectangle for the three other datasets. The OMAERUV AAOT is at 500 nm, from SU_AATSR at 550 nm, from SYNAER at 550 nm and from GRASP at 440 and 670 nm. The orange data are Mongu station AAOT data at 674 nm, while the black dots were computed by simple averaging of Mongu AAOTs at 674 nm and 441 nm (to compare with 500 nm), or 441 nm for comparison with GRASP at 440 nm.

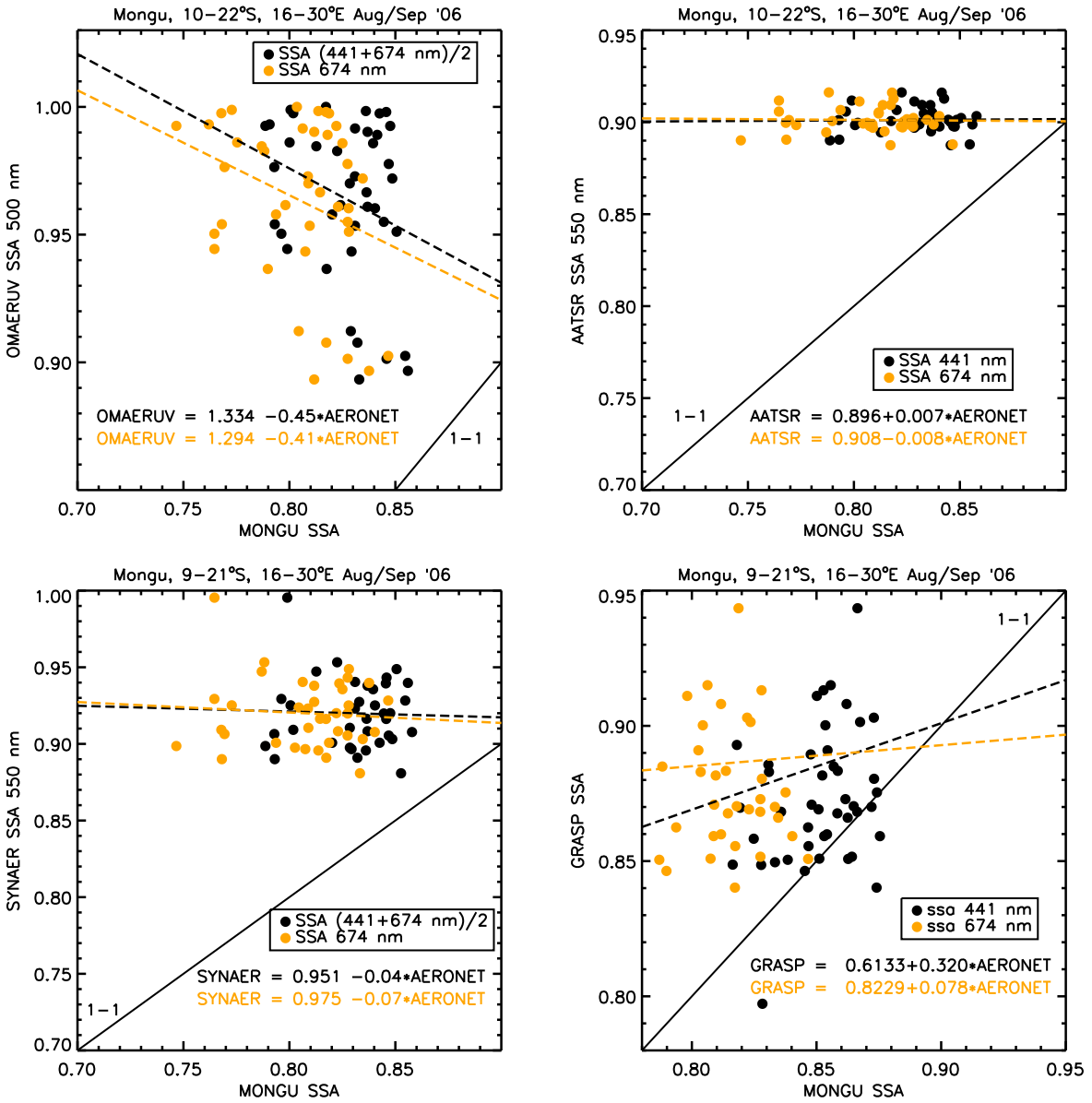

Figure 27: OMAERUV, SU_AATSR, SYNAER, and GRASP SSA averaged per day versus daily AERONET station Mongu SSA. The area over which is averaged is indicated in Fig 21, the smaller rectangle for OMAERUV, and the wider rectangle for the three other datasets. The OMAERUV SSA is at 500 nm, from SU_AATSR at 550 nm, from SYNAER at 550 nm and from GRASP at 440 and 670 nm. The orange data are Mongu station SSA data at 674 nm, while the black dots were computed by simple averaging of Mongu SSAs at 674 nm and 441 nm (to compare with 500 nm), or 441 nm for comparison with GRASP at 440 nm.

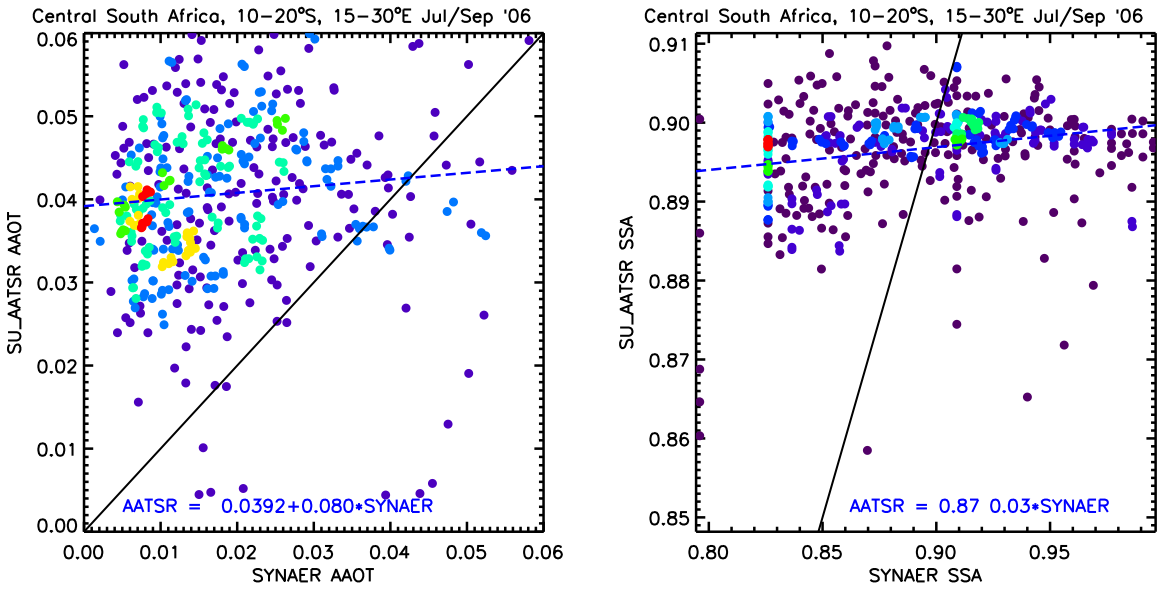

Figure 28: Comparison of SU_AATSR AAOT (left panel) and SSA (right panel) to that from SYNAER. The data were regridded to $0.5^\circ \times 0.5^\circ$ grid and averaged from 1 July to 30 September 2006.

data were used that were retrieved for an AOT larger than 0.2, because for smaller AOT no sensitivity for these parameters can be expected.

The black dots represent the satellite AAOT at 500 nm (OMAERUV), 550 nm (SU_AATSR and SYNAER), or 443 nm (GRASP). These are compared to a simple average of Mongu AAOT between 441 and 674 nm for the first three, and to AERONET AAOT at 441 nm for GRASP. The orange dots are the AAOT at 500, 550 or 670 nm compared to the AERONET AAOT at 674 nm. The plots shows that all but GRASP underestimate the AAOT compared to MONGU station data. Even the 674 nm AAOT from AERONET is still much lower than the satellite AAOT. All data sets except SYNAER show some correlation to AERONET. GRASP AAOT data are in the same range as the AERONET AAOT for both wavelengths, and they show a reasonable correlation, considering the crudeness of the comparison.

The upper left panel shows a good comparison between the OMAERUV AAOT and AERONET AAOT, even though the OMAERUV AAOT is much lower than that from the AERONET station. This suggest that a more correct choice of SSA or aerosol model might improve the AAOT retrieval and provide a product that has a good correlation with ground-based data, at least for this case. The correlation between AERONET AAOT and SU_AATSR AAOT is smaller, with both an offset and a smaller correlation, and decreases even further for SYNAER AAOT. However, the SYNAER data are sparse, which is disadvantageous for the comparison. SYNAER data were filtered for AOT550 $>$ 0.15, since below this value the retrieval of AAOT is replaced by a climatology, but filtering on AOT did not improve the correlation, no doubt because the data become even more sparse. The weak correlations seen in AAOT in Figure 26 are solely due to skill in retrieving AOT. It suggests (at least for this comparisonb) that the analysis fails to demonstrate that any of the retrievals have any skill at retrieving aerosol absorption properties.

The single scattering albedo from the satellite algorithms can likewise be compared to AERONET, see Figure 27. The order is the same for Figure 26. The upper left panel shows a lack of correlation between the OMAERUV SSA and AERONET SSA, even though the AAOT corresponds well between these two datasets. This suggest again that a better choice or retrieval of SSA may be most efficient to improve the OMAERUV dataset. The upper right panel shows the low variation that the SU_AATSR SSA has, as shown before. The same can be said about the SYNAER SSA (lower left), which shows no correlation with the AERONET SSA and a low variation, also suggesting a strong constraint of the SSA. The GRASP SSA (lower right) is the only dataset to show a positive correlation with the AERONET SSA, but the correlation is too low to be considered significant. This comparison shows that the SSA is the most challenging quantity of absorbing aerosols to be retrieved.

The comparison between the AAOT and SSA from SYNAER over central south Africa compared to the SU_G retrievals is shown in Figure 28. The left panel shows the AAOT and the right panel shows the SSA. The data were regridded to a $0.5^\circ \times 0.5^\circ$ grid, because of the scarcity of the data. Therefore, the number of points is 4 times smaller than that in Figure 23. All regridded data between 10–20°S and 15–30°E were averaged from 1 July to 31 September 2006, so again one extra month of data. The figures show no correlation for either AAOT or SSA, which is somewhat surprising, since both data products use SU_AATSR data in their retrieval. The lack of correlation points to very different assumptions used in the retrieval of the SSA.

6 Tropical Atlantic Ocean

Saharan dust is often transported over the tropical Atlantic Ocean, sometimes all the way to the Americas and beyond. This provides an opportunity to test the AOT and SSA retrievals over the ocean. In particular the FAME-A retrievals in sunglint areas can be compared here to other data.

6.1 FAME-A data

Figure 29 shows the FAME-A AOT and SSA over the tropical Atlantic, regridded to a $0.25° \times 0.25°$ grid and averaged from 1 June to 31 August 2007. Also shown in the same figure are the SU_AATSR AOT and SSA in the same area averaged over the same time. The main challenge with FAME-A, like SU_AATSR, is that the data are sparse, since they are only available in a small part of the AATSR swath where one of the AATSR cameras is brightened by sunglint and not cloud contaminated. Therefore, all data from the three available months are used. The FAME-A AOT plot shows that the sunglint areas are still visible even in data averaged over three month: There is a general southwest to northeast pattern in the AOT data which results from the sunglint areas that have the same orientation. However, the SU_AATSR data are even more sparse. Either because of cloud contamination or a very low AOT, the SU_AATSR AOT retrieval shows a lot of areas with no data, even averaged over three months.

From FAME-A also the SSA is available. The SSA from FAME-A and SU_AATSR are shown in the right panels in Figure 29. In general, the SSA is quite large, near one, which suggest an abundance of marine aerosols. This could

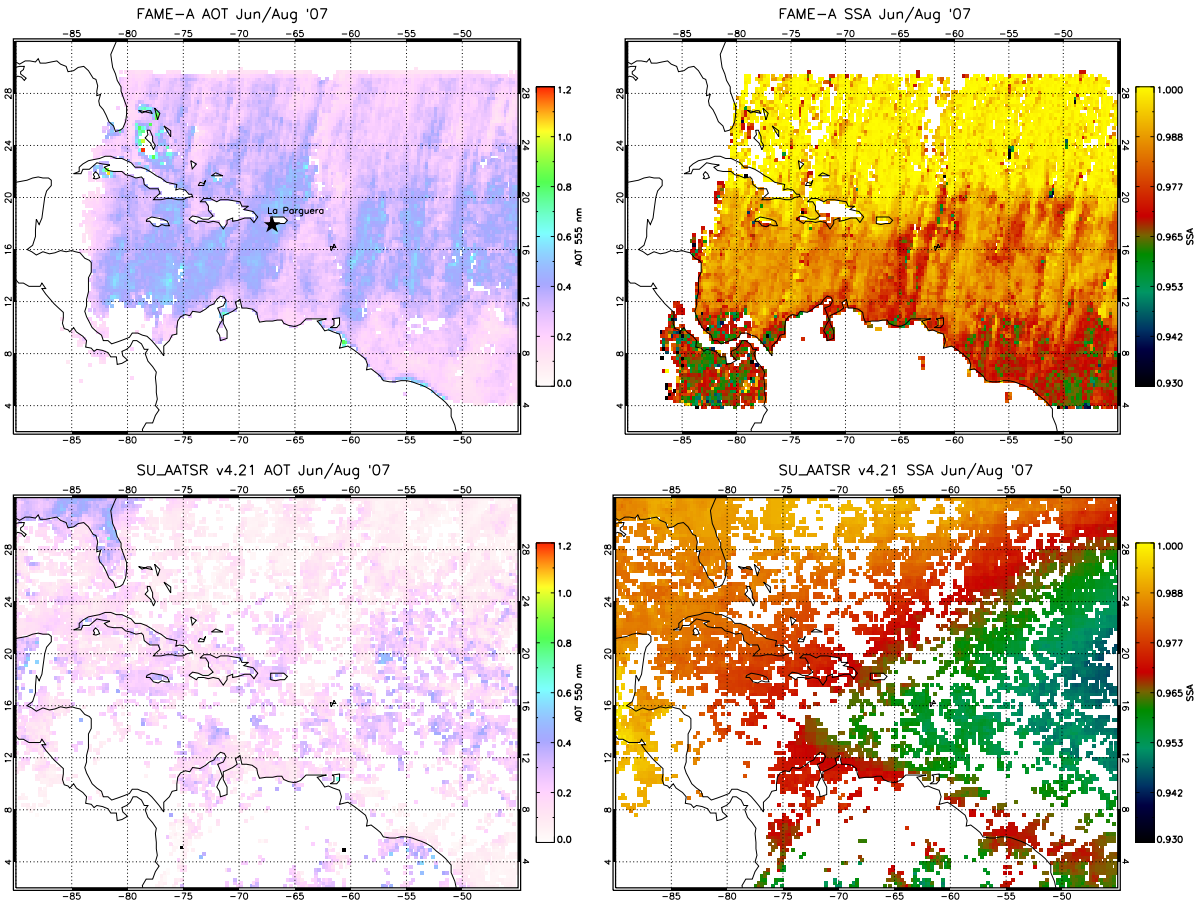

Figure 29: FAME-A AOT and SSA in sunglint areas (upper panels) and SU_AATSR AOT and SSA (lower panels) averaged from 1 June to 31 August 2007 over the tropical Atlantic Ocean.

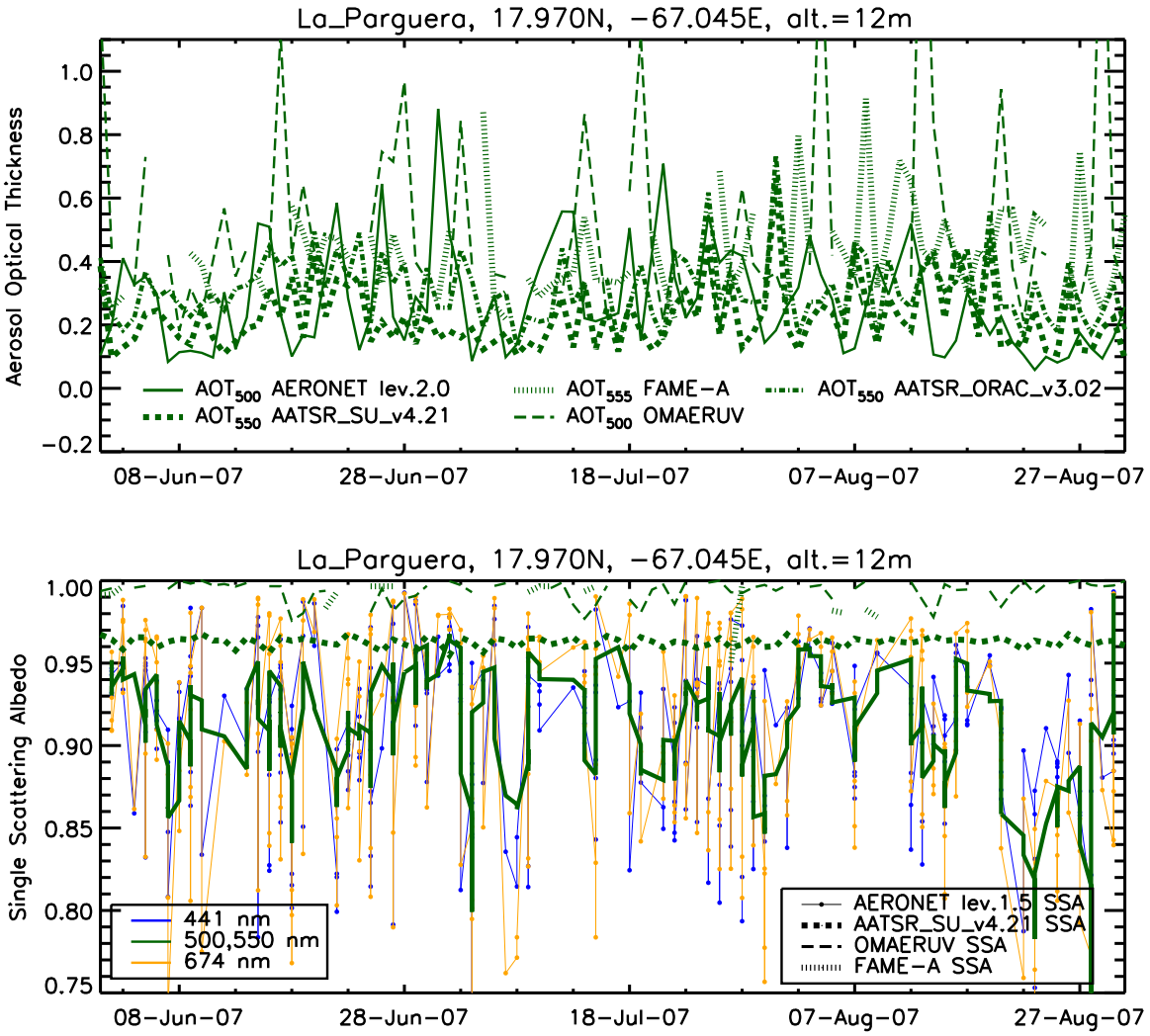

Figure 30: Upper panel: AOT (500 to 555 nm, see caption) from 1 June to 31 August 2007 averaged over the tropical Atlantic Ocean from the different algorithms compared to AOT from La Parguera AERONET station; Lower panel: SSA from three algorithms from 1 June to 31 August 2007 averaged over the tropical Atlantic Ocean compared to SSA from La Parguera AERONET station. Blue and yellow data are AERONET L1.5 data at 441 nm and 674 nm, respectively, the green line is a simple average of these data.

be correct over the tropical ocean. However, there is an artificial increase in FAME-A SSA to the south of the whole area, which is clearly an algorithm artifact. Similarly, the SSA from SU_AATSR shows a strange gradient from southeast to northwest.

The daily variation of the FAME-A AOT and SSA is depicted in Figure 30, together with AOT and SSA from OMAERUV, SU_AATSR and from AERONET station La Parguera. The location of La Parguera is depicted in Figure 29. For all satellite instruments the AOT and SSA were averaged each day over the entire domain shown in Figure 29, because of the scarcity of the data. Reducing the domain to an area closer around La Parguera resulted in a loss of comparable data. The AOT from La Parguera was version 2.0 AOT data at 500 nm. Although the absolute value is in the right order of magnitude, the AOT from the satellite instruments shows no correlation to the AERONET data. This may result from the large area around the AERONET station that was used to average the data. As seen before, increasing this domain reduces the correlation with the AERONET data quickly. However, the satellite data show no correlation between themselves either, even though the averaging areas are the same for all

of these instruments. Some strong events can be seen in OMAERUV data (AOT $>$ 1) and also in FAME-A data (up to 0.8) and AERONET data, but there seems to be no clear correlation between the events.

In the same Figure 30 the SSA from the various instruments is also compared. From La Parguera the level 1.5 SSA data at 441 nm and 674 nm was available, which is shown in the plot. To compare this to the SSA at 500-550 nm like from the satellite instruments, the two curves were averaged and a 5-point running mean was applied to the data, to get a curve comparable to the satellite SSA. This is the green thick solid curve. The SSA comparison shows that the AERONET SSA is much lower than the SSA from any of the satellite instruments, indicating weakly to moderately absorbing aerosols, with a variation of 0.1 SSA during the three month shown. The satellite SSA on the other hand, show much larger SSA, indicating weakly absorbing to scattering aerosols. As before, the SU_AATSR SSA has virtually no variation during the three months, between 0.95 and 0.96 on average. The OMAERUV has a larger spread, but values up to 1.0 most of the time. Unfortunately, the SSA from FAME-A is too sparse to draw definite conclusions. It seems to show both high and low numbers, down to about 0.91 on average, but it is hard to show a correlation with any of the other SSA data.

6.2 ORAC AATSR data

The Atlantic Ocean case also provides an opportunity to show the behavior of the Absorption Aerosol Optical Thickness (AAOT) of the ORAC AATSR data set. This dataset provides both AOT and AAOT, and the AOT can be compared to the AOT from FAME-A and SU_AATSR in Figure 29. The three-month averaged AOT shows a smooth aerosol field, albeit with structuring over the ocean that are unlikely to be physical. There is also a very strong land/sea contrast of the AOT derived over Latin America and the adjacent ocean. Furthermore, the AOT seems to show a remnant of the satellite orbit in the northeast to southwest direction.

Derived from the AOT is the AAOT, which is shown in the right panel of Figure 31. It shows a fairly well-behaved AAOT field, resembling the AOT field with a land/sea contrast and some structuring, but to a much lesser extend. However, anomalous values appeared in this figure around 30 degrees north latitude, of AAOT up to 3.5. Investigation of this phenomenon led to the discovery of very high AAOT values in the ORAC data in the northern hemisphere. An example is shown in Figure 32 for June 2007. It shows the AAOT over most of the globe, which shows the parts where high AOT and AAOT is expected, like over the deserts and biomass burning areas and the outflow regions. However, more obvious are the northeast to southwest stripes of high AAOT over the northern hemisphere oceans. The reasons for these values are unclear, but they are restricted to the northern hemisphere and always a fraction of the AOT, so in fact the retrieved AOT is very large here. This might hint to cloud contamination or sunglint, although the strict north-south division makes an algorithm error more likely. Figure 32 shows more interesting high values of AAOT near the coasts of the continents in the extreme northern regions. Again, the reason for these is unclear, they may be chlorophyll effects, since these regions are known for high

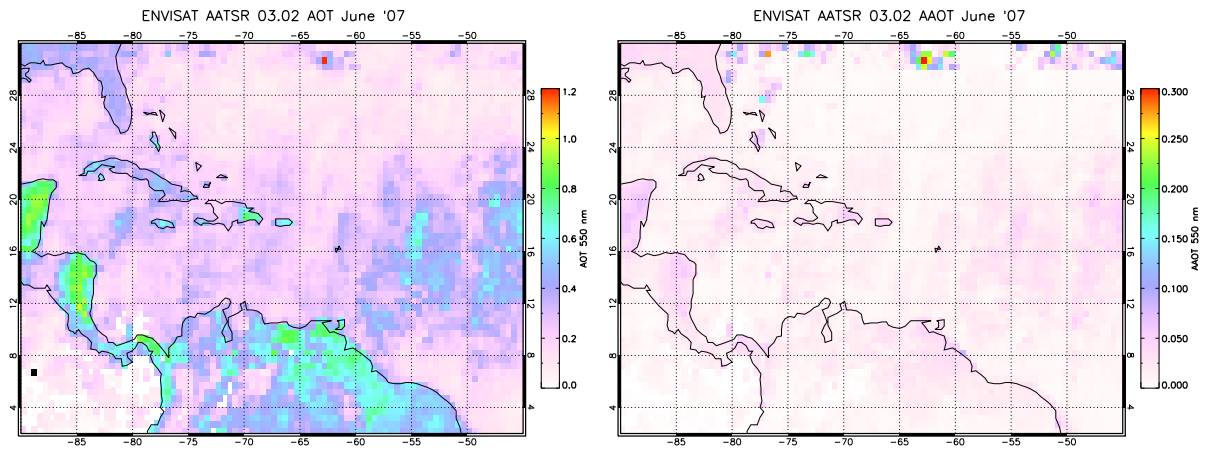

Figure 31: ORAC AATSR v3.02 AOT and AAOT over the tropical northeast Atlantic, averaged from 1 June to 31 August 2007.

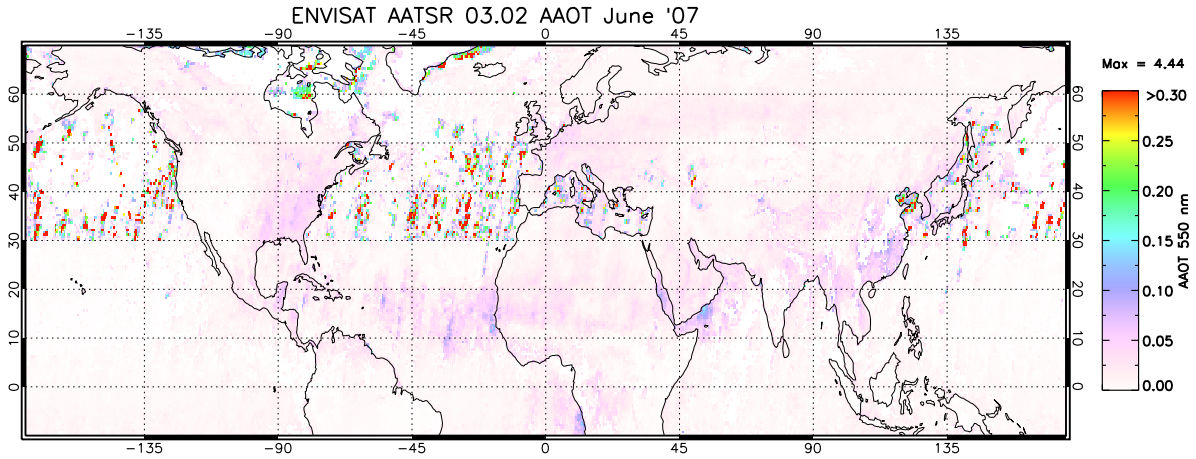

Figure 32: ORAC AATSR v3.02 AAOT over the Atlantic, averaged from 1 to 30 June August 2007.

biological activity, or they may be retrieval artifacts, since also these value are only present in the northern hemisphere.

6.3 Absorption Aerosol Optical Thickness

The oceanic region around AERONET station La Parguera was used to compare the various satellite derived AOT and AAOT with the AOT and AAOT from La Parguera, see Figure 33. Daily averaged level 2.0 AERONET data were used for the daily AOT, while level 1.5 AAOT data were averaged to derive a mean daily AAOT product. The satellite products were all averaged daily over the region shown in Figures 31 and 29. This is a fairly large area, and the AAOT and even AOT show little correlation among each other, which is consistent with Figure 30. However, choosing a much smaller region around La Parguera (18–24°N, 65–80°W) did nothing to increase the correlation and resulted only in many data points being lost, due to the scarcity of the satellite data.

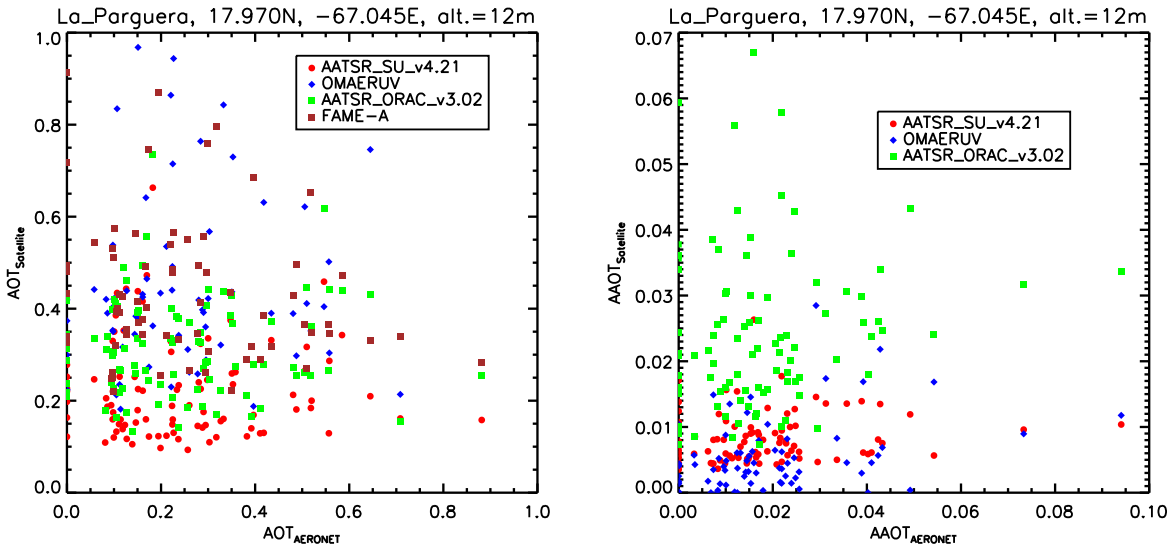

Figure 33: Satellite AOT and AAOT averaged over tropical northeast Atlantic around La Parguera AERONET station compared to AOT and AAOT from this AERONET station. Data were daily averaged from 1 June –31 August 2007.

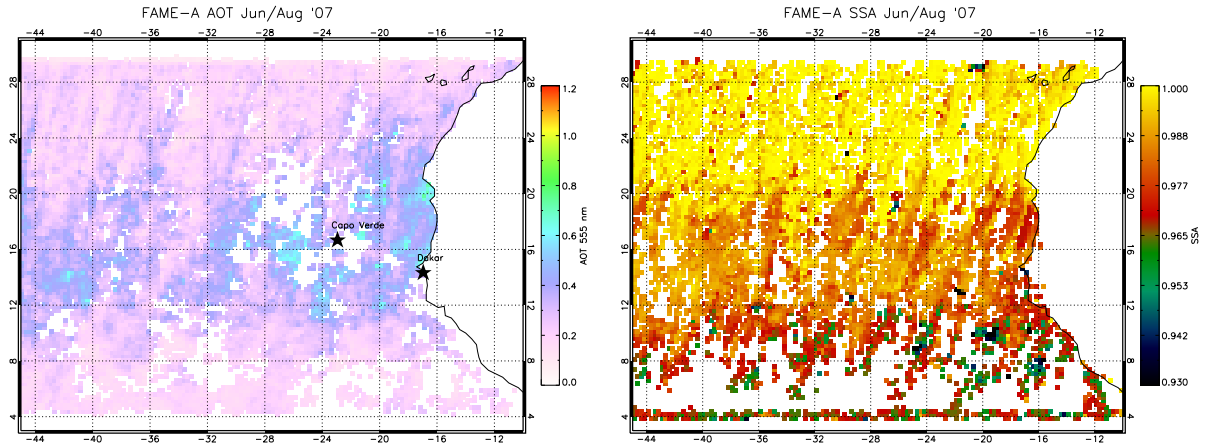

Figure 34: FAME-A AOT and SSA in sunglint areas averaged from 1 June to 31 August 2007 over the tropical Atlantic Ocean.

6.4 Saharan dust

Somewhat closer to the dust source over the ocean, the FAME-A data set may contain a larger signal, therefore the AOT and SSA over the north Atlantic Ocean, averaged from 1 June to 31 August 2007 were plotted in Figure 34. It shows the dust from the Sahara being blown over the ocean, which is a common feature here. The single scattering albedo, however, again shows the artificial gradient from south to north, with high numbers overall, indicating scattering aerosols.

The SSA from two AERONET stations located in the area, Dakar and Capo Verde were compared to the satellite data, see Figure 35. The locations of the AERONET stations are indicated in Figure 34. The single scattering albedo from the AERONET stations were only available as version 1.5 data at 440 nm and 670 nm, so they were again averaged and presented as SSA around 500 nm. The AERONET data were not available at all days, so they show some erratic behavior, but it is clear that the single scattering albedo is lower than that retrieved by the FAME-A algorithm and OMAERUV. Both are constrained to about 0.98, which is indicative of scattering aerosols, so no dust is detected by these algorithms. The SSA from SU_AATRS is lower and somewhat in the range of the AERONET SSA, but again, the SU_AATSR shows no variability, so it is most probably constrained too much. The AERONET SSA shows rather high values up to 0.98, with regular events of lower SSA, indicative of dust events. These events are not present in the satellite data.

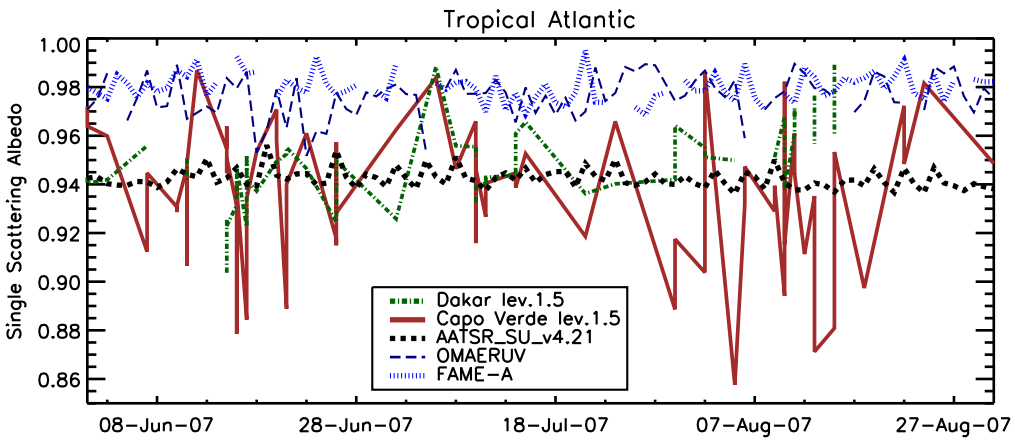

Figure 35: Satellite SSA over the tropical Atlantic Ocean, averaged from 1 June to 31 August 2007, compared to AERONET SSA from Dakar and Capo Verde stations.

7 Global Absorption Aerosol Optical Thickness

The important contribution of satellites to climate research is the continuous global monitoring of the atmosphere. However, the large differences between retrievals of Absorption Aerosol Optical Thickness (AAOT) and Single Scattering Albedo (SSA) from different instruments raises the question of the suitability of satellite data for the retrieval of these complicated aerosol properties. Most of the algorithms rely on the selection of a certain type of aerosol, based on geographic distribution or some macro-physical retrieved property, from which the micro-physical properties are inferred. This makes the selection of the correct aerosol type a very critical part of the algorithm, where an incorrect selection can have drastic effects on the inferred aerosol properties.

The global distribution of AAOT and SSA should give a indication of the consistency between the various global satellite datasets. The global distribution of AAOT from various instruments and algorithms shows a large variability, as shown in the world plots in Figure 36. All the available data for this project were used, resulting in an almost global coverage for SU_AATSR, OMAERUV and SYNAER, and a small spatial coverage for GRASP in this year. The spatial distribution of AAOT seems to be biased to the source region of various absorbing aerosols. The SU_AATSR AAOT is noticeably strong over desert regions, especially the Sahara, which is known for its large desert dust production. The AAOT from SYNAER is not retrieved over the Sahara, but rather shows high values over the Eastern deserts, like the Taklamakan, and densely populated areas, which may point to a preference for absorbing pollution aerosols. The AAOT from OMAERUV, finally, shows high AAOT only over the south-east Atlantic Ocean. This area is known for its extensive plumes of biomass burning smoke, spread over the ocean in an elevated layer at about 2–4 km altitude, with boundary layer clouds underneath during the boreal summer. The AAOT is not necessarily biased in this case, since high AAOT is commonly found over the Sahara and north Atlantic

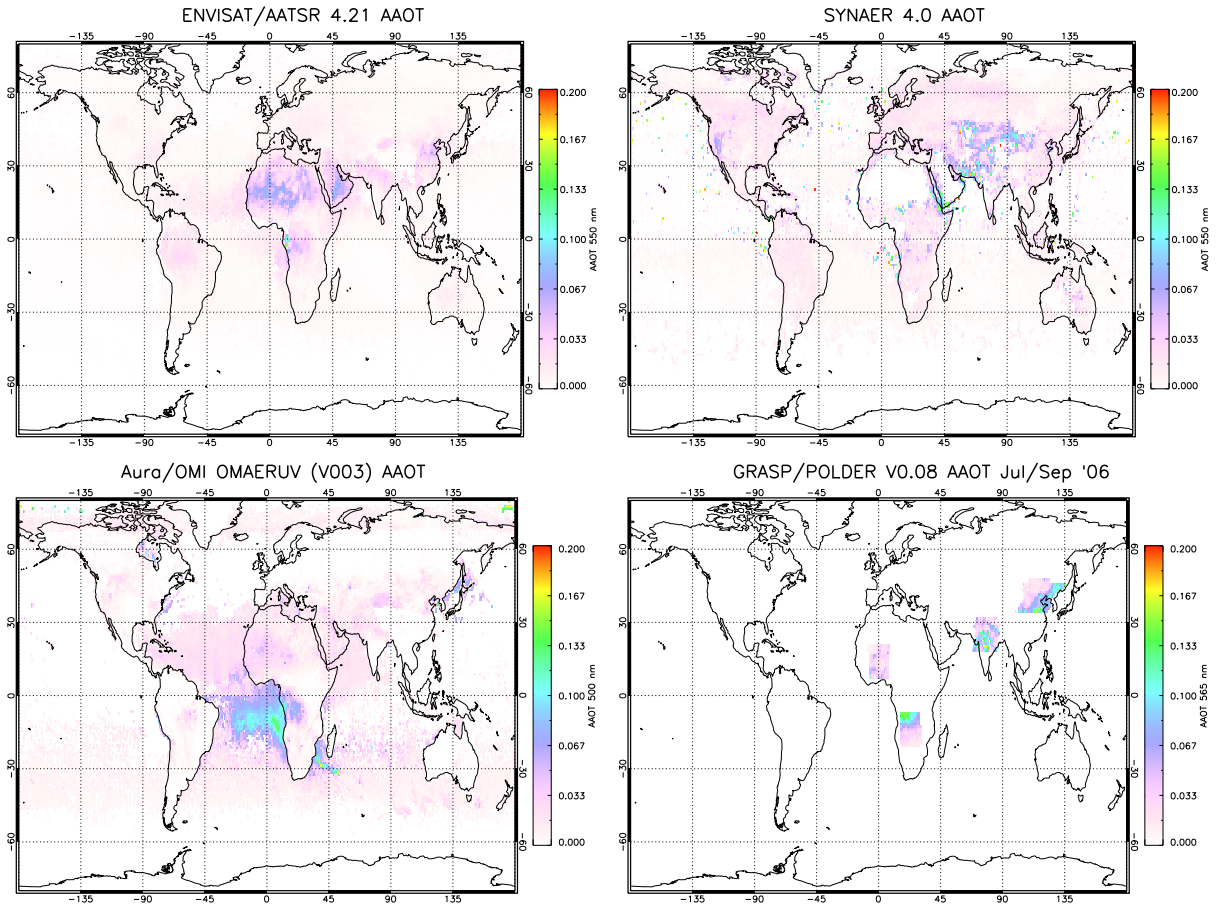

Figure 36: Absorption Aerosol Optical Thickness from various retrievals, averaged from July to September 2007. All data were regridded to a $1^\circ \times 1^\circ$ global grid. All available data from this period was used.

Ocean in the boreal winter months (not shown). This indicates a proper selection of aerosol type in this area for OMAERUV at least. The GRASP data are not covering the entire world, but rather are limited to areas close to important AERONET stations, currently four in total. The retrieved AAOT, however, shows realistic values and a large variation between 0 and values larger than 0.2, being sensitive to all known absorbing aerosols, like smoke, desert dust, and pollution aerosols.

8 Global Single Scattering Albedo

The Single Scattering Albedo (SSA) seems to be the most challenging parameter to be retrieved from space-based instruments. The previously presented absorbing aerosol cases show a large variability between the retrieved SSA from different instruments and algorithms. In order to show the current status of this parameter at a world scale, global plots of SSA averaged over the months July to September 2007 are presented in Figure 37. Figure 37 shows the large difference in retrieved SSA, reflecting the strong dependence of retrieval assumptions on the retrieved SSA. Only the SSA from SU_AATSR and SYNAER show some similarity, with slightly smaller SSA values over the known source regions of absorbing biomass burning smoke, like southern Africa, Australia and the Amazon basin. The similarity may be partly due to the shared use of AATSR data in both algorithms, and the use of similar aerosol climatologies. As noted before, the SSA from SU_AATSR shows little variation in the absolute value. SYNAER shows values as low as 0.8 for the averaged SSA, but still higher than AERONET values.

The SSA from OMAERUV is much higher, with only lower values for the southern African region, but never much lower than 0.9. Also these SSA values seem constrained, although values in boreal winter are lower, indicating more absorbing aerosols, especially near desert areas. However, the correlation to AERONET values and other satellite retrievals is low.

The coverage from GRASP/PARASOL is limited, as only data from areas around four AERONET stations are available. However, the SSA values are very realistic, showing a strong variability of the SSA between 0.7 and 1.0 and strong spatial gradients. These values are the closest match to AERONET SSA values, and represent the most valuable contribution of SSA from satellite imagery. This shows that accurate retrievals are more valuable than large datasets.

The SSA from FAME-A is hard to judge because of the limited coverage, and as noted before, it shows a strong non-physical north-south gradient and high absolute values.

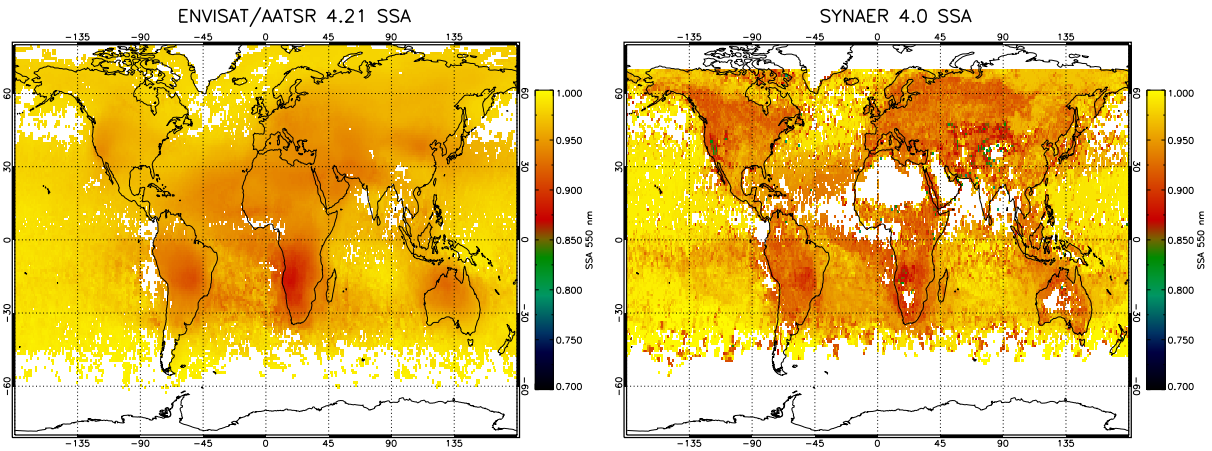

Figure 37: Single scattering albedo from various retrievals, averaged from July to September 2007. All data were regridded to a $1^\circ \times 1^\circ$ global grid. All available data from this period was used. (Figure continued on next page.)

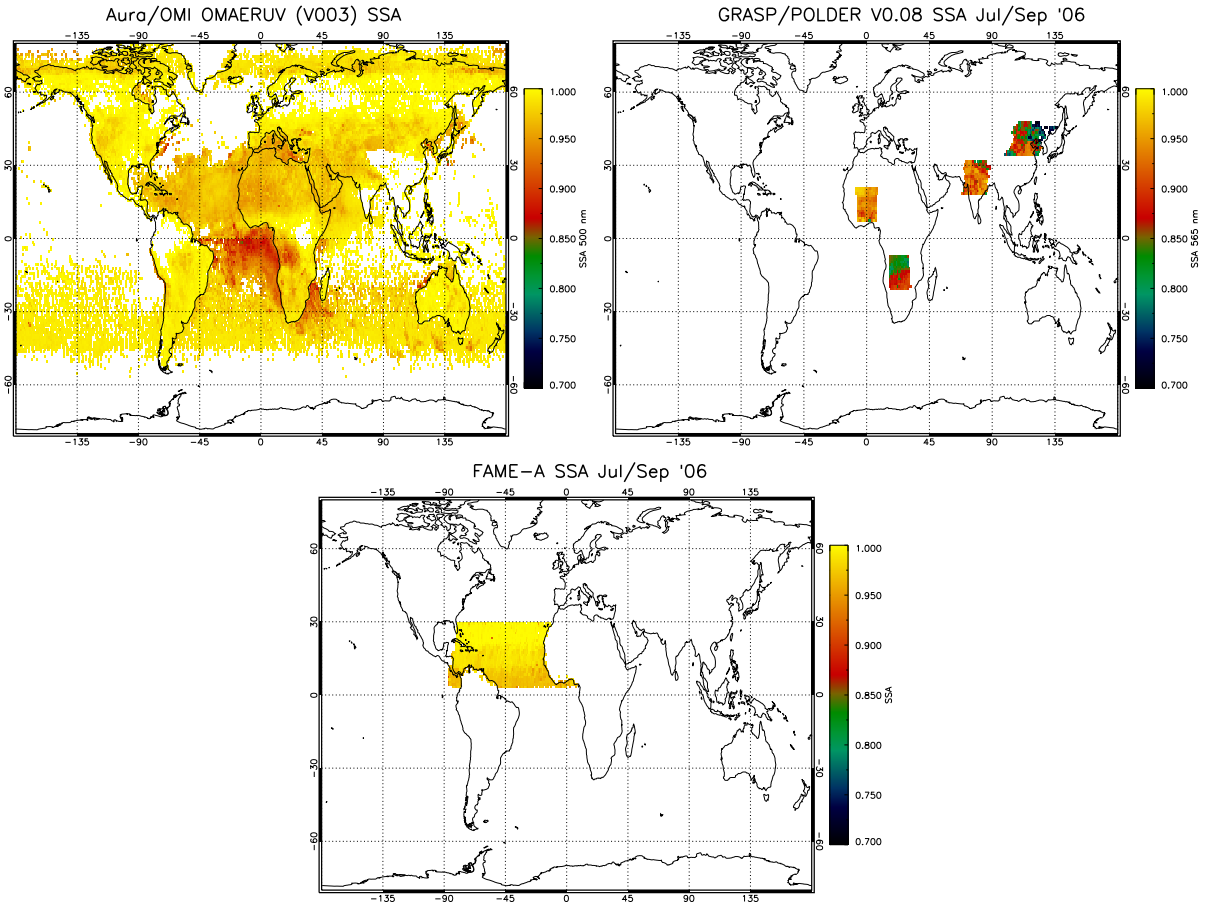

Figure 37 (Cont.): Single scattering albedo from various retrievals, averaged from July to September 2007. All data were regridded to a $1^\circ \times 1^\circ$ global grid. All available data from this period was used.

9 Absorbing AOT validation against AERONET

Absorbing AOT (AAOT) was retrieved by the Aerosol_CCI retrievals SU 4.3, ORAC v4.02 and PARASOL_GRASP_v0.08. This data is compared to AAOT data derived from the AERONET network. While there is AAOT data in the AERONET inversion product for AOT > 0.4, a data workup produced by Stefan Kinne was used for this comparison, which contains also AAOT for smaller AOT. The data set used is a later version of the one that was used in [*Bond et al.*, 2013]. In agreement with earlier work in the Aerosol_cci project this contribution will focus on the single year 2008. This has been the year Aerosol_cci phase 1 ended with and is the year where the PARASOL_GRASP_v0.08 retrieval provided data with the greatest spatial coverage.

9.1 Maps

In this chapter the data of the three retrievals will be compared based on their maps of the yearly mean calculated from the 12 monthly means. This is done for two regions: The whole globe and southern Africa. Note that the southern Africa region was defined in the HTAP project and covers only land regions. Figure 38 shows the maps of absorbing AOT for the three retrievals AATSR_ORAC_v4.01 (referenced as ORAC later on), AATSR_SU_v4.3 (referenced as SU later on) and PARASOL_GRASP_v0.08 (referenced as GRASP later on). The patterns look very different as is the weighted mean shown above the individual figures. The retrievals agree on the areas of the maximum AAOT occurrence (Africa, Asia) but outside these regions the values are very different. Especially over ocean ORAC and GRASP show very high values. While SU also shows low yearly means of AAOT, ORAC and GRASP do not.

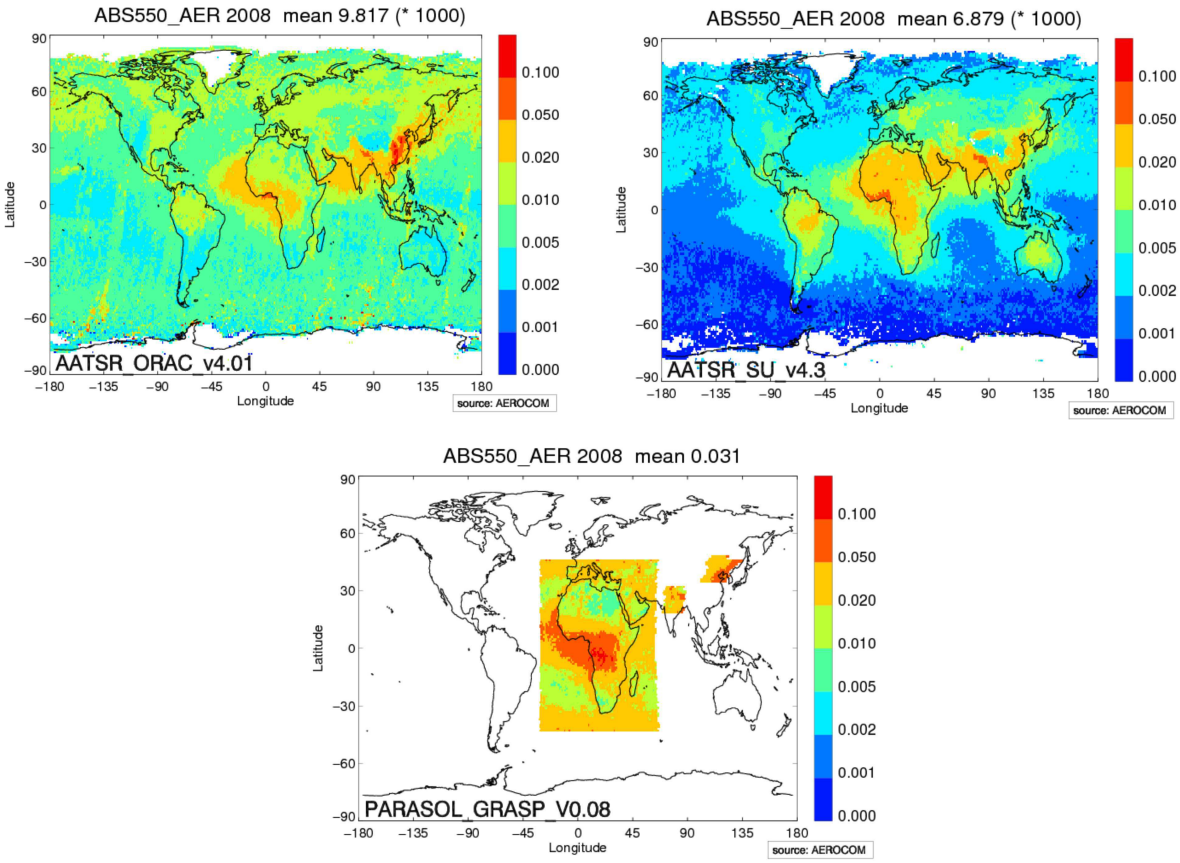

Figure 38: World maps of absorbing AOT

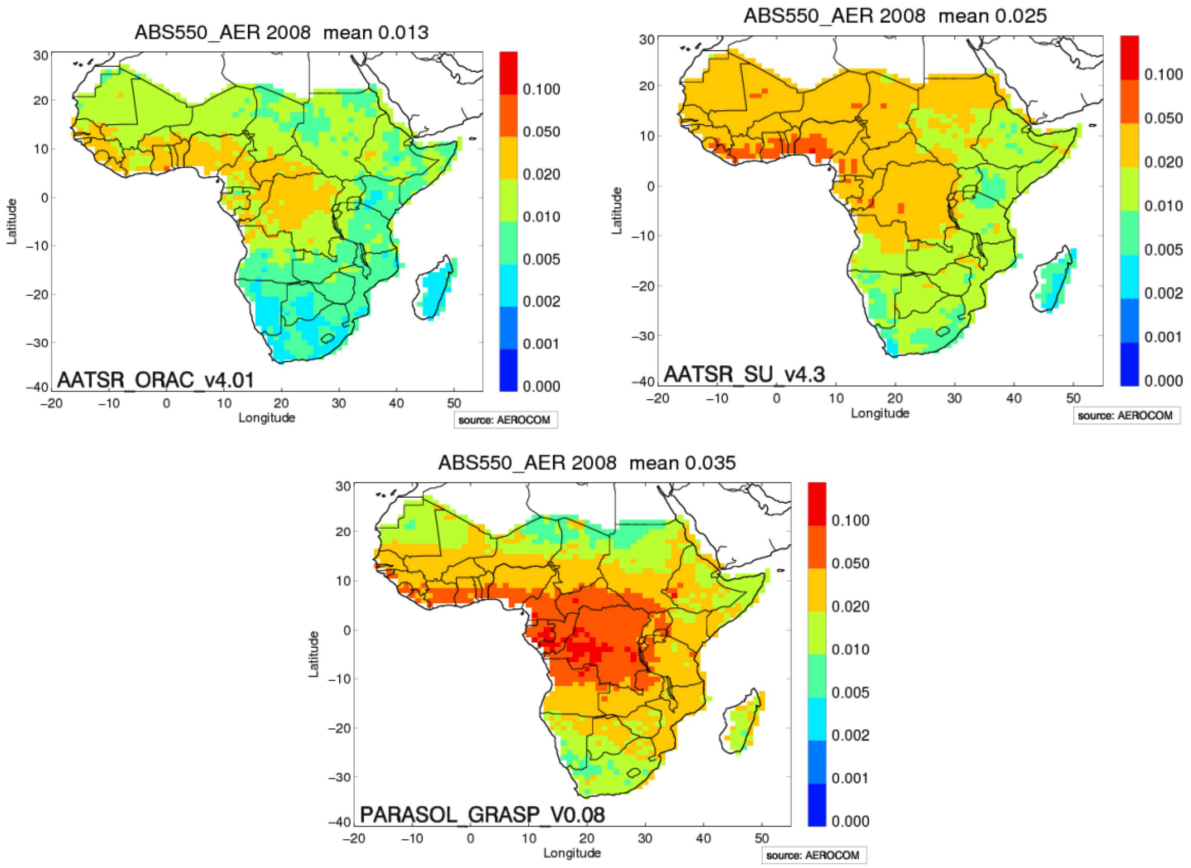

Figure 39: Maps of absorbing AOT in the southern Africa region

Figure 39 shows the same plot as before but for the southern Africa region. Because Africa was entirely covered by the GRASP retrieval, these plots are more comparable and show exactly the same area with retrievals. It can be seen that the retrievals do not agree very much in terms of the weighted mean with ORAC retrieving the lowest value of 0.013 AAOT, SU being in the middle with a value of 0.025 and GRASP having the highest value with 0.035. However, the retrievals agree in terms of where they retrieve the highest value (between a latitude of -15 to +10 degrees, and up to a longitude of 35 degrees east).

9.2 Comparison to observations

In this chapter the results of the three retrievals are compared to the earlier described absorbing AOT of AERONET. This is done on a daily basis where pixels are collocated in time and space to the ground based measurements. For collocation a nearest neighbour approach is used. The results of the two regions “WORLD” and “southern Africa” are shown.

For GRASP it has to be noted that the retrieval did not cover the whole globe. Because the comparison shows some features of the GRASP retrieval, the comparison for the WORLD region is shown here anyway.

Figure 40 shows scatterplots of the three retrievals analysed. The one for the GRASP retrieval (lower panel) shows some interesting patterns: Although it covers a far smaller part of the globe than the AATSR based retrievals, GRASP is able to retrieve data for more data points (GRASP: 3538, ORAC: 3406 and SU: 2738) using just approximately one third of the stations. Another interesting fact is that GRASP seems to have discrete low values as output of the retrieval. These can be seen in the values forming lines parallel to the x-axis at the lower values of GRASP. The statistics of GRASP for the WORLD region are not discussed here since they are not comparable to the ones of the other retrievals.

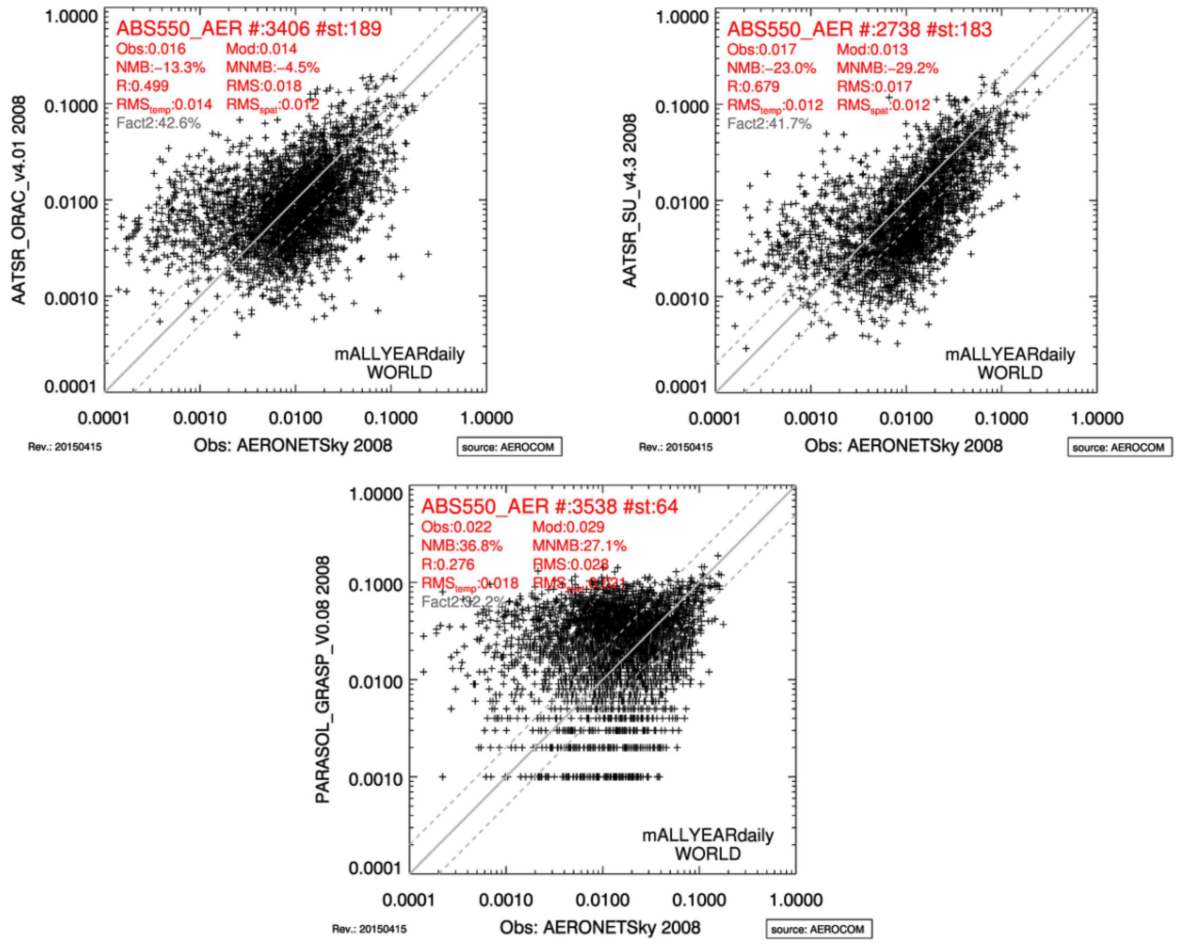

Figure 40: Scatterplots of absorbing AOT for the WORLD region

The two AATSR retrievals (upper panels) show comparable skill. The codes are comparable by RMS, and by the number of pixels within a factor of 2 between observations and satellite retrieval. In terms of correlation SU is better (0.68 compared to 0.5) while in terms of bias ORAC performs better (MNMB of -4.5% for ORAC compared to -29.2% for SU). Coverage measured by the number of days and the number of stations is 20% lower for SU as for ORAC, but the number of stations used is comparable (ORAC 189 vs. 183 for SU).

Figure 41 shows scatterplots for the southern Africa region. Because GRASP retrieved the whole area as well, statistical measures are comparable here. Note though that the analysis was not done for common pixels, just the area and time frame analysed is the same.

As before, GRASP shows a higher temporal coverage than the AATSR retrievals yielding more than the double number of days during the year 2008. The number of stations used is nearly the same (GRASP 10, AATSR: 9).

Although the mean of the observations is quite similar for all retrievals (between 0.033 AND 0.035), the means of the retrievals compared shows quite some difference (ORAC 0.020, SU 0.043, GRASP 0.030). Due to the very high negative bias of ORAC (-58.3%) SU is clearly the best AATSR retrieval for AAOT in the southern Africa region (also in terms of correlations, where GRASP again is affected by discrete low values of AAOT).

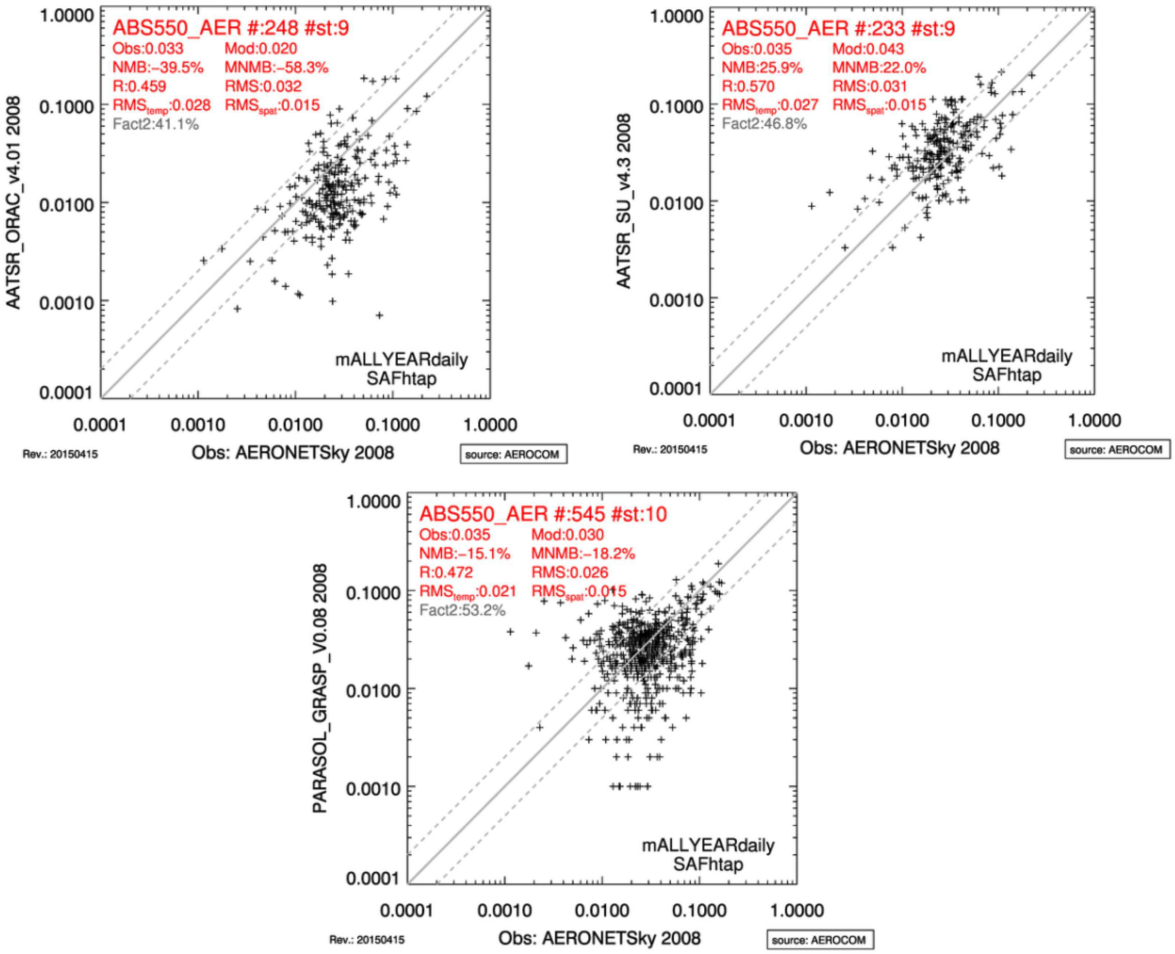

Figure 41: Scatterplots for the South Africa region

9.3 Zonal mean at observation sites

The goal of this comparison is to see, if the zonal dependency of observational data is also captured by the satellite retrievals. For this all monthly means from stations within a latitude of 10 degrees are averaged (e.g. between 30 and 40 degrees east). This average is then plotted as a dot at the middle point (35 degrees in the example). This plot is also shown for total AOT to see if the properties of the ASAOT retrieval is different to those of the quality proved AOT retrieval.

Figure 42 shows the zonal means of the different retrievals. The left hand panels show these means for absorbing AOT, the right hand side the same for total AOT for comparison. A perfect retrieval the blue and red lines in every plot show minimal differences.

For the ORAC retrieval the zonal means of AAOT differ quite a lot, especially in mid latitudes. Below -30 degrees and above 30 degrees the numbers agree quite well. Comparing the differences to the AOT zonal means, shows that the agreement is worse at AAOT. The existing agreement also happens in different regions of the globe.

For the SU retrieval the zonal mean of AAOT agrees quite nicely in general, but with a small low bias above 30 degrees compared to the observations. The difference in AAOT is similar to that for total AOT.

The zonal mean for the GRASP retrieval looks in general very different to the same plot for the AATSR retrievals due to different coverage. Comparing the zonal mean for AAOT and AOT shows that for AOT the zonal average is nearly same as for the AERONET measurements, but for AAOT this is not the case except for a small area between 20 and 40 degrees east.

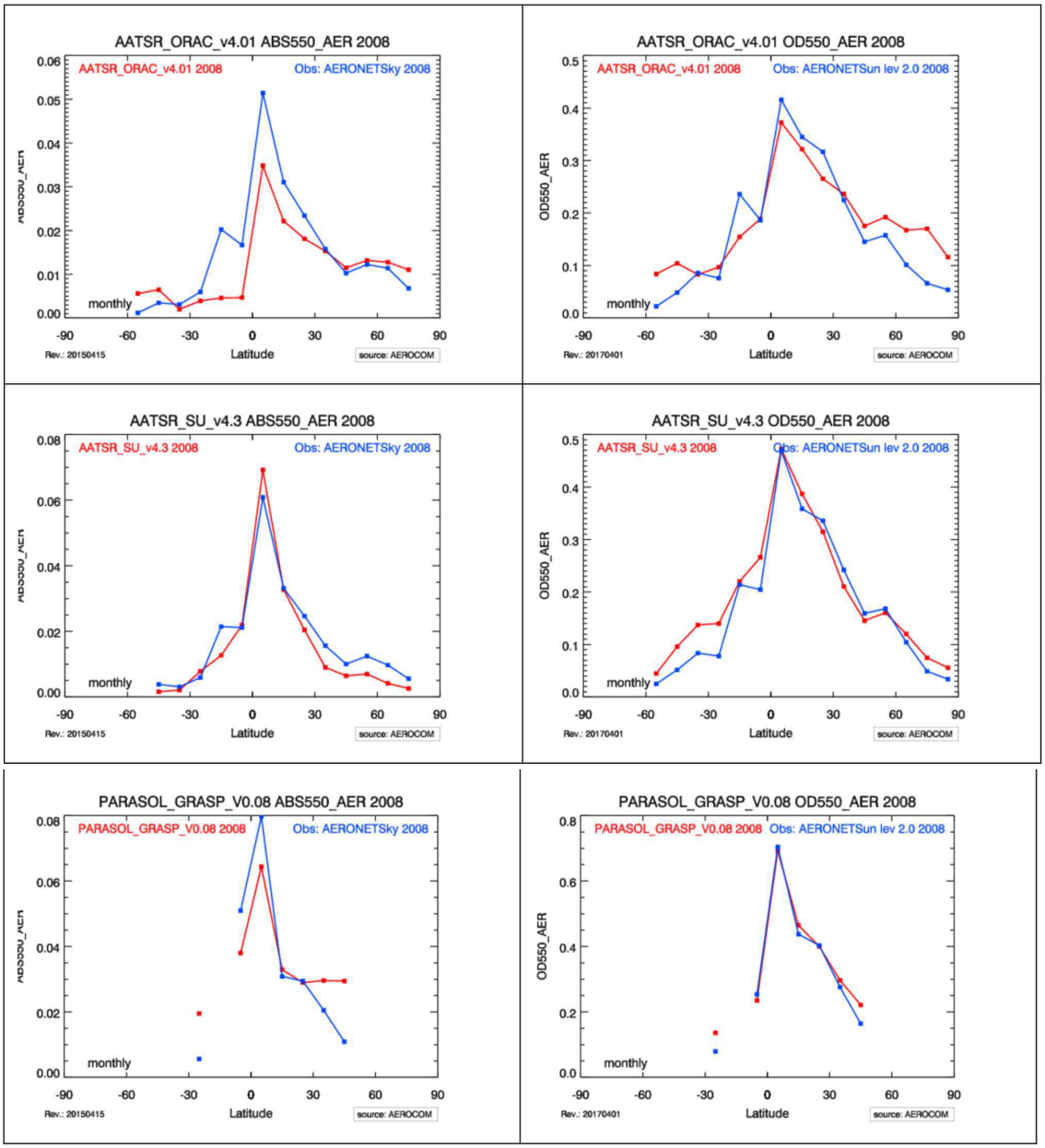

Figure 42: Zonal means of absorbing and total AOT

9.4 Bias at observation sites

For this plot, stations within an area of 10×10 degrees in latitude and longitude are averaged over time. The bias in percent is then calculated with the formula (ABS_{Sat} - ABS_{Obs}) / ABS_{Obs}. Reddish colours in the plot therefore indicate too high values from the satellite, blueish colours indicate too low values from the satellite. The paler the colours are, the more similar the values are.

For SU, the plot shows underestimation of AAOT in most parts North America and all over Europe, and a slight over estimation in the Sahel area. In South America and India there is no clear indication, because over and under estimation are present.

For ORAC the picture is less clear. There is underestimation in South America and the Sahel Zone, but for Europe, North America and Asia there is no clear picture as under and over estimation are present.

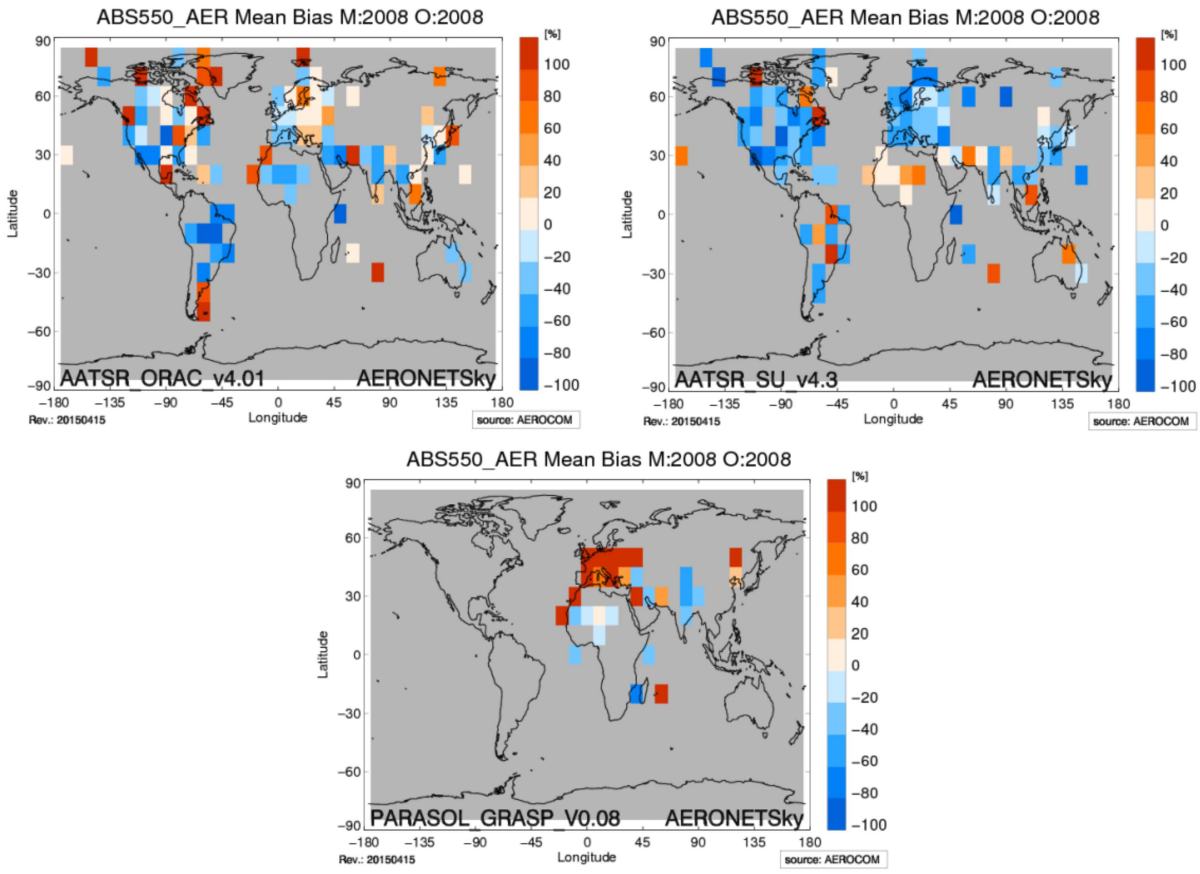

Figure 43: Bias at observational stations

For the GRASP retrieval, the plot shows some distinct patterns: good agreement in the Sahel area, large over estimation in southern Europe (not all Europe was covered by the data set), moderate underestimation in India and over estimation in east Asia.

9.5 Summary tables

In this chapter the statistical parameters from the AAOT comparison with AERONET are summarised and discussed compared to the same comparison for AOT and for two areas: The whole globe and southern Africa.

Table 7 shows the parameters for AAOT for the WORLD region, while Table 8 shows the same numbers for the AOT comparison. It can be seen that in general the bias is of comparable order of magnitude for both variables, the RMS is better for AAOT, but Correlation and the number of data pairs within a range of a factor of two is much higher for AOT.

Table 9 shows the parameters for AAOT for the SAF region, while Table 10 shows the same numbers for the AOT comparison. It can be seen that in general the RMS for AAOT is lower than the one of AOT. Correlation, RMS and values with a factor of 2 within each other are comparable between the AAOT retrievals, but the bias is significantly higher for ORAC than for SU and GRASP. Correlation around 0.5 for AAOT is significantly worse than for AOT (between 0.73 and 0.83). For both variables GRASP has roughly twice the amount of data points compared to the AATSR based retrievals.

Table 1: Statistics table AAOT daily values for the whole year 2008 WORLD

Retrieval	# of days	# of stations	Obs	Sat	MNMB	R	RMS	Fact2
AATSR_ORAC 4.01	3406	189	0.016	0.014	-4.5%	0.499	0.018	42.6%
AATSR_SU 4.3	2738	183	0.017	0.013	-29.3%	0.679	0.017	41.7%
PRARASOL GRASP V 0.08	3538	64	0.022	0.029	27.1%	0.276	0.028	32.2%

Table 2: Statistics table AOT daily values for the whole year 2008 WORLD

Retrieval	# of days	# of stations	Obs	Sat	MNMB	R	RMS	Fact2
AATSR_ORAC 4.01	6436	204	0.193	0.211	21.0%	0.754	0.144	60.9%
AATSR_SU 4.3	4668	199	0.221	0.227	2.9%	0.838	0.135	76.5%
PRARASOL GRASP V 0.08	5455	68	0.280	0.309	16.7%	0.841	0.163	62.7%

Table 3: statistics table AAOT daily values for the whole year 2008 SAF

Retrieval	# of days	# of stations	Obs	Sat	MNMB	R	RMS	Fact2
AATSR_ORAC 4.01	248	9	0.033	0.020	-58.3%	0.459	0.032	41.1%
AATSR_SU 4.3	233	9	0.035	0.043	22.0%	0.570	0.031	46.8%
PRARASOL GRASP V 0.08	454	10	0.035	0.030	-18.2%	0.472	0.026	53.2%

Table 4: statistics table AOT daily values for the whole year 2008 SAF

Retrieval	# of days	# of stations	Obs	Sat	MNMB	R	RMS	Fact2
AATSR_ORAC 4.01	492	11	0.415	0.329	-29.8%	0.730	0.248	72.4%
AATSR_SU 4.3	453	11	0.421	0.474	4.7%	0.809	0.235	76.8%
PRARASOL GRASP V 0.08	981	11	0.451	0.424	-2.4%	0.834	0.190	79.2%

10 Conclusions

The Aerosol CCI Absorbing Aerosol Round Robin exercise was designed to inter-compare satellite datasets of absorbing properties of aerosols world-wide, especially those datasets that have been developed under the auspices of the Aerosol CCI. However, many more datasets have been used in the inter-comparison, including ground-based data from the global AERONET network. Using several carefully selected periods and areas where absorbing aerosols were abundant, the retrieval of absorption properties from various absorbing aerosols, like desert dust and biomass burning aerosols (smoke), were compared.

This is the first time during the run of the Aerosol_cci phase 2 project an aborbing AOT product is analysed. It is therefore expected that the retrievals of AAOT do not show the same maturity as the ones of total AOT.

The study shows large inconsistencies between retrievals of the Absorbing Aerosol Optical Thinkness (AAOT) and Single Scattering Albedo (SSA) from satellite data. No correlation was found between any of the datasets for either quantity. The main reason for these discrepancies is the known dependence of most retrievals of these quantities on the (correct) choice of aerosol type in the algorithms. AOT from single view instruments is known to depend strongly on *a priori* assumptions [e.g. *Kokhanovsky et al.*, 2010; *Wu et al.*, 2016], and derived products like AAOT and SSA will even more depend on correct assumptions. The aerosol type selection is a critical step, and even with a large selection of aerosol types, the AAOT shows a bias to a certain type of absorbing aerosols, while the SSA is strongly constrained. Comparison to ground-based AERONET retrieved SSA shows a lack of variation of the absolute value of the SSA for all algorithms, except the GRASP algorithm. Correlations with AERONET data are weak or non-existent.

The GRASP/PARASOL data shows realistic values for both AAOT and SSA around AERONET stations, which is promising for future developments. It is an open source package, which combines as many observations as possible, which is necessary for complicated aerosol property retrievals. The OMAERUV data also shows promising correlations with AERONET data, albeit with known restrictions for single view instruments. The dependence on *a priori* information like aerosol type is strong, which should be taken into account when interpreting the data. The AAI and UVAI give reliable qualitative information about the presence of absorbing aerosols, and has a strong correlation with AAOT. The AAI is a quantity that is difficult to interpret, but is easy to retrieve globally, and is still one of the most used quantities for absorbing aerosols. Proper radiometric calibration of satellite instruments is essential for this product, but its sensitivity to radiometric offsets makes it a useful tool for degradation monitoring and correction. Unfortunately, the ORAC and FAME-A algorithms were difficult to judge, due to the limited amount of data and obvious retrieval problems apparent in the datasets. Future assessment should give more conclusive results about their accuracies. The SYNAER and SU_AATSR algorithms provide interesting global datasets on aerosol absorption parameters, but currently rely too much on *a priori* information, especially aerosol type, to provide accurate aerosol micro-physical information.

Of the three retrievals analysed, SU shows the highest skill at this point, but also having the lowest coverage. ORAC has a slightly higher covarage, but also slighly lower skill.

GRASP can be only judged by its performance in Africa at this point since it did not deliver data for the whole globe. It shows similar skill as ORAC for AAOT, but has a much better coverage than the AATSR based retrievals. Overall it can be stated that the AAOT retrievals have a similar skill as the AOT retrievals had at the beginning of the Aerosol_cci phase 2 project.

11 Recommendations

The round robin exercise summarized in this report shows the challenges in retrieving aerosol absorption properties from space-based instruments. A growing dataset of AOT from various instruments covering several decades is being generated, but the retrieval of AAOT and SSA from space still suffers from large inconsistencies. These quantities are important for climate studies on a global scale, and therefore deserve attention from the satellite community. The proper retrieval of these quantities should be a focus for the coming years.

The retrieval of aerosol micro-physical properties is a complex problem, and the inversion problem is usually under-determined. Single-view, intensity-only measurements are insufficient to fully characterize the aerosol content in the atmosphere and the aerosol properties [e.g. *Hasekamp and Landgraf*, 2005], especially from space as the underlying surface and clouds have a large impact on the retrieval accuracy. To better characterize micro-physical aerosol properties, several options are available, like the use of multi-angle measurements [e.g. *Kahn and Gaitley*, 2015; *Kokhanovsky et al.*, 2015], polarimetric measurements [e.g. *Wu et al.*, 2015; *Kokhanovsky et al.*, 2015], better characterization of the angular effects of the underlying surface [e.g. *Wu et al.*, 2016], and the synergistic use of instruments. In the near future, better characterisation of aerososol properties, including absorption, can be expected from current and planned satellite missions that focus on air quality, like ESA's Sentinel 5P (launched in October 2017), Sentinel 4 and Sentinel 5 missions. Furthermore, the EarthCARE mission is planned to characterise aerosols, clouds and radiation in the Earth's atmosphere.

SSA is defined by WMO/GCOS as an Essential Climate Variable (ECV) for Atmosphere Composition. The requirements are an SSA product every four hours on a 5-10 km resolution and a measurement uncertainty of 0.03. It is clear from the current analysis that this will not be met in the near future. The spatial resolution is feasible with current satellite instruments. The temporal requirement is not met by polar orbiting satellite, which provide measurements typically once per day, but the diurnal variation can be provided by geostationary satellites and simulated using global climate models, especially the slowly varying aerosol spatial distribution. Notably, the Copernicus Atmosphere Monitoring Service (CAMS) shows very promising developments, providing a daily 5-day forecast based on a global monitoring system of the state of the atmosphere. However, it is clear from the current analysis that the uncertainty requirement cannot be met with the algorithms described in this report. This study shows that the problem is complicated, and that careful evaluation of the retrieved parameters remains an essential part of the development. Attention should be focused on accuracy assessment before processing large datasets. To accurately characterize aerosol absorption properties, the best available information from ground-based instruments, space-based instruments, *in situ* observations, and models should be combined and exploited, and the uncertainties should be well characterized.

End of the document